DEVELOPMENT AND VALIDATION OF A NOVEL MICROFLUIDIC PLATFORM FOR STUDYING LOCAL MICROVASCULAR BLOOD FLOW REGULATION IN VIVO

by © Gaylene M. Russell McEvoy

A Thesis submitted to the School of Graduate Studies in partial fulfillment of the requirements for the degree of **Master of Science in Medicine (Cardiovascular Sciences)**

Division of Biomedical Sciences, Faculty of Medicine

Memorial University of Newfoundland

May 2020

St. John's, Newfoundland and Labrador

Abstract

Currently, there is no effective way to restrict administration of vasoactive drugs to capillary networks of skeletal muscle and observe the effects on blood flow. The purpose of this project was to develop and validate the efficacy of a novel liquid microfluidic device (LMFD) to manipulate a microscale region of tissue while simultaneously allowing for visualization and quantification of microvascular blood flow. The LMFD was developed and fabricated using soft lithographic techniques. Devices were molded in polydimethylsiloxane and bound to a glass coverslip with a 600 x 300 μm laser cut micro-outlet. Sprague-Dawley rats were anaesthetized with sodium pentobarbital and instrumented to monitor systemic parameters. The extensor digitorum longus muscle was dissected, externalized, and reflected across the LMFD on the stage of an inverted microscope. Doses (10^{-8} to 10^{-3} M) of adenosine triphosphate (ATP), acetylcholine, and phenylephrine (PE) were sequentially administered to the muscle via perfusion through the LMFD. Videos of microvascular blood flow at multiple focal planes were recorded directly overlying the micro-outlet. Recordings were analyzed offline for red blood cell (RBC) velocity, supply rate, and hematocrit. ATP significantly increased RBC velocity and supply rate. Increasing concentrations of PE caused a decrease in RBC velocity and supply rate. Changes in perfusion were restricted to areas directly overlying the micro-outlet and within 500 μm. This novel LMFD allows for a controlled delivery of dissolved substances to constrained regions of microvasculature while simultaneously allowing for visualization and measurement of blood flow within discrete vessels and networks.

Acknowledgements

This thesis would not be possible without the support and guidance of my supervisor Dr. Graham Fraser. I am grateful for his dedication, patience, and time that he has taken to provide me with excellent training and advice. The lessons I've learned have helped me grow personally and professionally. He has always made it a priority to ensure voices are heard, and emergency Oreos are stocked.

Secondly, an enormous thank you to my fellow lab members, past and present, for their encouragement and patience along the way. A special and much deserved thank you to Hamza Shogan for teaching me how to use CAD, being a helping hand throughout the entire project from device fabrication, the validation experiments and analysis, and above all a friend.

I would like to thank Dr. Bruce Van Vliet and Dr. John McGuire for their direction, and expertise. I also extend my thanks out to the rest of the Cardiovascular group who have all taken time to learn about the project and extend their words of wisdom and advice.

Thank you to NSERC and MUN Faculty of Medicine for the financial support of this project.

Lastly, thank you to all of the faculty members, support staff, MUN Med3D, and fellow graduate students past and present who have been there for support, advice, and coffee breaks.

Table of Contents

List of Tables

List of Figures

List of Abbreviations and Symbols

Standard chemical formulas, symbols and units were used throughout the thesis and were not included in this list.

10X	ten times magnification
2A	second order arteriole
3A	third order arteriole
3D	three-dimensional
ACh	acetylcholine
ANOVA	analysis of variance
ATP	adenosine triphosphate
CAD	computer aided design
cGMP	cyclic guanosine monophosphate
COX-1	cyclooxygenase-1
COX-2	cyclooxygenase-2
EDF	extended depth of field
EDHF	endothelium-derived hyperpolarizing factor
EDL	extensor digitorum longus
eNOS	endothelial nitric oxide synthase
ET-1	endothelin-1
FiO_2	fraction of inspired oxygen
GPU	graphical processing unit

IP3	inositol trisphosphate
IVVM	intravital video microscopy
LMFD	liquid microfluidic device
MAP	mean arterial pressure
NE	norepinephrine
PCO_2	partial pressure of carbon dioxide
PDMS	polydimethylsiloxane
PE	phenylephrine
PGH_2	prostaglandin H_2
PGI_2	prostacyclin
PO_2	partial pressure of oxygen
PSS	physiological salt solution
RBC	red blood cell
SAD	sum of absolute difference
sO_2	oxygen saturation
STI	space-time image
TCO_2	total carbon dioxide
U	international unit

Co-Authorship Statement

This thesis is structured in 3 chapters. Chapter 1 provides background knowledge, chapter 2 is a manuscript that describes original research, and chapter 3 is a summary chapter.

This thesis contains the following manuscript that is in preparation:

GM Russell McEvoy, H Shogan, RJ Sové, GM Fraser.
Development and validation of a novel microfluidic device for the manipulation of skeletal muscle microvascular blood flow in vivo. (In preparation for submission to *Microcirculation*)

The project was designed by GM Russell McEvoy and GM Fraser.

Animal surgeries were completed by GM Russell McEvoy and GM Fraser.

H Shogan provided occasional technical assistance in 3D stage insert and stage model conceptualization, device fabrication and data collection contributing to Tables 2.4-6, Figures 2.3, 2.4, 2.6-2.14.

RJ Sové provided mathematical modeling expertise based on experimental conditions for the study contributing to Table 2.1, Figures 2.17-2.19.

Data collection, data analysis, interpretation of data, preparation of figures and the manuscript in the current thesis was completed by GM Russell McEvoy with supervisor review. Co-authors contributed to critical revision of the manuscript in preparation for submission.

1. Introduction and Overview

1.1. Purpose and Objective

The circulatory system of mammals carries blood to all tissues through a series of organized branching vascular networks. Large arteries in the vascular tree are responsible for carrying the blood and distributing of blood flow to organs in response to downstream stimuli. Arterioles are resistance vessels that branch from arteries and are responsible for blood flow regulation at the tissue level as well as the regulation of flow from arteries. Smaller vessels, known as the microcirculation, are composed of arterioles, capillaries, and venules under 100 μm in diameter in rodents (Bosetti et al., 2016). These microvessels provide the major site of exchange of nutrients and waste products between the systemic circulation and the tissues of the body. Metabolic need is an important determinant in blood flow regulation between discrete regions of tissue. As a result, the associated regulatory mechanisms are of great interest (Segal, 2005; Bagher & Segal, 2011b).

Microcirculation and microvascular blood flow regulation mechanisms of various tissues can be studied using intravital video microscopy (IVVM). IVVM of skeletal muscle preparations, such as cremaster, gluteus maximus, and extensor digitorum longus (EDL), have been used to study the microcirculation in response to various experimental manipulations. Selection of a microvascular preparations largely depends on the proposed research question. Each preparation is suitable for different applications depending on characteristics such as the accessibility of vessels of interest, organization of tissue vasculature, and function. The selection also depends on the tissue structure, as planar

shaped muscle tissues (i.e., gluteus maximus and cremaster) lend themselves to superfusion techniques for the interrogation of arterioles, whereas fusiform muscle tissues (i.e., EDL) are better suited to isolation techniques for measurements at the capillary level (Duling & Berne, 1970; Sullivan & Pittman, 1982). Application of substances to IVVM preparations can only be achieved through intravascular injection, superfusion application, and via a micropipette at the surface of the muscle (Kurjiaka & Segal, 1995; Moore et al., 2010; Bagher & Segal, 2011a). Measurements following experimental manipulation include red blood cell (RBC) velocity, and RBC supply rate in capillaries, and vessel diameter changes at arterioles for quantifications of changes in the vasculature.

A potential avenue to administer substances to a specific region of tissue is through a microfluidic device. Microfluidics encompasses the techniques and technology for precise control and manipulation of fluids of small volume in a system. The use of microfluidic devices in research has been expanding over the past several decades (Wolfe et al., 2010). Microfluidic devices are used to manipulate small volumes of fluid and can be fabricated in silicon elastomers using soft lithography techniques.

Fabrication of a novel microfluidic device to restrict administration to spatially confined regions of interest provides a modality to experimentally manipulate the microcirculation to study blood flow regulation. In this thesis, I have described a novel microfluidic approach for the continuous delivery of substances, such as vasoactive drugs, at known concentrations, to a well-defined microscale region of tissue. Administration of biologically relevant molecules, vasoactive drugs, and pharmacological targets to rat EDL skeletal muscle will serve as a test of the efficacy and validation of this device.

Purpose: Develop a novel microfluidic device suitable for incorporating with a well-established microvascular preparation, that is capable of the continuous delivery of substances, such as vasoactive drugs, at known concentrations, to a well-defined microscale region of tissue with simultaneous visualization of capillary blood flow.

Objective: Validate the capability of a novel microfluidic platform to manipulate microvascular blood flow by administering vasoactive drugs to a confined micro scale region of skeletal muscle tissue.

1.2. Microvascular Preparations

The series of organized branching vascular networks of the circulatory system is responsible for the delivery of blood to all tissues. Blood carries oxygen (O_2) and nutrients while removing waste products, including carbon dioxide (CO_2), from tissues in order to maintain the metabolic needs of cells, and communication among the organs through hormonal and other signaling molecules. The exchange between the blood and tissue requires a high surface area for diffusion to occur. The majority of this surface area lies in the microcirculation, which is composed of the smallest vessels within the circulatory system. In humans, the microcirculation is considered to be vessels which are less than 300 μm in diameter (Levy et al., 2001). However, in rodents, due to the smaller size of their body and vasculature we define the microcirculation as vessels less than 100 μm in diameter (Bosetti et al., 2016). The microcirculation is made up of arterioles, capillaries, and venules, with capillaries forming the major site of exchange between the blood and the tissues.

Experimental manipulation of microvascular beds allows researchers to study the mechanisms of blood flow regulation in the microcirculation. In an intact, integrated vascular system, this is achieved by evaluating the effects of biochemical, pharmacological and physical manipulations, as well as O_2 perturbations through direct observation of microvascular blood flow and vessel diameters using intravital microscopy. Intravital microscopy has been used for investigations into the microcirculation of several tissues, with different preparations being developed and refined based on the structure of interest, imaging equipment available, the research question being addressed, and the specific field of study.

Intravital microscopy has been applied to whole organ preparations including brain (Kleinfeld et al., 1998), heart (Lee et al., 2012), liver (Scott & Fox-Robichaud, 2002), kidney (Hato et al., 2018), spleen (Ferrer et al., 2012), and mesentery (Dixon et al., 2005). A brief overview of these preparations and related applications is provided in this section. The complex vascular geometry, and unique function of each organ influences the research questions undertaken. The liver, kidney, and heart preparations are challenging due to the movement of the tissue imposed by the animal's breathing and heartbeat. For example, in the liver, where much of the microvasculature is composed of hepatic sinusoids, intravital microscopy has been used to study inflammation and motility of leukocytes following induction of experimental sepsis (Scott & Fox-Robichaud, 2002). Imaging hepatic microcirculation involves isolation of the liver through an incision in the anterior abdominal wall for the reflection of the liver onto the microscope stage. This form of experimental preparation has led to many discoveries in leukocyte recruitment in animal models of disease states such as in inflammatory bowel disease, inflammation,

and cancer cell metastasis (MacDonald et al., 2002; Scott & Fox-Robichaud, 2002; Ondiveeran & Fox-Robichaud, 2004). Similar to liver preparations, isolation of the kidney can be achieved via an incision through the overlying tissue of the abdomen. Direct observation of renal microcirculation with the help of IVVM equipment has been beneficial in understanding the progression of renal failure (Zhi et al., 2011; Hato et al., 2018). Interventions including artery occlusion and release have been used as models for human renal ischemia, and renal failure (Yamamoto et al., 2001; Zhi et al., 2011). Use of this system to study glomerular function and microcirculation has been valuable for evaluating the effect of renal artery blockages, reperfusion, and the resulting change in microcirculation blood flow (Zhi et al., 2011).

Development of IVVM techniques for heart and brain tissues has allowed research questions to be addressed in the cerebral and coronary microcirculation. Imaging the brain and heart preparations are more complex as the skull impedes easy access to the brain, and the heart is continuously moving. Kleinfeld et al. (1998) described the use of intravital imaging on a laser scanning microscope in conjunction with a craniotomy, and injections of fluorescein isothiocyanate-labeled dextran in Sprague-Dawley rats (Kleinfeld et al., 1998). Desired areas of interest are typically below the pia therefore, fluorescence confocal imaging is required to achieve imaging at the required depth. The coupling of a craniotomy and injection of fluorescent dye allows for the imaging of blood flow up to 600um below the pia. As well this technique allows the capillary RBC velocity to be quantified both at rest and following vibrissae and cutaneous stimulation, with both stimulations causing a transient increase in RBC velocity. This method to study the cerebral microvasculature has been applied in several studies to examine the response to

inflammatory agents, and the redistribution of blood flow following vessel occlusion (Schaffer et al., 2006).

In the past decade, with development of new elongated or "stick" objectives there has been success in the use of IVVM in the heart to image individual cells within tissues (Lee et al., 2012). This preparation involves dissection of the pericardial sac of an anaesthetized animal for access to the visceral layer of the epicardium. To stabilize the tissue, a ring is bound to the visceral layer of the epicardium using a bonding agent and returned to the resting position. A further limitation of imaging the heart is the requirement for short capturing periods coinciding with the non-dynamic periods of ventilation and cardiac cycle that minimizes excess movement of the tissue. This technique has been used to study leukocyte recruitment in the myocardium following ischemic reperfusion injury and computer reconstruction of vessels of the heart (Lee et al., 2012). Intravital imaging of these organs are challenging due to the thick nature of the tissue, making them unsuitable for transillumination.

Studying the microcirculation in organs throughout the body provides valuable insight into the impact that perturbations have on various tissue. The musculoskeletal system is frequently used as a model to evaluate the responsiveness of the microcirculation to a variety of factors including exercise and oxygen perturbations. Individual muscle preparations have been selected based on their physical characteristics, particularly their ability to be transilluminated and used with IVVM equipment. Viable muscle preparations must lend themselves to surgical isolation and externalization. Characteristics of viable muscle preparations include muscles being of adequate size, the ability to separate the muscle from surrounding structures, preservation of nervous

innervation, and the ability to situate the muscle on imaging equipment without impairing blood supply. These characteristics are not the same for each muscle and therefore require consideration when developing the specific muscle preparation.

With the above considerations in mind, preparations applying IVVM have been developed to study the microcirculation of muscles throughout the body, including cheek pouch, cheek pouch retractor, cremaster, gluteus maximus, and the EDL muscle. The cheek pouch is a unique anatomical structure in some rodents (hamster) that forms a sac and was among the first tissues to be used as a method to study the microcirculation of hamsters (Lutz et al., 1950). The cheek pouch has provided valuable insight into the role of conducted signaling in arterioles (Duling & Berne, 1970) and blood flow regulation (Fox & Frame, 2002). There have been two main preparations related to the hamster cheek pouch; one for studies at low magnification to observe effects in a larger area of tissue, and a second technique which can be used for studies at high magnification for improved imaging of arterioles. However, due to the necessary removal of one of the two layers of tissue, the surgical preparation of the cheek pouch for high magnification requires more skill, is more challenging, and is time consuming (Duling & Berne, 1970).

Following the cheek pouch preparation, the hamster cheek pouch retractor muscle preparation was developed to facilitate studying O_2 transport from the microcirculation into the tissue (Sullivan & Pittman, 1982). The length of the retractor muscle is desirable for intravital setups that are equipped for transillumination as the cross-section is thin and oblong. Structurally, the vasculature, particularly the capillaries, are oriented parallel to the muscle fibers running along the long axis of the muscle. This preparation was used to develop several techniques and tools to determine the O_2 saturation of RBCs along the

length of capillaries (Ellsworth & Pittman, 1986). An additional advantage of this preparation is the ability to use both superfusion and isolation techniques. However, the retractor preparation is not ideal for microscopy setups that cannot transilluminate a muscle with a thickness greater than 400 μm.

The use of common skeletal muscle preparations that are thin and able to be easily transilluminated for blood flow regulation studies is highly desirable. Due to this, other muscle preparations have been developed to satisfy the need for a thin tissue suitable for visualizing multiple branches of the arteriolar tree. One of these easily externalized preparations is the cremaster muscle. This muscle is responsible for the raising and lowering of testicles in males and to provide appropriate temperature control in order to produce viable sperm. The cremaster preparation was first outlined by Grant as a way to study the microcirculation in living animals (Grant, 1964). The cremaster is pinned out radially for imaging, and a superfusion fluid is used to bath the muscle with a bicarbonate buffer (Bagher & Segal, 2011a). Tubing directs superfusion fluid to the cremaster preparation where the solution is continuously dripped over the muscle. The cremaster preparation has been regularly used for numerous studies investigating vascular tone and arteriolar blood flow regulation, which include recent studies into the conducted signalling response to CO_2 and hydrogen (Charter et al., 2018) and vasoactive drugs (Kurjiaka & Segal, 1995; Lamb et al., 2018).

Interests in the role of muscle microcirculation during locomotion and exercise, prompted the development of skeletal muscle preparations, as they are often used for locomotion and mobility. The gluteus maximus, for example, is responsible for locomotion of the lower hind limb in both rodents and humans. This fan-shaped muscle

has been used for microcirculatory studies as it provides not only the ability to use the superfusion preparation as described with the cremaster muscle but also is a striated muscle that can be stimulated to simulate exercise. The gluteus maximus muscle is isolated and reflected out onto the stage of an upright microscope with care to ensure the supply of blood is not interrupted, and the muscle is pinned out in the fan shape similar to *in situ* orientation (Bearden et al., 2004). Other applications of this preparation include studying conducted signalling in response to exercise with aging. Specifically, the ability to simulate exercise through electrical stimulation has been used to evaluate the effect of aging on exercise-induced conducted vasodilation at the arteriolar level in mice (Jackson et al., 2010). During exercise, the nutrient and O_2 demands of the tissues increase, triggering mechanisms to increase in blood flow to support higher metabolic demand.

Some muscles, due to the orientation and shape of the tissue, are better suited to either superfusion preparations or to preparations which involve isolation from the atmosphere through the use of an impermeable membrane. The EDL muscle is a skeletal muscle preparation that does not require superfusion techniques as it can be isolated from the atmosphere once externalized. This preparation was used for the experimental study in the current thesis and will be discussed in detail. Tyml and Budreau first described the EDL muscle preparation (Tyml & Budreau, 1991). The rat EDL is a striated muscle of the lower hind limb and, similar to its function in humans, is responsible for paw mobility by raising the toes during locomotion. In rats, the EDL has two feed vessels, the proximal and medial arteries, each with paired venous collaterals and nerves (Williams & Segal, 1992). The location of these feed vessels allows for externalization and reflection of the muscle while keeping the neurovascular bundle intact. The capillaries and capillary beds

are typically oriented parallel to the muscle fibers with terminal arterioles and venules being perpendicular to the muscle fibers. The EDL preparation, as described by Tyml, involves the blunt dissection of the muscle and isolating it from the adjacent tibialis anterior and the biceps femoris muscles (Tyml & Budreau, 1991). Imaging the EDL is achieved by covering the exposed surface of the EDL and tibialis anterior with a glass coverslip and covering adjacent muscles in an impermeable plastic film (e.g. polyvinylidene chloride, Saran). The EDL preparation is advantageous for studying O_2 transport in capillaries and also mechanisms of blood flow regulation at terminal arterioles.

The EDL isolation technique is essential for not only limiting the muscle's exposure to the atmosphere and reducing tissue movement due to the animal's respiratory motion, but also to provide a suitable optical surface for epi-illumination of the muscle to evaluate and record microvascular hemodynamic measurements. This preparation is advantageous compared to superfused preparations due to the lack of prolonged bathing in a bicarbonate buffered solution and the ability to isolate the muscle from the atmosphere. However, the ability to interact with the muscle is limited by the overlying coverslip in this non-externalized orientation.

The progression to combine externalization and transillumination of the EDL preparation involves similar techniques to those described above (Fraser et al., 2012b). However, to externalize the muscle, care must be taken to ensure the dissection is close to the extensor retinaculum, under which the EDL tendons passes, to avoid damaging the muscle belly. Once dissected, a silk ligature is tied firmly to the distal tendon of the EDL, and the muscle tendon is cut near the retinaculum to eliminate severing or damaging

vascular beds within the distal portion of the muscle. Once the tendon is free, caution is taken to ensure the feed vessels, primarily the medial feed artery, vein, and associated nerve, are not damaged or stretched. These vessels maintain the blood flow supply to the muscle, and any damage to these can result in a decrease or lack of blood flow to the muscle. The animal is placed on the stage of an inverted microscope with the EDL muscle secured to the stage surface ensuring the length and orientation of the EDL is similar to that seen in *in situ* condition (Fraser et al., 2012b).

To achieve isolation from the atmosphere with the externalized muscle, the muscle is covered with an impermeable plastic film (e.g. polyvinylidene chloride, Saran), a standard glass coverslip secured with vacuum grease, and a standard glass slide with vacuum grease on top of the coverslip to improve optical coherence and provide slight compression across the muscle while also eliminating the need for superfusion solution (Fraser et al., 2012b). Transillumination of the muscle is achieved using an inverted microscope allowing vessels within the first 100 μm of the surface of the muscle to be visualized. This externalization of the EDL provides the same benefits as previously mentioned. However, it also allows for transillumination of the muscle for visualization and recording of microvascular networks enabling quantification of capillary hemodynamic and RBC oxygen saturation (sO_2). The EDL can be reflected onto a variety of surfaces for simultaneous manipulation and observation of blood flow regulation in response to physical or chemical manipulation (Fraser et al., 2012b). Typically, a glass coverslip is used, thus isolating the muscle from the atmosphere and limiting direct interactions via intravascular injection. This preparation has also been adapted for the development and use of a gas exchange chamber paired with micro-outlets of various

sizes capable of local gas manipulation (Ghonaim et al., 2013). The characteristics of the EDL provides a promising platform for the development of other techniques including a microfluidic device to manipulate a microscale region of tissue to study blood flow regulation.

Unique preparations for IVVM of muscles have advantages and disadvantages. Superfusion preparations provide researchers with the opportunity to administer doses of pharmacological agents to the surface of the muscle, allowing for some spatial localization beyond that which can be achieved through intravascular administration. However, the superfusion preparation, results in the muscle being exposed to room air, as well as subjects the tissue to being continuously washed in a bicarbonate buffered solution for extended periods of time. This preparation also has limitations when administering drugs to a spatially specific site due to the flow of the superfusion solution across the muscle. Isolation preparations do not require the use of a bicarbonate buffered solution to maintain the muscle, but rather protects the tissue from the atmosphere to avoid drying out the muscle. As a result, this preparation has comparatively few methods to interact with the underlying vasculature. These approaches include intravascular injections of agents which limits the ability to administer to a spatially specific location, and gas perturbations that can be imposed using custom built gas based microfluidic devices.

1.3. Intravital Video Microscopy

The use of IVVM is a common technique used to visualize the microcirculation and quantify microvascular blood flow *in vivo*. IVVM imaging systems allow for direct observation of microvessels in a way that other imaging technologies are unable to provide. The optical resolution of IVVM systems is necessary for making fine measurements on discrete vessels and complete networks in an intact tissue. Along with the ability to directly observe the microcirculation *in vivo*, recording microscopic fields for offline analysis is highly valuable. The optical resolution and high frame rates of digital cameras in modern IVVM setups are particularly advantageous for measuring vascular geometries, hemodynamics, and capillary RBC O_2 saturation (Ellis et al., 1992; Japee et al., 2004; Fraser et al., 2012a).

The following characteristics of intravital imaging systems make them well suited for studying blood flow in capillary networks. Flowing capillaries within an intravital field are focused upon during video capture, ensuring that in focus capillary segments are well defined with clearly resolved red cells. Recorded sequences of capillary blood flow can then be processed offline to generate functional images through a series of mathematical transformations (Japee et al., 2004). Generation of functional images from intravital sequences aids in the identification of discrete vessel segments for further analysis. Fundamentally, a video sequence is composed of a series of individual still images, or frames (Figure 1.1, Panel A), each of which is defined as an array of pixel values, representing the light intensities detected spatially across the field by the camera. Calculations performed at each pixel location over the duration of a captured video

sequence are then used to create various functional images. For example, a mean functional image (*M)* is generated by calculating the arithmetic mean of pixel intensities (*I*) from the first to the *N*th frame in a sequence at each individual pixel location (*x,y*), and an image is constructed from the resulting values as follows (Japee et al., 2004):

$$M(x,y) = \frac{1}{N}\sum_{i=1}^{N} I_i(x,y)$$

The equations used for generation of other functional images including max, min, and variance images has been previously described (Japee et al., 2004). Generation of various functional images that provide high contrast between vessels and surrounding tissue allow for mathematical determination of vessel locations within an intravital field. Sum of absolute difference (SAD) functional images were employed for this purpose in the present thesis and are defined by:

$$SAD(x,y) = \frac{1}{N}\sum_{i=2}^{N} |I_{i-1}(x,y) - I_i(x,y)|$$

Flowing capillaries including those with RBCs and plasma gaps visually appear brighter in the SAD functional images compared the surrounding tissue due to the variation in light intensity between series of frames (Figure 1.1, Panel B). These steep gradients in pixel intensity allow for semi-automated edge detection algorithms to delineate the geometry of individual capillary segments and describe the centerline along the vessel (Fraser et al., 2012a). Selection of in focus vessels using this method is necessary for quantitative hemodynamic and sO_2 measurements. Such functional images eliminate uncertainty during selection, ensuring values from analysis algorithms are accurate and consistent.

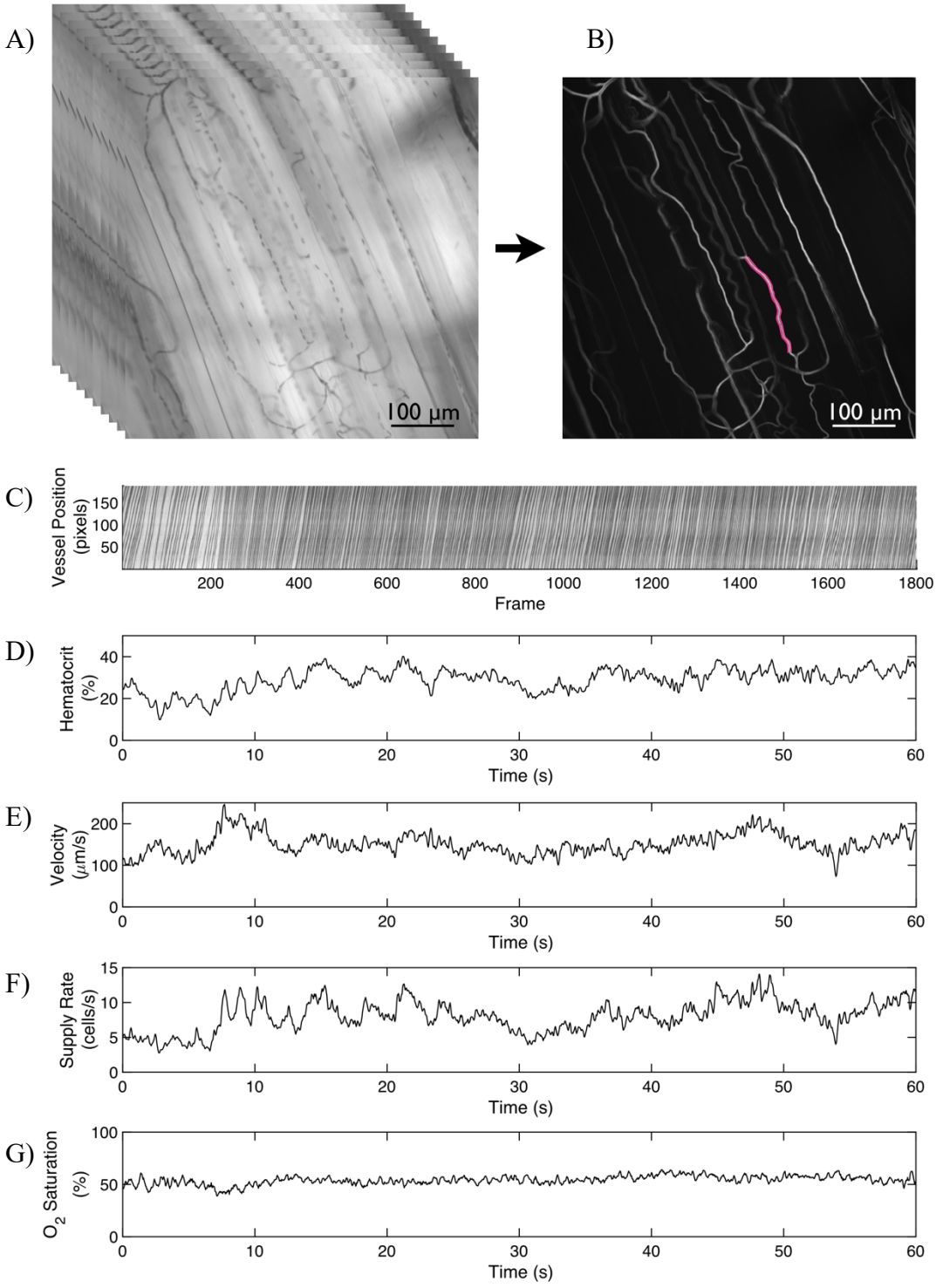
A)
B)
100 µm
100 µm
C)
Vessel Position (pixels)
150
100
50
200
400
600
800
1000
1200
1400
1600
1800
Frame
D)
Hematocrit (%)
40
20
0
0
10
20
30
40
50
60
Time (s)
E)
Velocity (µm/s)
200
100
0
0
10
20
30
40
50
60
Time (s)
F)
Supply Rate (cells/s)
15
10
5
0
0
10
20
30
40
50
60
Time (s)
G)
O2 Saturation (%)
100
50
0
0
10
20
30
40
50
60
Time (s)

Figure 1.1 Single vessel offline analysis for quantification of capillary hemodynamics. A) 10 frames of a ten times magnification intravital video microscopy recording of extensor digitorum longus muscle (every 200th frame over a one minute capture is shown) and B) MATLAB generated sum of absolute difference image (pink highlight) shows a single traced in focus capillary segment with single file red blood cell flow as an example. C) Space-time image of individual pixel intensity fluctuations along the centerline of the highlighted vessel with time, in frames, on the x-axis and distance on the y-axis. Hemodynamic and oxygen saturation measurements of panel C space-time image showing D) capillary hematocrit (%), E) red blood cell velocity (μm/s), F) red blood cell supply rate (cells/s), and G) red blood cell O_2 saturation (%).

Hemodynamic measurements are made using the same video sequences (Figure 1.1, Panel A) used to construct functional images from intravital microscopy recordings (Figure 1.1, Panel B). The passage of RBCs through capillaries causes fluctuating changes in light intensity due to cells being interspersed with plasma gaps. Space-time images (STI) (Figure 1.1, Panel C) are generated to trace these fluctuations along the centerline of a selected vessel resulting in an image structure with time on the x-axis and distance along the vessel centreline on the y-axis (Ellis et al., 1992). The location of the red cell is mapped both along the position in the vessel (space) and throughout the sequence of the recording (time) (Figure 1.1, Panel C). STIs provide the basis for the measurement of velocity of each red cell throughout the recorded sequence (Figure 1.1, Panel E). Lineal density is also measured from selected vessel segments to determine the density, or number of RBCs along a capillary per millimeter of vessel. RBC supply rate is the number of cells passing through the capillary per unit time, calculated as a product of velocity and lineal density, and reported in cells per second (Figure 1.1, Panel F). Lastly, tube hematocrit of the vessel segment is calculated from the measured lineal density, vessel volume, and the average volume of RBCs (Figure 1.1, Panel D). Hemodynamic values including velocity, supply rate, and lineal density allow for the quantification of RBC flux, and blood flow within a given IVVM recording field.

IVVM recording of capillaries at two wavelengths allows for the determination of RBC sO_2 within capillaries due to the differential light absorption of oxy- and deoxyhemoglobin (Figure 1.2). The selected wavelengths include one isosbestic wavelength and one oxygen-dependent wavelength for spectrophotometric measurement of sO_2 (Ellis et al., 1990). The light absorption by red cells with the isosbestic wavelength (e.g. 450 or 420 nm) is insensitive to a change in hemoglobin sO_2 as the molar extinction coefficient for both oxy- and deoxyhemoglobin is the same (Figure 1.2). However, the second wavelength used, the oxygen-dependent wavelength (e.g. 438 nm) is dependent on the oxygen-saturation of hemoglobin and therefore is sensitive to the relative concentrations of oxy- and deoxyhemoglobin within the red cell. Optical density, an effective surrogate for light absorption, is determined by using the incident light intensity of a plasma gap when no red cells are present and the light intensity of a red cell (Figure 1.1, Panel G). sO_2 measurements are based on the ratio of optical densities of the oxygen-dependent wavelength and the isosbestic wavelength. The ratio of the optical density at the two wavelengths and the oxygen-saturation of hemoglobin is linearly related, allowing for the spectrophotometric analysis of hemoglobin concentration, as per the Lambert-Beer's law, and adjusted via an *in vivo* calibration (Ellsworth et al., 1987; Ellis et al., 1990). The imaging system used to collect the experimental data set in this thesis (outlined in chapter 2) applies these principles which also relate to the process for hemodynamic measurements as described above. The EDL is well suited for the application of these approaches to study capillary geometry, blood flow, regulation, and sO_2 using the IVVM system described in chapter 2.

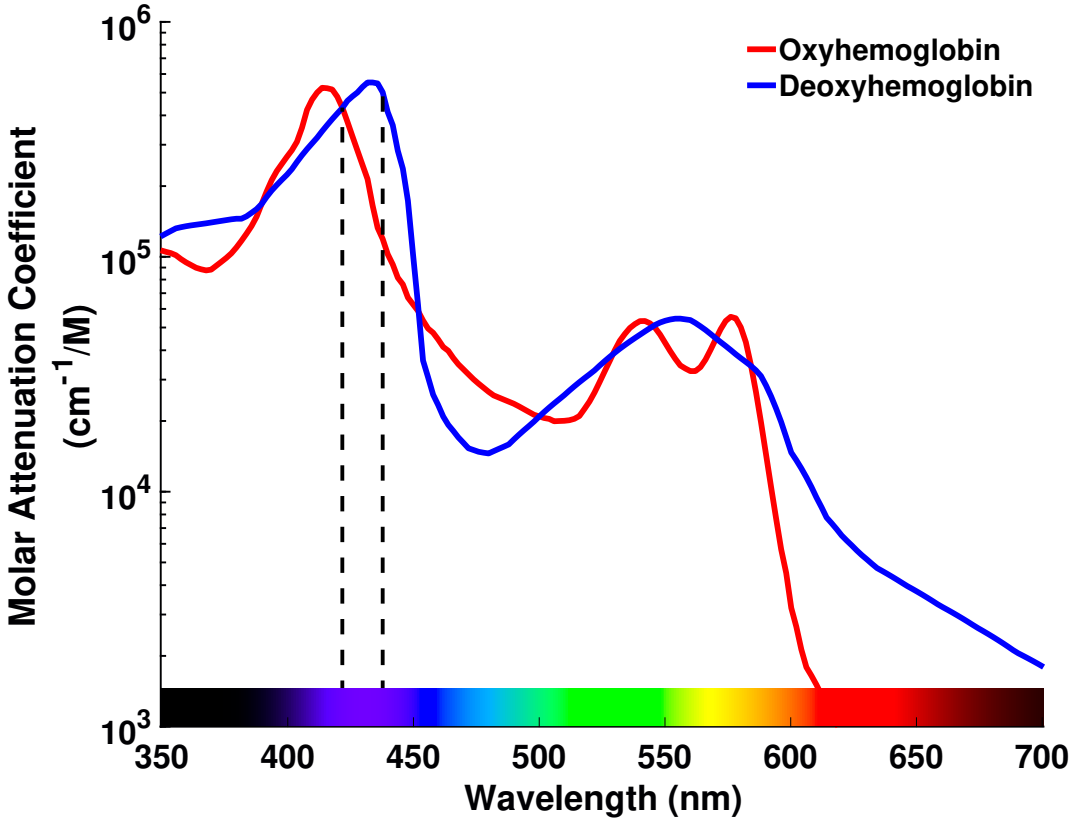

Figure 1.2 Molar attenuation curves for oxyhemoglobin and deoxyhemoglobin. Isosbestic (420 nm) and oxygen-dependent wavelength (438 nm) indicated with dotted lines. Colour bar provides a visual reference for the spectral wavelengths indicated on the x axis. Figure was generated with data from Prahl (1999) and visual representation was based on Fraser (2012) (Prahl, 1999; Fraser, 2012).

1.4. Microfluidic Device Uses

Microfluidic devices refer to the techniques and technology that can be used for the precise control and manipulation of small fluid volumes in a micro-delivery system. The ability for researchers to manipulate and simulate environments on handheld devices has been used in many fields including engineering, microbiology, bioengineering and developmental biology. The development of devices to manipulate small volume fluid flow within microenvironments is beneficial in many ways including accessibility, cost-effective tests and the ability to minimize reagents required for testing (Xia & Whitesides, 1998). Rapid prototyping of microfluidic devices has also increased the accessibility to use microfluidics in a variety of disciplines. Methods for development and fabrication of microfluidic devices has expanded since the conceptualization of microfluidic devices (Xia & Whitesides, 1998; Lathrop, 2013).

As the ubiquity of microfluidic devices increases, the methods to develop and fabricate these devices range from simple to complex. The first methods to fabricate device channels through photolithography and micromachining were accomplished using oxidized silicone and glass. Fabricating devices from glass and oxidized silicone is time consuming, difficult, and expensive to mold and form custom designed channels. The ability to manipulate and modify microfluidic channels was a desirable feature. To circumvent this problem, plastics and elastomers, including polydimethylsiloxane (PDMS), were introduced for rapid prototyping. PDMS allows for the rapid prototyping that is highly desirable when developing microfluidic devices for novel applications.

Use of PDMS and similar elastomers has enabled the rapid development of microfluidic devices. Microfluidic devices usually involve fluid volumes from picolitres to microlitres. Flow conditions within microfluidics are typically highly laminar (with a Reynolds number under 2000) i.e. particles flow past the layers surrounding them in the absence of lateral mixing, and fluid flows orderly through the device without forming vortices or irregular flow patterns (Kjeang et al., 2009). Velocity is consistent within discrete layers. However, the flow near the walls moves at a lower velocity than the flow at the center. Indeed, it is reasonable to assume a no-slip condition at the wall of a microfluidic flow channel, which assumes that at the wall the flow velocity will be zero. This allows the delivery of solute in a fluid within the device to be reproduced consistently due to the properties of laminar flow.

The use of microfluidic devices has expanded across many disciplines allowing researchers to manipulate and modify existing technologies for desired uses. Some of the current common uses of microfluidic devices in industry, clinical practice, and research include point of care diagnostics, drug discovery, and lab-on-a-chip devices. Specialized features are often integrated into devices to facilitate specific ends such as implementation of a screw valve to control the fluid flow from one channel to another (Fang et al., 2012). Another example of implementation of specialized features occur in drug discovery to improve the speed and associated high cost. The development of high throughput microfluidic devices has replaced previously used methods which relied on higher volumes of fluid, and overall longer periods of time to determine if the pharmacological agent was targeting the appropriate receptor (Dittrich & Manz, 2006). A key aspect in the use of microfluidics in drug discovery is the ability to simultaneously

impose manipulation at the cellular level while also replicating physiologically relevant conditions. Microfluidic devices have been developed to be used to study the effects a compound of interest has on cellular signalling and chemotactic cell migration (Wu et al., 2018).

Commercialized lab-on-a-chip technologies are used in clinical settings and research environments for on demand blood analysis. Testing a sample of blood with an i-STAT handheld device has become common practice, requiring only 50 - 100 µL of blood and 2 minutes to perform multiple tests simultaneously ("Abaxis | Better at Point of Care," 2019). These commercial devices are made of a plastic polymer that is fashioned into a disposable cartridge to measure the blood sample's gas partial pressures, lactate levels, O_2 saturation, and electrolytes. The commercialization of lab-on-a-chip technology has improved the accessibility to receive on demand blood gas analysis using handheld diagnostic tools. These devices have specialized aspects which are used in unique ways depending on their intended application. Common techniques can be applied to many different areas of specialization depending on the intended use of the device.

While microfluidic devices have been used in many *in vitro* applications, the ability to interact with an intact organism has enormous potential to increase the impact on several fields of study. For example, the use of microfluidics for interrogation into active neuronal migration in Drosophila was one of the first *in vivo* microfluidic techniques to be described (van Giesen et al., 2016). This PDMS microfluidic device, molded using a master mold with a 300 µm deep channel, can expose neuronal cell bodies to chemicals of interest while simultaneously imaging the resulting neuronal activity (van Giesen et al., 2016). This preparation has been used to study the response of

thermosensitive cells to a change in microfluidic fluid temperature. The technique is advantageous as the recording of cellular activity in response to thermal and chemical cues can now be done at the organism level in Drosophila larvae. Refinement of this device and progression of the technique to include adult larvae for the manipulation of sensory neurons as well as other signalling processes could be advantageous to better understand developmental processes and neuronal signalling. Use of microfluidics in this system enables the controlled chemical and thermal interaction in a constrained region of an organism to study the responses to stimuli in the intact system of a living organism. The constrained area of effect is due to the ability for microfluidic devices to manipulate small volumes in a specific manner over and to a specific region.

As the use of microfluidic devices slowly expands into organism based *in vivo* work, the interest of using devices to refine *in vivo* preparations has become appealing yet remains particularly challenging to implement. As such, proposals of device development have been limited. One such proposed idea involves the use of a skin fold chamber for drug delivery to mice with simultaneous visualization of the surrounding area (Myneni et al., 2014). The conceptual design of this microfluidic device includes a skin fold chamber with a channel etched into a glass portion that isolates the desired area from the atmosphere. Designing the microfluidic in glass would be favorable as the ability to clean and flush the device between uses without the potential of damaging the channel is improved. Once the device is in place, perfusion fluid would be pumped into the microfluidic device such that administration can be targeted to the area of interest. A major advantage to using microfluidics in conjunction with IVVM is the ability to target delivery to a localized area of the tissue and directly observe and record the response.

Simultaneous manipulation of cell signalling through administration with prolonged periods of observation are of value when considering the roles of any interrogation has on the integrated nature of a living system. At the time of writing, this microfluidic device concept has not been used in any scientific study. Manipulation of *in vivo* tissues with a microfluidic device is challenging as the techniques of fluid manipulation cannot be applied when interfacing with tissue (i.e. increasing the pressure exerted on the tissue to drive fluid).

Manipulations of local tissue microenvironments *in vivo* have been pursued using various techniques. Gas based microfluidic devices have been developed to dynamically deliver specific gas concentrations to the surface of a skeletal muscle in order to manipulate blood flow in localized areas (Ghonaim et al., 2011). This microfluidic device is designed to accommodate a gasket between a coverslip and the upper channel covering. The gasket provides a space for the gas to travel from inlet to the gas permeable exchange membrane and to the outlet. Spatially confined perturbations within the tissue can be made using the gas based device using micro-outlets of varying dimensions (1000 x 200 μm, 100 μm in diameter). A proof of concept to alter spatially confined regions of tissue allowed for the progression of the refinement of the technique to manipulate gas conditions within the tissue. Although the gas based microfluidic elicits a strong stimulus for blood flow control to the area, the manipulations are limited to only changes in gas concentrations with no way to use non-gaseous stimuli.

1.5. Fabrication Techniques

Microfluidic device fabrication techniques have been evolving since the advent of the use of microfluidic devices in areas beyond microelectronics. The most common methods used to fabricate microfluidic devices include soft lithography and photolithography. Both of these general techniques have advantages and disadvantages associated with them including the ability to generate structures at micrometer vs nanometer scale, the cost and time associated with generation, and the accessibility of the techniques to a wide range of practitioners.

Device fabricators prototype a variety of similar devices to test the effectiveness, efficiency, and reliability of each device model to determine which design best suits the application. Soft lithography is the most cost-effective method to generate microfluidic devices as it involves the use of inexpensive elastomers to form the desired structures of devices (Taggart & Wray, 1998). Generation of devices using soft lithography techniques consists of using structures that form the desired channel pattern of the microfluidic device (Xia & Whitesides, 1998; Rogers & Nuzzo, 2005). Since structures do not need to be planar, soft lithography can accommodate a wider range of patterned structures. Structure formation has included the use of polyvinyl adhesive tape, three-dimensional (3D) printed structures, and wax. However, features can be generated using any substance that is able to produce well defined shapes and structures (Rogers & Nuzzo, 2005). The flexibility in generating a range of surface features improves the cost effectiveness of device fabrication for soft lithography. Researchers are able to generate microfluidic

devices quickly for prototyping at low cost by using soft lithography and because of this, soft lithography has increased in popularity over the past several decades.

Photolithography has been a standard fabrication technique in microelectronic circuit fabrication since the 1950's (Lathrop, 2013). Photolithography involves generating a master mold for device molding followed by the use of an elastomer to generate a device (Gale et al., 2018). Briefly, to generate a master mold, a layer of photoresist resin, such as Bisphenol A Novolac epoxy, is spun coat onto a pre-cleaned silicon-coated wafer. A mask with corresponding device pattern cut-out is placed between the wafer and light source inhibiting light from reaching the photoresist layer. Upon exposure to the light, a reaction occurs solidifying the exposed photoresist, and the unexposed soluble photoresist is removed. The underlying exposed silicon and the remaining photoresist layer is then chemically removed. Following this removal the chip is then coated in silicon dioxide. Additional layers with varying patterns can be layered onto this mold to generate the desired master mold. The silicon layer beneath each layer of the cured photoresist will form the boundaries of the resulting master mold. This technique is beneficial when designing structures to nanometer precision. However, this process is very time consuming and also expensive due to the clean room facilities and specialized equipment required to generate high quality master molds using photolithography.

The development and improvement of fabrication processes to generate microfluidic devices has increased the accessibility of microfluidic device modification by users who are new to these techniques. Cost effective strategies have enabled users to develop and prototype devices quickly and efficiently allowing for the expansion of microfluidic device uses into many fields and a variety of preparations from

microenvironment manipulation in cell culture to manipulation of *in vivo* tissues, such as determining mechanisms associated with blood flow regulation.

1.6. Blood Flow Regulation

Blood flow to organs is regulated to match the nutritive requirements of each tissue, particularly in response to changing metabolic demand. This distribution is constrained by the overall capacity of the cardiovascular system and the relative needs amongst tissues. An example of this regulation is the fight or flight response, where increased demand for blood flow to working muscle results in decreased blood supply to the digestive system and renal systems due to increased sympathetic activity in resistance vessels (Gordan et al., 2015). Similarly, blood flow distribution within a tissue is heterogeneous as the demand for O_2 and nutrients fluctuates between capillary networks and the tissue surrounding them. This blood flow regulation is controlled at various levels of vasculature from high order arterioles to terminal arterioles. The regulation of blood flow can be achieved through fine spatial regulation and regulating vascular tone of arterioles.

Fine spatial regulation of blood flow within capillary networks had once been thought to be due to the action of precapillary sphincters, rings of smooth muscle at the arteriolar end of capillaries, and metarterioles, which act as a thoroughfare for shunting blood to areas in need. Zweifach and colleagues were first to illustrate the presence of precapillary sphincters and metarterioles based on observations made within the mesenteric microcirculation of rats (Zweifach et al., 1953). It was proposed that the regulation of blood flow between capillaries is regulated by the constriction and

relaxation of precapillary sphincters located along the arterioles (Zweifach et al., 1953). However, studies on other tissues have shown that the presence of precapillary sphincters and metarterioles is not ubiquitous. Muscle, for example, has neither metarterioles nor precapillary sphincters as defined by Zweifach and colleagues (Klitzman & Johnson, 1982). The occurrence of precapillary sphincters and metarterioles has remained a topic of debate amongst microvascular researchers since Krogh's first proposal of these structures as flow controllers (Krogh, 1919; Poole et al., 2013). Indeed, description of these structures is common in most physiology textbooks, which regularly suggest they are a ubiquitous feature of all tissues (Sakai & Hosoyamada, 2013). It is now understood that the distribution of blood flow within individual capillary networks within skeletal muscle depends on the vascular tone of the terminal arteriole and passive rheological factors (Pries et al., 1996) rather than precapillary sphincters. Although precapillary sphincters do not control the supply of blood flow to individual capillaries, the capillaries are thought to contribute to blood flow regulation through conducted signalling. The ability to regulate blood flow from arterioles to capillary networks relies on the communication of vasoconstriction and vasodilation stimuli to upstream vessels in response to transient changes in local metabolic demand.

Vascular tone is the state of arteries and arterioles under basal conditions with a partial constriction of vascular smooth muscle cells. This partial constriction maintains the vessel in a state where vessels are neither fully contracted nor dilated. This state allows vessels to increase or decrease in diameter based on signals from various sources. Resting vascular tone is accomplished through the partial constriction of the vascular smooth muscle cells that control arteriolar diameter and thereby modulate blood flow

through vasodilation and vasoconstriction. To establish this control there are several mechanisms that maintain vessels within a functional range. These inputs on resting tone include extrinsic factors such as autonomic nerve activity (Buckwalter & Clifford, 2001), and intrinsic factors including myogenic and biochemical stimuli (Sandoo et al., 2010). Under normotensive conditions, changes in blood flow to capillary networks ostensibly rely on the dynamic modulation of arteriolar vascular tone.

Regulation of arteriolar tone is partially achieved through the sympathetic innervation of arterioles. Extrinsic sympathetic nerve activity in skeletal muscle can lead to vasoconstriction through the release of norepinephrine (NE) from postganglionic sympathetic nerve fibers that binds to α_1- and α_2-adrenergic receptors on arterioles and the α_2-adrenergic receptors on terminal arterioles (Buckwalter & Clifford, 2001). NE can also bind to postsynaptic β_2-adrenergic receptors leading to vasodilation, or to presynaptic α_2 receptors on the postganglionic sympathetic nerve to inhibit the release of NE. Sympathetic stimulation can lead to either dilation or constriction because of these opposing interactions on the post ganglionic nerve and arterioles.

Intrinsic mechanisms that act on vascular tone arise from several different sources including myogenic and biochemical or metabolic mechanisms. Myogenic mechanisms that control vascular tone regulation occur in response to a change in transmural pressure within the vessel, causing it to stretch leading to constriction of the vessel (Davis & Hill, 1999). Biochemical mechanisms associated with blood flow regulation and vascular tone include nitric oxide, prostacyclin (PGI_2), endothelium derived hyperpolarizing factor, endothelin-1 (ET-1), and thromboxane. These mechanisms act on vascular smooth muscle cells surrounding arterioles to regulate the dilation and constriction of vessels

(Sandoo et al., 2010). The release of the former 3 molecules stimulate vasodilation whereas the latter two lead to vasoconstriction.

Nitric oxide (NO), one of the most potent endothelial derived vasodilators, is produced through the endothelial nitric oxide synthase (eNOS) pathway. An increase in intracellular Ca^{2+} allows Ca^{2+} to bind to calmodulin that can bind to eNOS. In the presence of eNOS, L-arginine, NADPH, and O_2 are metabolized into L-citrulline, NADP, and NO (Sandoo et al., 2010; Madigan & Zuckerbraun, 2013). NO is produced and acts on the vascular smooth muscle cells of arterioles, activating guanylate cyclase responsible for converting guanosine triphosphate to cyclic guanosine monophosphate (cGMP) (Madigan & Zuckerbraun, 2013). This leads to a decrease in intracellular Ca^{2+} and myosin light chain kinase activity within smooth muscle cells resulting in relaxation and thus, vasodilation of the blood vessel (Sandoo et al., 2010).

Another mechanism regulating vascular tone is the production of PGI_2 and thromboxane. PGI_2 and thromboxane are produced by the cyclooxygenase-1 (COX-1) and cyclooxygenase-2 (COX-2) enzymes (Wong et al., 2010). COX-1 and COX-2 enzymes are expressed in all endothelial cells and damaged endothelial cells, respectively, and are responsible for the conversion of arachidonic acid to prostaglandin H_2 (PGH_2). PGI_2 is produced in damaged endothelial cells from PGH_2 with prostacyclin synthase. Additionally, PGI_2 binds to the prostaglandin I_2 G protein coupled receptor on smooth muscle cells activating adenylate cyclase, thereby increasing the production of cyclic adenosine monophosphate. Thromboxane is produced in all endothelial cells from PGH_2 by thromboxane synthase. Thromboxane A_2 acts on the thromboxane receptor of smooth muscle cells and increases the intracellular calcium concentration to cause

vasoconstriction of the arterioles. These opposing mechanisms act to ensure resting tone of vessels is sustained and to regulate blood flow to areas downstream.

ET-1, a vasoconstrictor, is released from the endothelial cells after being produced by endothelin converting enzyme (La & Reid, 1995). Briefly, ET-1 binds to ET-B1 receptors on endothelial cells resulting in vasodilation due to the release of NO and PGI2 as previously described. However, ET-1 further binds to the ETA and ET-B2 that are coupled to a Gq-protein on vascular smooth muscle cells (Unic et al., 2011). This pathway is responsible for the conversion of phosphatidylinositol-4-phosphate to inositol trisphosphate (IP_3), which leads to an increase in intracellular calcium from the sarcoplasmic reticulum leading to vasoconstriction (Bouallegue et al., 2007). Therefore, ET-1 can act as both vasoconstrictor and vasodilator depending on the local physiological conditions of the vessel and tissue. These regulators of vascular tone are important as the regulation of blood flow within a tissue relies on the ability to vasoconstrict and vasodilate the upstream arterioles.

1.7. Conducted Signalling

In addition to local stimuli that can influence arteriolar tone, vessels are capable of propagating a stimulus over a distance due to the electrical coupling among vascular smooth muscle and endothelial cells lining the vascular tree. Conducted signalling along the microvascular tree is suggested as a mechanism for regulating blood flow to vessels downstream based on capillary signalling. Conducted signalling consists of electrical transmission of signals from vessels at a distance for control of the vascular tone and overall blood flow. This signal is sustained until the origin of the stimulus is remediated.

Electrical stimuli are generated by altering the membrane potential from the resting membrane voltage (Bagher & Segal, 2011b; Welsh et al., 2018). This alteration is accomplished by the movement of ions through channels resulting in a change in membrane potential. The efflux of K^+ in response to increased intracellular Ca^{2+} produces hyperpolarization which is spread between endothelial cells through gap junctions. The electrical signal is spread through alteration of the membrane potential via activation of ion channels which are responsible for forming transmembrane gradients. Conducted signals are thought to spread along the endothelial wall through electrical coupling via gap junctions between endothelial cells, between smooth muscle cells, and between endothelial cells and smooth muscle cells (Segal & Duling, 1989).

Conducted dilation in arteries was previously described in several preparations including rodent and cat femoral artery (Lutz et al., 1950; Hilton, 1959). Duling and Berne demonstrated the effect of conducted vasodilation up to 2 mm from the site of administration in the microcirculation in response to acetylcholine (ACh) application on the hamster cheek pouch (Duling & Berne, 1970). The resulting conducted vasodilation spread farther, up to 2 mm, as higher doses of ACh were applied. Previous work has demonstrated that the occlusion of the vessel did not impede the conduction of the signal (Segal & Duling, 1986). However, administration of a depolarizing solution, 137 mM KCl, resulted in conduction spreading to the point of KCl administration, but not beyond the treated area (Segal & Duling, 1989). Conduction was also impaired in vessel segments treated with 18α-glycyrrhetinic acid, a gap junction uncoupler (Yu et al., 2000).

Vasodilation signal conduction via the smooth muscle cells is spread via the K^+ influx through various channels including voltage gated, adenosine triphosphate (ATP)-

sensitive, Ca^{2+} activated, and inward rectifying K^{+} channels (Dora, 2017). These channels work together to generate cell-to-cell communication amongst the vascular smooth muscle cells to cause vasodilation both locally and along the vascular tree. Vasoconstriction conducted signalling in response to vasoconstrictors varies with the mechanism through which they act (Segal et al., 1999). Reports of conducted signalling of vasoconstriction in response to phenylephrine (PE) and NE differ across several tissue types as administration to cheek pouch results in a conducted signal. However, in hamster and mouse cremaster preparations there is no conducted response to PE, and in hamster retractor muscle there is no response to PE or NE (Welsh et al., 2018). This difference in reported signal conduction is thought to be based on differences in preparations, or due to differences in the innervation of different tissues (Segal et al., 1999; Welsh et al., 2018). Biphasic vasoactive effects in response to KCl have been observed and are dependent on the concentration of the dose applied as depolarization of smooth muscle cells leads to vasoconstriction and hyperpolarization of endothelial cells resulting in vasodilation (Dora, 2017).

In response to local administration, the conducted responses to vasoactive substances are due to the mechanisms through which the substances act (Delashaw & Duling, 1991). Conducted vasodilation can be triggered through the release of NO from vessels downstream that require a higher flow rate (Sandoo et al., 2010). The vasodilator substances discussed in Chapter 2 are ACh and ATP. When applied locally, ACh effects are mediated by binding to muscarinic receptors and through the ability of ACh to induce hyperpolarization through the endothelium-derived hyperpolarizing factor (EDHF). Binding of the muscarinic receptors leads to an increase in intracellular Ca^{2+}

concentration that binds to calmodulin. Ca^{2+} and calmodulin bind eNOS which activates eNOS to then increase the production of NO (Winter & Dora, 2007). Application of ATP also leads to a production of NO after binding to the purinergic G protein coupled receptors $P2X_4$, $P2Y_1$ and $P2Y_2$ on endothelial cells which leads to an increase in intracellular Ca^{2+} (Burnstock & Verkhratsky, 2010). ACh and NO have both local and conducted vasodilatory effects as the production of NO from endothelial cells leads to vascular smooth muscle cell relaxation due to increased cGMP. The conduction of vasodilation at a distance from the site of administration has been shown previously to correspond to the production of NO along endothelial cells. However, the administration of ACh may stimulate vasodilation through the EDHF pathway after inducing hyperpolarization when NO production is inhibited (Budel et al., 2003). The induced hyperpolarization originates in endothelial cells caused by an increase in intracellular Ca^{2+} (Clifford, 2004). The increase in intracellular Ca^{2+} in endothelial cells results in the hyperpolarization of vascular smooth muscle cells through gap junctions, or through an increase in activity of the Na^+-K^+-ATPase, or inward-rectifier potassium channels (Busse et al., 2002). Conducted dilation along the length of a vessel allows for signal to travel to larger vessels upstream that can control delivery of blood to an area that is being stimulated.

Conducted signalling for vasodilation from downstream vessels through NO release is common in the case of ACh and ATP. However, conducted signalling in response to vasoconstriction caused by PE application has not been well documented in the microcirculation. When applied, PE acts on the α_1-adrenergic receptor leading to constriction of smooth muscle cells (Brozovich et al., 2016). This occurs through the

increase in the phospholipase C pathway which increases IP_3 and leads to an increase in Ca^{2+} in smooth muscle cells. Vasoconstriction in response to PE is thought to occur locally, yet there is no conduction along the vascular tree (Bagher & Segal, 2011b).

Lastly, there remains the possibility that the RBCs themselves are involved in conducted signalling via their ability to serve as a sensor for O_2. Erythrocytes release several vasodilator molecules under low O_2 conditions including NO, S-nitrosothiols, and ATP (Helms et al., 2018). RBCs as a sensor would potentially play a role in vascular control due to the oxygen-saturation dependent release of ATP from RBCs at various O_2 levels. Fully saturated RBCs release ATP at a basal level, and as these cells desaturate, there is an increase in ATP release (Jagger et al., 2001). This increasing release of ATP acts on the endothelial cells through the $P2X_4$, $P2Y_1$ and $P2Y_2$ receptors resulting in vasodilation (Burnstock & Verkhratsky, 2010). O_2 sensing and blood flow regulation via the RBCs themselves would be an elegant mechanism to regulate flow to capillary networks via local and conducted signalling to upstream arterioles. There are some reports in the literature that suggests hemolysis under hypoxic conditions may contribute to the ATP release observed. However, ATP release has not been observed or documented to this extent *in vivo* and is due to release through a combination of mechanisms other than cell lysis (Mairbäurl et al., 2013; Sikora et al., 2014). Several factors play key roles in the control of blood flow including fine spatial control, regulation of vascular tone, and conducted signalling that result in a broader area of effect. These mechanisms of regulation work in tandem to modulate the delivery of blood to the tissues that require it.

References

Abaxis | Better at Point of Care. (2019). Retrieved from https://www.abaxis.com/veterinary/products/vetscan-iStat1

Bagher, P., & Segal, S. S. (2011a). The Mouse Cremaster Muscle Preparation for Intravital Imaging of the Microcirculation. *Journal of Visualized Experiments*(52). doi:10.3791/2874

Bagher, P., & Segal, S. S. (2011b). Regulation of blood flow in the microcirculation: role of conducted vasodilation. *Acta Physiologica (Oxford, England), 202*(3), 271-284. doi:10.1111/j.1748-1716.2010.02244.x

Bearden, S. E., Payne, G. W., Chisty, A., & Segal, S. S. (2004). Arteriolar network architecture and vasomotor function with ageing in mouse gluteus maximus muscle. *The Journal of Physiology, 561*(2), 535-545. doi:10.1113/jphysiol.2004.068262

Bosetti, F., Galis, Z. S., Bynoe, M. S., Charette, M., Cipolla, M. J., del Zoppo, G. J., . . . Zlokovic, B. V. (2016). "Small Blood Vessels: Big Health Problems?": Scientific Recommendations of the National Institutes of Health Workshop. *Journal of the American Heart Association, 5*(11), 657-612. doi:10.1161/JAHA.116.004389

Bouallegue, A., Daou, G. B., & Srivastava, A. K. (2007). Endothelin-1-induced signaling pathways in vascular smooth muscle cells. *Current Vascular Pharmacology, 5*(1), 45-52.

Brozovich, F. V., Nicholson, C. J., Degen, C. V., Gao, Y. Z., Aggarwal, M., & Morgan, K. G. (2016). Mechanisms of Vascular Smooth Muscle Contraction and the Basis for Pharmacologic Treatment of Smooth Muscle Disorders. *Pharmacological Reviews, 68*(2), 476-532. doi:10.1124/pr.115.010652

Buckwalter, J. B., & Clifford, P. S. (2001). The paradox of sympathetic vasoconstriction in exercising skeletal muscle. *Exercise and Sport Sciences Reviews, 29*(4), 159-163.

Budel, S., Bartlett, I. S., & Segal, S. S. (2003). Homocellular conduction along endothelium and smooth muscle of arterioles in hamster cheek pouch: unmasking an NO wave. *Circulation Research, 93*(1), 61-68. doi:10.1161/01.RES.0000080318.81205.FD

Burnstock, G., & Verkhratsky, A. (2010). Long-term (trophic) purinergic signalling: purinoceptors control cell proliferation, differentiation and death. *Cell Death and Disease, 1*(1), e9-e9. doi:10.1038/cddis.2009.11

Busse, R., Edwards, G., Félétou, M., Fleming, I., Vanhoutte, P. M., & Weston, A. H. (2002). EDHF: bringing the concepts together. *Trends in Pharmacological Sciences, 23*(8), 374-380. doi:10.1016/s0165-6147(02)02050-3

Charter, M. E., Lamb, I. R., & Murrant, C. L. (2018). Arteriolar and capillary responses to CO2 and H+ in hamster skeletal muscle microvasculature: Implications for active hyperemia. *Microcirculation (New York, N.Y. : 1994), 25*(7), e12494. doi:10.1111/micc.12494

Clifford, P. S., & Hellsten, Y. (2004). Vasodilatory mechanisms in contracting skeletal muscle. *Journal of Applied Physiology, 97*(1), 393-403. doi:10.1152/japplphysiol.00179.2004

Davis, M. J., & Hill, M. A. (1999). Signaling mechanisms underlying the vascular myogenic response. *Physiological Reviews, 79*(2), 387-423. doi:10.1152/physrev.1999.79.2.387

Delashaw, J. B., & Duling, B. R. (1991). Heterogeneity in conducted arteriolar vasomotor response is agonist dependent. *The American Journal of Physiology, 260*(4 Pt 2), H1276-1282. doi:10.1152/ajpheart.1991.260.4.H1276

Dittrich, P. S., & Manz, A. (2006). Lab-on-a-chip: microfluidics in drug discovery. *Nature Reviews Drug Discovery, 5*(3), 210-218. doi:10.1038/nrd1985

Dixon, J. B., Zawieja, D. C., Gashev, A. A., & Coté, G. L. (2005). Measuring microlymphatic flow using fast video microscopy. *Journal of Biomedical Optics, 10*(6), 064016. doi:10.1117/1.2135791

Dora, K. A. (2017). Conducted dilatation to ATP and K+ in rat skeletal muscle arterioles. *Acta Physiologica (Oxford, England), 219*(1), 202-218. doi:10.1111/apha.12656

Duling, B. R., & Berne, R. M. (1970). Propagated vasodilation in the microcirculation of the hamster cheek pouch. *Circulation Research, 26*(2), 163-170. doi:10.1161/01.RES.26.2.163

Ellis, C. G., Ellsworth, M. L., & Pittman, R. N. (1990). Determination of red blood cell oxygenation in vivo by dual video densitometric image analysis. *The American Journal of Physiology, 258*(4 Pt 2), H1216-1223. doi:10.1152/ajpheart.1990.258.4.H1216

Ellis, C. G., Ellsworth, M. L., Pittman, R. N., & Burgess, W. L. (1992). Application of image analysis for evaluation of red blood cell dynamics in capillaries. *Microvascular Research, 44*(2), 214-225. doi:10.1016/0026-2862(92)90081-Y

Ellsworth, M. L., & Pittman, R. N. (1986). Videodensitometric determination of oxyhemoglobin saturation (SO2) in muscle capillaries. *Advances in Experimental Medicine and Biology, 200*(Chapter 1), 1-11. doi:10.1007/978-1-4684-5188-7_1

Ellsworth, M. L., Pittman, R. N., & Ellis, C. G. (1987). Measurement of hemoglobin oxygen saturation in capillaries. *The American Journal of Physiology, 252*(5 Pt 2), H1031-1040. doi:10.1152/ajpheart.1987.252.5.H1031

Fang, X., Chen, H., Xu, L., Jiang, X., Wu, W., & Kong, J. (2012). A portable and integrated nucleic acid amplification microfluidic chip for identifying bacteria. *Lab on a Chip, 12*(8), 1495-1499. doi:10.1039/c2lc40055c

Ferrer, M., Martin-Jaular, L., Calvo, M., & del Portillo, H. A. (2012). Intravital microscopy of the spleen: quantitative analysis of parasite mobility and blood flow. *Journal of Visualized Experiments : JoVE*(59), e3609. doi:10.3791/3609

Fox, R. J., & Frame, M. D. (2002). Regulation of flow and wall shear stress in arteriolar networks of the hamster cheek pouch. *Journal of Applied Physiology (Bethesda, Md. : 1985), 92*(5), 2080-2088. doi:10.1152/japplphysiol.00984.2001

Fraser, G. M. (2012). Modeling Oxygen Transport in Three-Dimensional Capillary Networks.

Fraser, G. M., Goldman, D., & Ellis, C. G. (2012a). Microvascular flow modeling using in vivo hemodynamic measurements in reconstructed 3D capillary networks.

Microcirculation (New York, N.Y. : 1994), 19(6), 510-520. doi:10.1111/j.1549-8719.2012.00178.x

Fraser, G. M., Milkovich, S., Goldman, D., & Ellis, C. G. (2012b). Mapping 3-D functional capillary geometry in rat skeletal muscle in vivo. *American Journal of Physiology. Heart and Circulatory Physiology, 302*(3), H654-664. doi:10.1152/ajpheart.01185.2010

Gale, B., Jafek, A., Lambert, C., Goenner, B., Moghimifam, H., Nze, U., & Kamarapu, S. (2018). A Review of Current Methods in Microfluidic Device Fabrication and Future Commercialization Prospects. *Inventions, 3*(3), 60-25. doi:10.3390/inventions3030060

Ghonaim, N. W., Fraser, G. M., Ellis, C. G., Yang, J., & Goldman, D. (2013). Modeling steady state SO2-dependent changes in capillary ATP concentration using novel O2 micro-delivery methods. *Frontiers in Physiology, 4*, 260. doi:10.3389/fphys.2013.00260

Ghonaim, N. W., Lau, L. W. M., Goldman, D., Ellis, C. G., & Yang, J. (2011). A micro-delivery approach for studying microvascular responses to localized oxygen delivery. *Microcirculation (New York, N.Y. : 1994), 18*(8), 646-654. doi:10.1111/j.1549-8719.2011.00132.x

Gordan, R., Gwathmey, J. K., & Xie, L.-H. (2015). Autonomic and endocrine control of cardiovascular function. *World Journal of Cardiology, 7*(4), 204-214. doi:10.4330/wjc.v7.i4.204

Grant, R. T. (1964). Direct Observation Of Skeletal Muscle Blood Vessels (Rat Cremaster). *The Journal of Physiology, 172*(1), 123-137. doi:10.1113/jphysiol.1964.sp007407

Hato, T., Winfree, S., & Dagher, P. C. (2018). Kidney Imaging: Intravital Microscopy. *Methods in Molecular Biology (Clifton, N.J.), 1763*(4), 129-136. doi:10.1007/978-1-4939-7762-8_12

Helms, C. C., Gladwin, M. T., & Kim-Shapiro, D. B. (2018). Erythrocytes and Vascular Function: Oxygen and Nitric Oxide. *Frontiers in Physiology, 9*, 125. doi:10.3389/fphys.2018.00125

Hilton, S. M. (1959). A peripheral arterial conducting mechanism underlying dilatation of the femoral artery and concerned in functional vasodilatation in skeletal muscle. *The Journal of Physiology, 149*(1), 93-111. doi:10.1113/jphysiol.1959.sp006327

Jackson, D. N., Moore, A. W., & Segal, S. S. (2010). Blunting of rapid onset vasodilatation and blood flow restriction in arterioles of exercising skeletal muscle with ageing in male mice. *The Journal of Physiology, 588*(Pt 12), 2269-2282. doi:10.1113/jphysiol.2010.189811

Jagger, J. E., Bateman, R. M., Ellsworth, M. L., & Ellis, C. G. (2001). Role of erythrocyte in regulating local O2 delivery mediated by hemoglobin oxygenation. *American Journal of Physiology. Heart and Circulatory Physiology, 280*(6), H2833-2839. doi:10.1152/ajpheart.2001.280.6.H2833

Japee, S. A., Ellis, C. G., & Pittman, R. N. (2004). Flow visualization tools for image analysis of capillary networks. *Microcirculation (New York, N.Y. : 1994), 11*(1), 39-54.

Kjeang, E., Djilali, N., & Sinton, D. (2009). Microfluidic fuel cells: A review. *Journal of Power Sources, 186*(2), 353-369. doi:10.1016/j.jpowsour.2008.10.011

Kleinfeld, D., Mitra, P. P., Helmchen, F., & Denk, W. (1998). Fluctuations and stimulus-induced changes in blood flow observed in individual capillaries in layers 2 through 4 of rat neocortex. *Proceedings of the National Academy of Sciences of the United States of America, 95*(26), 15741-15746. doi:10.1073/pnas.95.26.15741

Klitzman, B., & Johnson, P. C. (1982). Capillary network geometry and red cell distribution in hamster cremaster muscle. *The American Journal of Physiology, 242*(2), H211-219. doi:10.1152/ajpheart.1982.242.2.H211

Krogh, A. (1919). The supply of oxygen to the tissues and the regulation of the capillary circulation. *The Journal of Physiology, 52*(6), 457-474. doi:10.1113/jphysiol.1919.sp001844

Kurjiaka, D. T., & Segal, S. S. (1995). Conducted vasodilation elevates flow in arteriole networks of hamster striated muscle. *The American Journal of Physiology, 269*(5 Pt 2), H1723-1728. doi:10.1152/ajpheart.1995.269.5.H1723

La, M., & Reid, J. J. (1995). Endothelin-1 and the regulation of vascular tone. *Clinical and Experimental Pharmacology and Physiology, 22*(5), 315-323.

Lamb, I. R., Novielli, N. M., & Murrant, C. L. (2018). Capillary response to skeletal muscle contraction: evidence that redundancy between vasodilators is physiologically relevant during active hyperaemia. *The Journal of Physiology, 596*(8), 1357-1372. doi:10.1113/JP275467

Lathrop, J. W. (2013). The Diamond Ordnance Fuze Laboratory's Photolithographic Approach to Microcircuits. *IEEE Annals of the History of Computing, 35*(1), 48-55. doi:10.1109/MAHC.2011.83

Lee, S., Vinegoni, C., Feruglio, P. F., Fexon, L., Gorbatov, R., Pivoravov, M., . . . Weissleder, R. (2012). Real-time in vivo imaging of the beating mouse heart at microscopic resolution. *Nature Communications, 3*(1), 1054. doi:10.1038/ncomms2060

Levy, B. I., Ambrosio, G., Pries, A. R., & Struijker-Boudier, H. A. (2001). Microcirculation in hypertension: a new target for treatment? *Circulation, 104*(6), 735-740. doi:10.1161/hc3101.091158

Lutz, B. R., Fulton, G. P., & Akers, R. P. (1950). The neuromotor mechanism of the small blood vessels in membranes of the frog (Rana pipiens) and the hamster (Mesocricetus auratus) with reference to the normal and pathological conditions of blood flow. *Experimental Medicine and Surgery, 8*(2-4), 258-287.

MacDonald, I. C., Groom, A. C., & Chambers, A. F. (2002). Cancer spread and micrometastasis development: quantitative approaches for in vivo models. *BioEssays : News and Reviews in Molecular, Cellular and Developmental Biology, 24*(10), 885-893. doi:10.1002/bies.10156

Madigan, M., & Zuckerbraun, B. (2013). Therapeutic Potential of the Nitrite-Generated NO Pathway in Vascular Dysfunction. *Frontiers in Immunology, 4*, 174. doi:10.3389/fimmu.2013.00174

Mairbäurl, H., Ruppe, F. A., & Bärtsch, P. (2013). Role of hemolysis in red cell adenosine triphosphate release in simulated exercise conditions in vitro. *Medicine*

and Science in Sports and Exercise, 45(10), 1941-1947. doi:10.1249/MSS.0b013e318296193a

Moore, A. W., Jackson, W. F., & Segal, S. S. (2010). Regional heterogeneity of α-adrenoreceptor subtypes in arteriolar networks of mouse skeletal muscle. *The Journal of Physiology, 588*(Pt 21), 4261-4274. doi:10.1113/jphysiol.2010.194993

Myneni, P., Terekhov, A., Wright, G., Hofmeister, W., & Janetopoulos, C. (2014). Intravital Microfluidic Windows for Delivery of Chemicals, Drugs and Probes. *Microscopy and Microanalysis, 20*(S3), 1352-1353. doi:10.1017/S1431927614008496

Ondiveeran, H. K., & Fox-Robichaud, A. E. (2004). Pentastarch in a balanced solution reduces hepatic leukocyte recruitment in early sepsis. *Microcirculation (New York, N.Y. : 1994), 11*(8), 679-687.

Poole, D. C., Copp, S. W., Ferguson, S. K., & Musch, T. I. (2013). Skeletal muscle capillary function: contemporary observations and novel hypotheses. *Experimental Physiology, 98*(12), 1645-1658. doi:10.1113/expphysiol.2013.073874

Prahl, S. (1999). Optical absorptionof hemoglobin. Retrieved from https://omlc.org/spectra/hemoglobin/

Pries, A. R., Secomb, T. W., & Gaehtgens, P. (1996). Biophysical aspects of blood flow in the microvasculature. *Cardiovascular Research, 32*(4), 654-667.

Rogers, J. A., & Nuzzo, R. G. (2005). Recent progress in soft lithography. *Materials Today, 8*(2), 50-56. doi:10.1016/S1369-7021(05)00702-9

Sakai, T., & Hosoyamada, Y. (2013). Are the precapillary sphincters and metarterioles universal components of the microcirculation? An historical review. *The Journal of Physiological Sciences : JPS, 63*(5), 319-331. doi:10.1007/s12576-013-0274-7

Sandoo, A., van Zanten, J. J. C. S. V., Metsios, G. S., Carroll, D., & Kitas, G. D. (2010). The endothelium and its role in regulating vascular tone. *The Open Cardiovascular Medicine Journal, 4*(1), 302-312. doi:10.2174/1874192401004010302

Schaffer, C. B., Friedman, B., Nishimura, N., Schroeder, L. F., Tsai, P. S., Ebner, F. F., . . . Kleinfeld, D. (2006). Two-photon imaging of cortical surface microvessels reveals a robust redistribution in blood flow after vascular occlusion. *PLoS Biology, 4*(2), e22. doi:10.1371/journal.pbio.0040022

Scott, J. R., & Fox-Robichaud, A. E. (2002). Hepatic leukocyte recruitment in a model of acute colitis. *American Journal of Physiology-Gastrointestinal and Liver Physiology, 283*(3), G561-G566. doi:10.1152/ajpgi.00462.2001

Segal, S. S. (2005). Regulation of blood flow in the microcirculation. *Microcirculation (New York, N.Y. : 1994), 12*(1), 33-45. doi:10.1080/10739680590895028

Segal, S. S., & Duling, B. R. (1986). Flow control among microvessels coordinated by intercellular conduction. *Science, 234*(4778), 868-870. doi:10.1126/science.3775368

Segal, S. S., & Duling, B. R. (1989). Conduction of vasomotor responses in arterioles: a role for cell-to-cell coupling? *The American Journal of Physiology, 256*(3 Pt 2), H838-845. doi:10.1152/ajpheart.1989.256.3.H838

Segal, S. S., Welsh, D. G., & Kurjiaka, D. T. (1999). Spread of vasodilatation and vasoconstriction along feed arteries and arterioles of hamster skeletal muscle. *The Journal of Physiology, 516 (Pt 1)*(1), 283-291. doi:10.1111/j.1469-7793.1999.283aa.x

Sikora, J., Orlov, S. N., Furuya, K., & Grygorczyk, R. (2014). Hemolysis is a primary ATP-release mechanism in human erythrocytes. *Blood, 124*(13), 2150-2157. doi:10.1182/blood-2014-05-572024

Sullivan, S. M., & Pittman, R. N. (1982). Hamster Retractor Muscle - a New Preparation for Intravital Microscopy. *Microvascular Research, 23*(3), 329-335. doi:10.1016/S0026-2862(82)80005-8

Taggart, M. J., & Wray, S. (1998). Hypoxia and smooth muscle function: key regulatory events during metabolic stress. *The Journal of Physiology, 509 (Pt 2)*(2), 315-325. doi:10.1111/j.1469-7793.1998.315bn.x

Tyml, K., & Budreau, C. H. (1991). A new preparation of rat extensor digitorum longus muscle for intravital investigation of the microcirculation. *International Journal of Microcirculation, Clinical and Experimental, 10*(4), 335-343.

Unic, A., Derek, L., Hodak, N., Marijancevic, D., Ceprnja, M., Serdar, T., . . . Romic, Z. (2011). Endothelins -- clinical perspectives. *Biochemia Medica, 21*(3), 231-242.

van Giesen, L., Neagu-Maier, G. L., Kwon, J. Y., & Sprecher, S. G. (2016). A microfluidics-based method for measuring neuronal activity in Drosophila chemosensory neurons. *Nature Protocols, 11*(12), 2389-2400. doi:10.1038/nprot.2016.144

Welsh, D. G., Tran, C. H. T., Hald, B. O., & Sancho, M. (2018). The Conducted Vasomotor Response: Function, Biophysical Basis, and Pharmacological Control. *Annual Review of Pharmacology and Toxicology, 58*(1), 391-410. doi:10.1146/annurev-pharmtox-010617-052623

Williams, D. A., & Segal, S. S. (1992). Microvascular architecture in rat soleus and extensor digitorum longus muscles. *Microvascular Research, 43*(2), 192-204. doi:10.1016/0026-2862(92)90016-I

Winter, P., & Dora, K. A. (2007). Spreading dilatation to luminal perfusion of ATP and UTP in rat isolated small mesenteric arteries. *Journal of Physiology, 582*(1), 335-347. doi:10.1113/jphysiol.2007.135202

Wolfe, D. B., Qin, D., & Whitesides, G. M. (2010). Rapid Prototyping of Microstructures by Soft Lithography for Biotechnology. In (Vol. 583, pp. 81-107). Totowa, NJ: Humana Press, Totowa, NJ.

Wong, S. L., Wong, W. T., Tian, X. Y., Lau, C. W., & Huang, Y. (2010). Prostaglandins in action indispensable roles of cyclooxygenase-1 and -2 in endothelium-dependent contractions. *Advances in Pharmacology (San Diego, Calif.), 60*, 61-83. doi:10.1016/B978-0-12-385061-4.00003-9

Wu, J., Kumar-Kanojia, A., Hombach-Klonisch, S., Klonisch, T., & Lin, F. (2018). A radial microfluidic platform for higher throughput chemotaxis studies with individual gradient control. *Lab on a Chip, 18*(24), 3855-3864. doi:10.1039/c8lc00981c

Xia, Y., & Whitesides, G. M. (1998). Soft Lithography. *Angewandte Chemie (International ed. in English), 37*(5), 550-575. doi:10.1002/(SICI)1521-3773(19980316)37:5<550::AID-ANIE550>3.0.CO;2-G

Yamamoto, T., Hayashi, K., Tomura, Y., Tanaka, H., & Kajiya, F. (2001). Direct in vivo visualization of renal microcirculation by intravital CCD videomicroscopy. *Experimental Nephrology, 9*(2), 150-155. doi:10.1159/000052606

Yu, J., Bihari, A., Lidington, D., & Tyml, K. (2000). Gap junction uncouplers attenuate arteriolar response to distal capillary stimuli. *Microvascular Research, 59*(1), 162-168. doi:10.1006/mvre.1999.2192

Zhi, Z., Jung, Y., Jia, Y., An, L., & Wang, R. K. (2011). Highly sensitive imaging of renal microcirculation in vivo using ultrahigh sensitive optical microangiography. *Biomedical Optics Express, 2*(5), 1059-1068. doi:10.1364/BOE.2.001059

Zweifach, B. W., Shorr, E., & Black, M. M. (1953). The influence of the adrenal cortex on behavior of terminal vascular bed. *Annals of the New York Academy of Sciences, 56*(4), 626-633. doi:10.1111/j.1749-6632.1953.tb27383.x

2. Development and validation of a novel microfluidic device for the manipulation of skeletal muscle microvascular blood flow *in vivo*

2.1. Introduction

Skeletal muscle blood flow regulation has been a topic of interest since August Krogh's 1919 documentation of varying capillary perfusion with red cells at rest and in response to muscle contraction (Krogh, 1919). In rodent models, the microcirculation is considered to be composed of vessels which are less than 100 μm in diameter, including arterioles, capillaries, and collecting venules (Bosetti et al., 2016). First order arterioles branching off of the feed artery incrementally give rise to smaller daughter arterioles eventually leading to terminal arterioles that supply discrete capillary networks. Typically, terminal arterioles provide blood supply to pairs of capillary networks each of which connect to separate collecting venules, which then anastomose with increasingly larger venules as the vascular system leads back to the heart. Capillaries are the major site of exchange for nutrients and O_2 to be transported from blood into tissues while also removing waste and CO_2 (Poole et al., 2013). Determining the role of the capillaries in the regulation of blood flow is challenging as current methods used to study blood flow regulation interact with multiple levels of the microvasculature. The level of perfusion of capillary networks with RBCs is dynamically controlled to meet the demands of the tissues that the vessels supply (Segal, 2005; Bagher & Segal, 2011b). This regulation of blood flow to capillary networks is reliant on vasodilation and vasoconstriction of high

order arterioles (Segal, 2005). Vasodilation of first and second order arterioles leads to an increase in blood flow to a proportion of downstream vessels compared with the dilation of terminal arterioles which only influence flow conditions in capillary networks immediately downstream. An increase in blood flow facilitates the delivery of nutrients and O_2 to the tissues and simultaneous removal of CO_2 and waste products. Further investigation into the role of capillaries in blood flow regulation requires a novel approach of administration of vasoactive drugs to a microscale region of skeletal muscle achieved through development of a microfluidic device with simultaneous visualization of capillary blood flow.

There are two common types of preparations used to directly observe the microcirculation of muscle. Superfusion preparations are commonly used in cremaster, gluteus maximus, and spinotrapezius muscle (Marshall, 1982; Jackson et al., 2010; Bagher & Segal, 2011a). The experimental setup involves a reservoir of physiological salt solution (PSS) leading to the muscle. Another common methodology is the isolated muscle preparation commonly used with fusiform shaped muscles such as the EDL to isolate the tissue from the atmosphere with a polyvinylidene chloride film and a coverslip (Tyml & Budreau, 1991; Fraser et al., 2012b). Both of these techniques are the gold standard in the field. However, the ability to restrict experimental influence to a spatially specific area (e.g. the capillaries) is very challenging with each of these preparations.

Manipulation of the tissue microenvironment is possible with either of these preparation types by way of intravascular injection, abluminal delivery using a micropipette, or topical application of drugs dissolved in superfusion solution. The techniques for abluminal application of solutes used in superfusion preparations varies

with target size. Micropipetting a solution onto a target area involves the injection of the solute directly on, or near a vessel of interest allowing for a more directed administration compared to dissolving solutes of interest into the PSS and administering to the entire muscle preparation (Charter et al., 2018). Intravascular injection involves the cannulation of vessels to administer a substance via the systemic circulation, or through exposure to vascular beds of interest directly downstream of the cannulation. Drugs can be introduced intravascularly in both the isolation and superfusion preparations and will potentially provoke changes in all vessels downstream from the site of injection. The ability to administer these solutes to vessels of interest while not affecting other vessels would allow for targeting of specific signalling mechanisms as agonists and antagonists can be introduced either through the same technique of administration or a combination of the above techniques. However, there is currently no effective way to continuously administer drugs to well defined microscale levels of capillary networks and observe the resulting blood flow response while controlling for diffusional exchange to other regions within the preparation in order to focus on the role of the capillaries in signalling.

Techniques for targeted manipulation of tissue microenvironments have previously been developed using a gas exchange chamber (Ghonaim et al., 2011). This approach allows for a spatially confined gas perturbation to be imposed on the skeletal muscle tissue with simultaneous visualization. Previously, it has been demonstrated that perturbation of O_2 concentrations in tissue can modulate skeletal muscle blood flow. Ghonaim and colleagues used various micro-outlets including 100 μm diameter circular windows and 1000 x 200 μm rectangular windows to change blood flow in response to O_2 perturbations (Ghonaim et al., 2013). In the same study computer simulations were

used to describe the partial pressure of oxygen (PO_2) distribution in tissue overlying the micro-outlets (Ghonaim et al., 2013). *In silico* simulation predicted that the imposed PO_2 changes declined as distance from the micro-outlet increased up to 100 μm from the outlet as the tissue returned to the mean tissue PO_2 due to regulation. Although there was strong response to gas changes there are limited perturbations that can be administered to tissues in the gaseous phase. The ability to observe the microvascular response during alterations in gas concentrations within the channel served as a precursor to our development of a liquid based microfluidic for the dynamic delivery of dissolved solutes to microscale tissue environments in skeletal muscle. We set out to expand the versatility of the gas exchange chamber using a liquid microfluidic device capable of targeted delivery of solutes to a spatially confined region of skeletal muscle tissue *in vivo*.

Microfluidic devices have enormous versatility and can be custom designed to suit the needs of researchers for precise manipulation of tissue and cell microenvironments. Microfluidic devices have gained popularity within the past several years in many areas of research as they allow for fine manipulation (Abgrall & Gué, 2007; Wolfe et al., 2010; Yan et al., 2017). Devices can also be rapidly developed using inexpensive fabrication techniques through soft lithography (Wolfe et al., 2010; Yan et al., 2017). Development of devices can be customized to suit the need of researchers for a task of interest as the ability to modify prototypes and master molds is expeditious (Wolfe et al., 2010). These techniques have been used in many biomedical research environments including lab-on-a-chip (Abgrall & Gué, 2007) and organ-on-a-chip technology (Kimura et al., 2018), electrophysiology (Park et al., 2013), and cell culture (van Duinen et al., 2015). There are few examples in the literature where microfluidic

devices have been applied to study physiology *in vivo* (Ghannad-Rezaie et al., 2012). At the time of writing, conceptualized microfluidic devices for studying microvascular blood flow have been proposed (Myneni et al., 2014), but to date there have been no studies that apply this technology to deliver drugs to skeletal muscle *in vivo*.

Dynamic manipulation of the tissue microenvironment in a controlled fashion is highly sought after to study blood flow regulation as the microcirculation in an integrated system. A microfluidic device provides the ability to influence microscale regions of skeletal muscle using solutes dissolved in a PSS with a targeted delivery to a microvascular network of interest. This targeted delivery technique enables researchers to administer agonists or antagonists continuously while simultaneously recording the resulting change in blood flow. This device can then be used in many research areas for various tissues including interrogation of O_2 mediated blood flow regulation, as well as the impairment in blood flow regulation in diseased states in skeletal muscle.

In this study, we developed a novel microfluidic device, using soft lithographic techniques, which was applied *in vivo* to administer three vasoactive drugs to a microscale region of skeletal muscle tissue in order to study microvascular blood flow responses. This device is capable of delivering vasoactive substances with simultaneous visualization and IVVM recording of the microcirculation exposed to the fluid filled channel. In order to validate the microfluidic device, vasoactive agonists with well characterized actions were chosen as they are widely known and have been extensively studied in many microvascular preparations.

Vasoactive agonists are commonly used for studying the mechanisms of vasoconstriction and vasodilation in *in vivo* and *ex vivo* studies (Furchgott & Zawadzki,

1980; Buus et al., 1994). For our validation we chose ACh (Winter & Dora, 2007) as a vasodilator, and PE (Buus et al., 1994; Bridges et al., 2011) as the vasoconstrictor. Lastly, we also used ATP due to our interest in the role of ATP in O_2 mediated flow changes. For each substance we chose a dose range from 10^{-8} to 10^{-3} M based on literature values (Dua et al., 2009; Moore et al., 2010; Nyberg et al., 2013). ACh is used as a control vasodilator due to its action on muscarinic receptors of endothelial cells lining blood vessels; the production of nitric oxide leads to relaxation of vascular smooth muscle cells and results in vasodilation (Furchgott & Zawadzki, 1980). However, ACh also acts on vascular smooth muscle cells and can directly cause vasoconstriction (Ludmer et al., 2009). PE, the vasoconstrictor that we chose, binds to α_1-adrenoceptors activating phospholipase C producing inositol triphosphate which increases Ca^{2+} leading to smooth muscle contraction (Brozovich et al., 2016). ATP, however, has both vasoconstrictive and vasodilatory effects that can be observed at different doses. At low doses, ATP causes vasoconstriction through binding the $P2X_1$ receptors on vascular smooth muscle cells. Conversely, higher doses of ATP results in vasodilation through its action on the $P2X_4$, $P2Y_1$, and $P2Y_2$ receptors located on endothelial cells which produces nitric oxide leading to vasodilation (Lohman et al., 2012). In addition, conducted vasodilatation of arterioles (at a distance from application sites) has been documented for the two vasodilatory agents. Specifically, ACh causes vasodilation 2 mm from the site of application, and ATP up to 1.2 mm away (Duling & Berne, 1970; Duza & Sarelius, 2003; Bagher & Segal, 2011b). Local application of vasodilators to terminal arterioles can lead to vasodilation of upstream vessels that are beyond 1000 μm away which will have an effect on the downstream vessels of interest (Duza & Sarelius, 2003).

In summary, our objective was to develop and validate a novel microfluidic system that is capable of delivering solutes of fixed concentration to capillary networks and terminal arterioles of skeletal muscle while simultaneously observing blood flow changes in response to increasing doses of well characterized vasoactive substances. The device was designed for application to the well-established isolated EDL skeletal muscle preparation (Tyml & Budreau, 1991; Fraser et al., 2012b). In addition to the empirical validation of our microfluidic delivery system we also have applied a mass transport model to predict expected drug concentrations within the overlying tissue volume. Taken together, this represents the first comprehensive description of how a microfluidic device can be applied *in vivo* to manipulate tissue microenvironment and associated vasculature.

2.2. Methods

2.2.1. Computer Aided Design

Tinkercad (Tinkercad.com, Accessed October 2017 - September 2019) and AutoCAD for Mac software (Version Q.46.M.184) was used for the conceptualization of microfluidic devices and consideration of animal positioning on the device (Figure 2.1). Designs were developed taking multiple factors into consideration. These factors include development of a channel of sufficient width, minimum 3 mm, and height, between 0.3 and 0.7 mm, to ensure adequate channel fluid flow rate capable of rapid delivery and switching of perfusion solutions at the outlet and the adjacent tissue (Figures 2.1, 2.2). The positioning and total length of the channel was selected to maximize the available surface area of 25 x 75 mm standard glass slide and considering the arrangement of the animal's muscle and limb. Placement of the coverslip, with a centered laser-cut micro-outlet, and the device inlet and outlet were positioned to suit the limited range of movement of the limb and the angle to which the muscle can be reflected across the objective. Computer aided design (CAD) conceptualized devices were used to ensure the spacing of micro-outlet and the inlet/outlet tubing supports would not interfere with one another. During prototyping, careful consideration was given to developing a device that was within a functional working distance of the microscope objective that was to be used during the *in vivo* data collection portion of the validation.

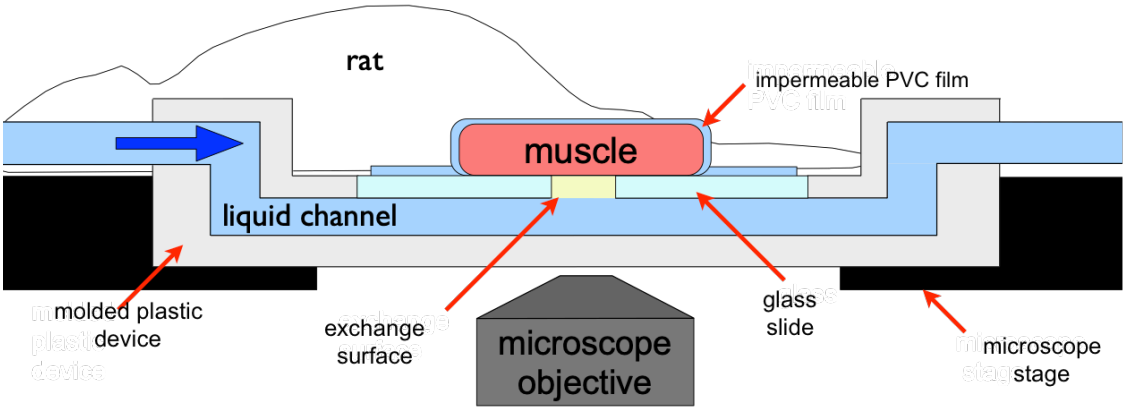

Figure 2.1 Cross sectional schematic of liquid microfluidic intravital video microscopy experimental setup. The rat extensor digitorum longus muscle was placed on a novel liquid microfluidic device apparatus for simultaneous intravital video microscopy and vasoactive drug administration. The liquid microfluidic device was positioned in a three dimensional printed stage insert of an inverted Olympus IX73 microscope. Schematic adapted with permission from Ghonaim et al. (Ghonaim et al., 2011).

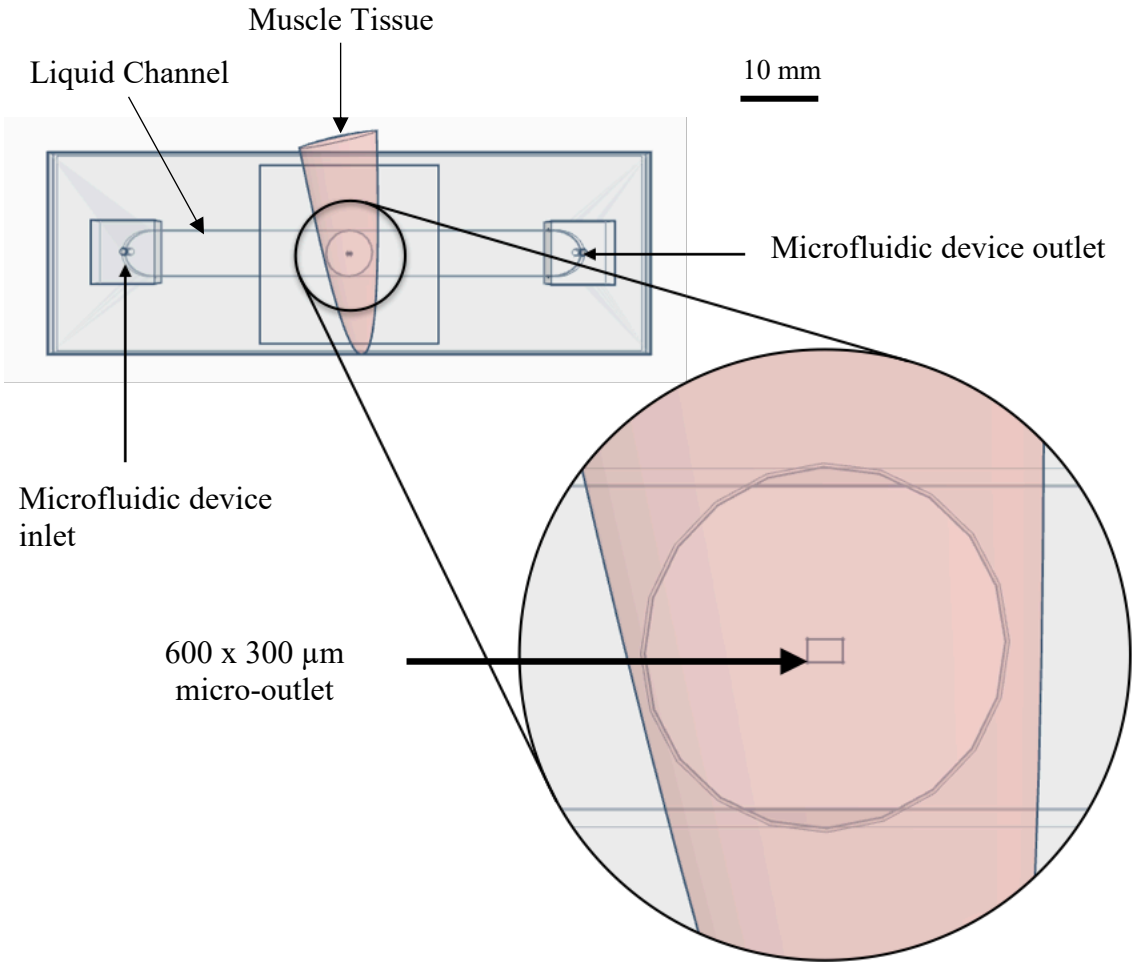

Figure 2.2 Computer aided design schematic of the orientation of the extensor digitorum longus muscle on the liquid microfluidic device. The schematic illustrates the microfluidic apparatus and includes the image of 600 x 300 µm micro-outlet positioning relative to the muscle. In use, perfusate travels from the inlet of the microfluidic device to the micro-outlet (where the muscle is exposed to the perfusate and any added vasoactive drugs), and then from the micro-outlet to the microfluidic device's outlet.

2.2.2. 3D Printing

To facilitate device fabrication, device mould barriers which have a slide insert and elevated walls were designed using free online Tinkercad software. Barriers were developed and printed to set a maximum thickness of devices and improve time of preparation. Barriers were also developed to reduce the amount of PDMS, a silicone elastomer, that was used. Barriers of sufficient size were designed to surround a standard 25 x 75 mm glass slide while also limiting the amount of mold flashing present along the surface of the device. The 3D print was done in acrylonitrile butadiene styrene material to withstand the repeated heating and cooling required for microfluidic device fabrication.

A previously designed microscope stage insert was modified to house the microfluidic device (Figure 2.3). The placement and design of the microfluidic device insert was to allow for precise fitting of microfluidic devices within the stage insert. The last consideration was the maximum thickness of the stage insert within the functional range of the microscope objectives. This was due to the necessity to be able to change the microscope objectives during an experiment without obstruction of the objectives and turret.

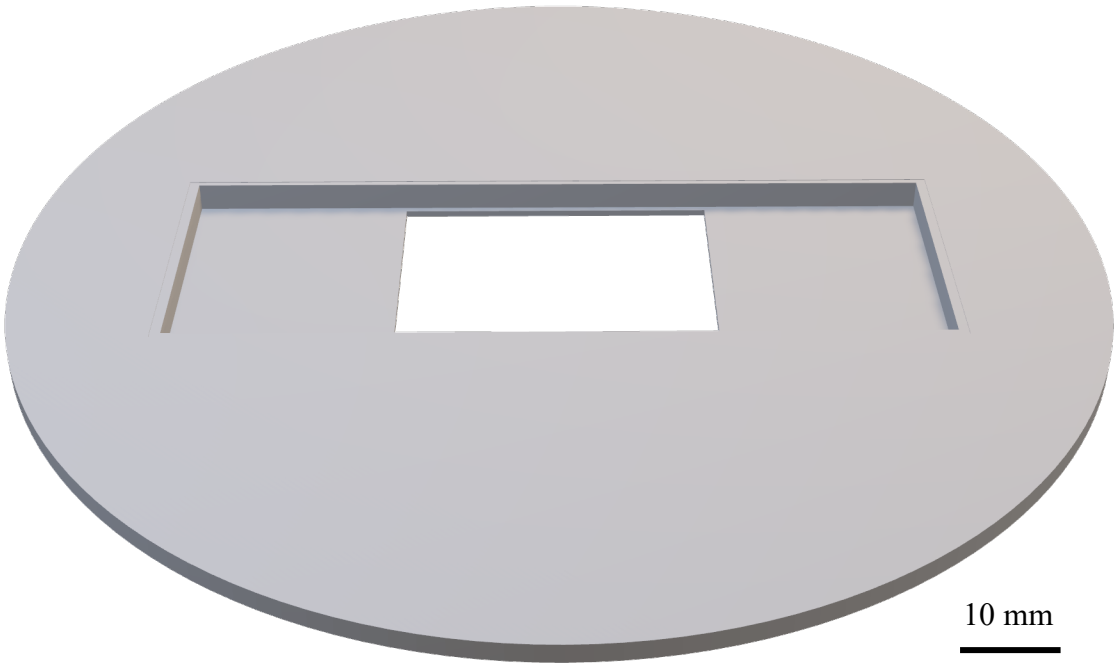

Figure 2.3 Computer aided design image of three dimensional printed microfluidic stage insert. The three dimensional printed insert was designed to fit the stage of an inverted Olympus IX73 microscope.

A custom designed stage platform was developed to provide additional surface area required for the microfluidic device apparatus (Figure 2.4) along with the limited space available on the Olympus IX73 standard microscope stage**.** The stage print was designed to include supports for the placement of the ventilator tubing, arterial and venous lines, and the area specified for the microfluidic reservoir. The animal positioning was largely fixed to ensure the optimal efficiency of the animal monitoring equipment. The reservoir access determined the location of the barriers for the reservoir container.

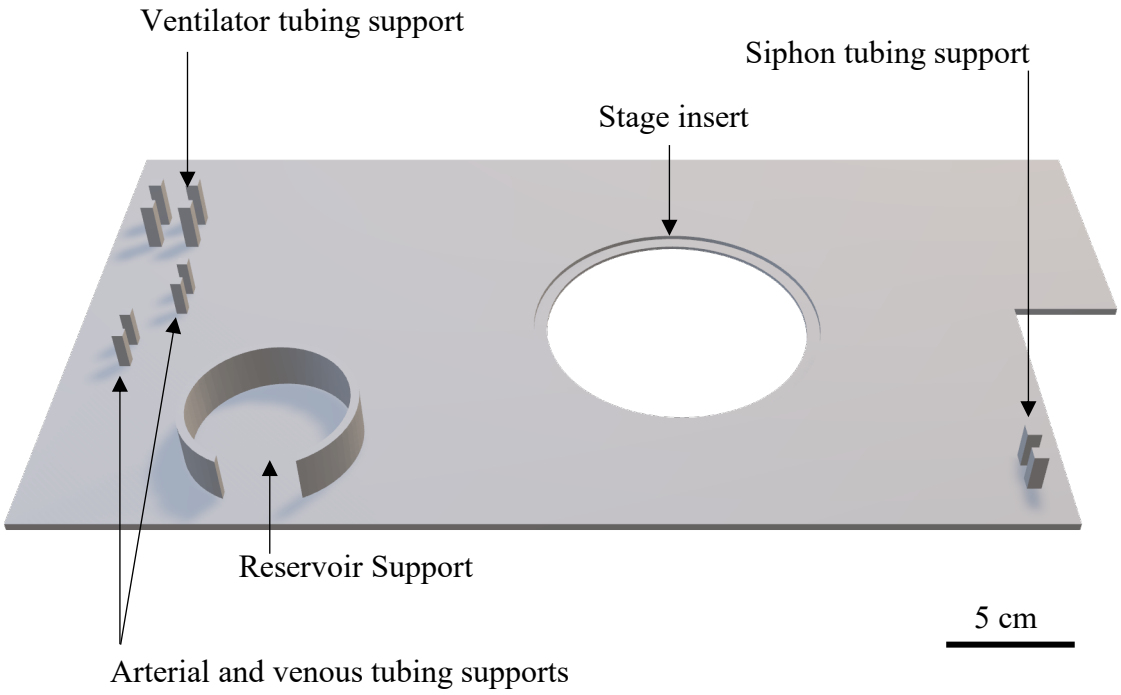

Figure 2.4 Custom computer aided design image of the three dimensional printed stage for an Olympus IX73 inverted microscope.

2.2.3. Device Fabrication

Channel structures were patterned using layers of polyvinyl adhesive tape. Channels were trimmed to 3 mm x 65 mm dimensions with rounded edges using scalpel and razor blades. Channels were then adhered to standard glass slides which were thoroughly cleaned with 99 % alcohol to minimize residue prior to device fabrication. Channel moulds were then left upside down overnight (12-16 hours) with a 5 kg weight to ensure that the polyvinyl tape had sufficient time to adhere to the glass. On the day of fabrication, the channel moulds were wiped with 70 % alcohol to remove any debris that may have been present. The moulds were then transferred to the 3D printed device barriers described above. The assembled moulds were then placed into large glass, levelled petri dishes lined with aluminum foil to reduce leakage from the moulds during curing.

PDMS was mixed from Sylgard 184 Silicone Elastomer Kit (Dow Corning, Midland, MI) at a 10:1 base: curing agent ratio in accordance with manufacturer specifications**.** 20 ml of base and 0.2 ml of curing agent was sufficient for the fabrication of 2 devices. Mixed PDMS was degassed in a vacuum chamber in 10-minute intervals to remove bubbles introduced during mixing, once the PDMS was sufficiently degassed extreme care was taken when pouring PDMS into the completed moulds held in glass dishes to ensure minimal bubble formation. Uncured devices were then degassed in the same vacuum chamber in 10-minute cycles to remove the bubbles that were present. Tubing supports were made prior to assembling the microfluidic devices by pouring PDMS mixtures in small plastic petri dishes until an approximate height of 8 mm. PDMS was then cured at 90 ℃ for 120 minutes, demoulded, and cut into 10 x 10 mm sections.

Sections were then punched with a 3 mm round punch. Tubing supports were placed in the liquified PDMS at both end of the channel, small pieces of polyethylene tubing were placed into each of the supports to ensure access to the channel and remaining support was filled with PDMS. The glass dishes holding completed devices were then placed into a preheated 90 ℃ bench oven and allowed to cure for 120 minutes.

The dishes containing devices were removed and allowed to cool for 5-10 minutes at room temperature to allow for safe handling. Cured devices were then carefully demoulded and trimmed with a razor blade to remove flashing and excess PDMS. Tubing pieces were carefully removed from supports. Access to the center of the channel was achieved by cutting a 4 x 15 mm rectangular opening into the centre of the channel using scalpel and razor blades. Devices were then cleaned to remove stray pieces of PDMS and mounted onto a standard 25 x 75 mm glass slide. Polyethylene 60 tubing was inserted into the inlet and outlet support as an interface between the reservoir and the device. The top surface of device was covered with clear tape and whole devices were placed into petri dishes to reduce dust accumulation prior to use. When preparing device for use, a coverslip with a 300 x 600 μm laser cut micro-outlet (Figure 2.5) (Potomac Photonics, Maryland) was centered over the channel opening.

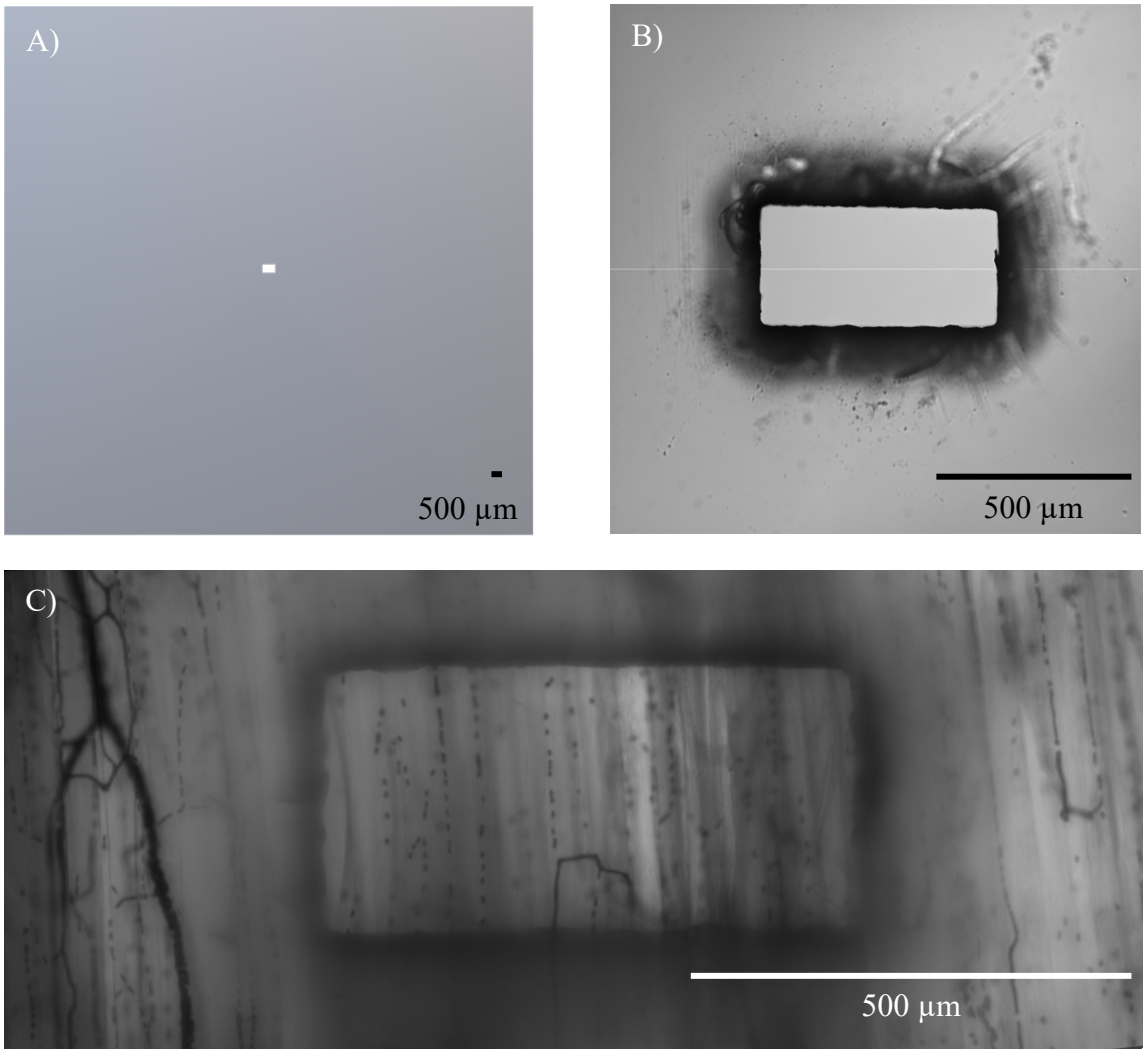

Figure 2.5 Laser cut 300 x 600 µm micro-outlet in 25 x 25 mm glass coverslip. A) Computer aided design model of 300 x 600 µm micro-outlet in 25 x 25 mm glass coverslip, B) ten times magnification view of in 25 x 25 mm glass coverslip that interfaces the muscle and liquid channel and C) brightfield ten times magnification view of the extensor digitorum longus microcirculation with a 300 x 600 µm micro-outlet.

2.2.4. Animal Protocol

Male Sprague-Dawley rats (n=18, 149-208 g) were received from Charles River laboratory 5 days prior to the experiment to ensure animals were acclimatized to animal care facilities. Animals were allowed to eat a standard Teklad 18 % Protein chow diet (Envigo, Madison, Wisconsin, USA) and drink *ad lib*. All animal protocols were approved by the Memorial University Animal Care and Use Committee. On the day of experiments animals were anaesthetized with an intraperitoneal injection of sodium pentobarbital (65 mg/kg) (Euthanyl, Bimeda-MTC, Cambridge, Ontario, Canada). Once the animals were sufficiently anaesthetized to a surgical plane, several sub cutaneous injections of lidocaine (20 mg/ml) were administered along the midline of the neck between the jawline and sternum. A rectal temperature probe was inserted to monitor the animal's core body temperature throughout the experiment. A heating pad (Harvard Apparatus) and heat lamp were used to maintain the animal's temperature between 36 and 37 ℃.

A neck incision was made to along the midline of the neck to dissect the left common carotid artery. Once the carotid was isolated, portions of the vagus nerve plexus surrounding the artery were carefully separated from the vessel and kept intact. The carotid was then cannulated towards the heart with polyethylene 50 tubing (Intramedic, inner diameter 0.58 mm, outer diameter 0.965 mm). The arterial cannula was constantly perfused with 1 international unit (U)/ml heparinized saline connected to a Digi-Med blood pressure analyzer to monitor and record animal status. Using the manufacturer's software, the animal's systolic, diastolic, mean arterial pressure (MAP), and heart rate

were recorded and stored. Following the arterial cannulation, the right external jugular vein was isolated and cannulated in the direction of the heart with 0.635 mm outer diameter Silastic tubing (Dow Corning, Midland, Michigan, United States) used for fluid resuscitation of heparinized saline (1 U/ml) (0.5 ml/hour) and maintenance anaesthetic administration as required. The animal's heart rate and blood pressure were evaluated every 30 minutes for variability as well as testing the palpebral reflexes and toe pinch to ensure acceptable depth of anaesthesia. Maintenance doses of sodium pentobarbital anaesthetic (22 mg/kg) were administered when the animal's MAP exceeded 110 mmHg or if the animal responded to adverse stimuli. A tracheotomy was performed, and the animals were mechanically ventilated with a gas mixture of ~30 % O_2 and 70 % Nitrogen. Respiratory rates and volumes were calculated based on the animal's weight. Respiratory rate, per minute, was automatically calculated by the Harvard Apparatus Inspira ventilator using the equation $53.5 \times M_b^{-0.26}$, where M_b is the animal's weight in kilograms. Respiratory volume, in litres, was determined automatically by using the equation $0.0062 \times M_b^{1.01}$. Following completion of the tracheotomy the neck incision was sutured closed with a continuous lock stich.

The right EDL, a muscle of the lower hind limb, was blunt dissected and isolated as previously described (Tyml & Budreau, 1991; Fraser et al., 2012b). The skin over the lateral portion of the leg was wiped with 70 % alcohol and 0.9 % sterile saline before being removed. The muscle was isolated using blunt dissection techniques. The distal tendon was located, and a 4-0 silk suture was tied to the tendon close to the retinaculum using a reef knot. The distal tendon was then cut, the muscle was lifted and cleared from the remaining tissue without damaging the feed artery and vein.

The animal was then transferred onto the 3D printed custom stage of an Olympus IX73 inverted microscope. The microfluidic device was filled with buffered Krebs solution (37 ℃, pH 7.4) with the following composition (in mM): sodium chloride (NaCl) 114, potassium chloride (KCl) 4.7, potassium dihydrogen phosphate (KH_2PO_4) 0.8, magnesium chloride ($MgCl_2$) 1.2, calcium chloride ($CaCl_2$) 2.5, D-Glucose 11, sodium bicarbonate ($NaHCO_3$) 25, HEPES (4-(2-hydroxyethyl)-1-piperazineethanesulfonic acid) 10. Care was taken to avoid introducing bubbles into the tubing or flow channels. The device was inserted into the custom stage insert and shimmed such that it was level with the stage surface. The EDL was reflected over the microfluidic device micro-outlet at an *in situ* length and position. The muscle was then covered with polyvinylidene chloride film (Saran, Dow Chemical Canada inc., Toronto), and bathed in sterile saline warmed to 37 ℃. The muscle was gently sealed using a standard coverslip and standard glass slide with vacuum grease applied to the edges (Dow Corning, Midland, Michigan, United States). In a subset of experiments, a thermocouple was placed beside the muscle to measure the temperature at the muscle. The temperature probe, muscle suture and cannulas were secured to the stage with adhesive tape. Once transferred, the animals were acclimated on the stage for 30 minutes or until animal's core temperature reached 36.0 ℃ and the animal's MAP was above 80 mmHg.

After the acclimation period was complete, the arterial cannula was briefly disconnected, and a 0.5 ml arterial blood sample was taken. The blood sample was loaded into a CD4+ blood gas analyzer cartridge and inserted into a handheld VetScan iSTAT (Abbott Point of Care Inc., Princeton, New Jersey). The blood gas analyzer provided values for pH, partial pressure of carbon dioxide (PCO_2), PO_2, base excess in the

extracellular fluid compartment concentration, bicarbonate (HCO_3) concentration, total carbon dioxide, oxygen saturation (sO_2), and lactate concentration. Ventilation rates and volumes were adjusted to maintain PCO_2 and PO_2 within physiological range as required.

2.2.5. Capture Protocol

The IVVM apparatus was composed of a 300 W Xenon arc light source (Sutter Lambda LS, San Francisco, USA) connected to an inverted microscope (Olympus IX73, Tokyo, Japan). The muscle was trans-illuminated and transmitted through a beam splitter (Optosplit II, Cairn, Kent, UK) that allowed for simultaneous parfocal capture of an isosbestic wavelength (both 450 and 420 nm filters were used) and an oxygen-sensitive wavelength (438 nm). Recordings were taken using an OrcaFlash4.0 v3 digital camera (Hamamatsu, Japan), being viewed and controlled using HCImage Live software (Hamamatsu, Japan) on a desktop computer. Each capture consisted of a 60-second recording, at a 30 frames/second. Exposure rates were adjusted prior to each recording to maximize light intensity of the field and ranged between 5 – 30 ms.

IVVM recordings of in focus capillaries directly overlying the micro-outlet were taken at ten times (10X) magnification for multiple focal planes to maximize the number of in focus vessels. Recordings were made while MAP were between 90 – 100 mmHg, rectal temperatures between 36.0 - 37.0 ℃, and while the microfluidic device was perfused with various solutions. Baseline focal plane recordings were made following the equilibration period and once the arterial blood samples were within the physiological range. For each focal plane, focus was carefully maintained on selected vessels throughout the capture sequence. Following the focal plane recordings extended depth of

field (EDF) recordings were completed. EDFs were recorded by beginning at the surface of the muscle and progressively focusing into the first 100 μm of the muscle and returning back to the surface during a 60 second capture. These recordings were made at the window and the areas surrounding the micro-outlet to show all vessels perfused with red cells in the first 100 μm of the muscle.

2.2.6. Vasoactive Drug Administration

Doses of vasoactive substances were prepared on the day of the experiment in sequential doses of 10^{-7} to 10^{-3} M for ACh and PE, and 10^{-8} to 10^{-3} M for ATP. The microfluidic device was perfused with each dose allowing the dissolved drugs access to tissue directly overlying the micro-outlet. Doses were determined based on literature values which resulted in a significant change in arteriolar diameter for both suffusion and intravascular injections of the vasoactive drugs (Dua et al., 2009; Moore et al., 2010; Nyberg et al., 2013)**.** Sequential doses were loaded into the stage reservoir and conducted to the microfluidic device inlet. Flow through the device was controlled by a downstream siphon connected to a 4 way stopcock**.** Due to the siphon, there was a slight negative pressure exerted on the muscle from within the micro-outlet, this pressure provided a seal around the outlet and eliminated the possibility of leaks.

The device was perfused for 3 minutes with each drug concentration to ensure adequate time for washout and for the muscle to be exposed to each dose as the flow rate through the device was ~4 ml per minute. For all drug concentrations, the same focal planes were recorded within the window to maximize the number of analyzable capillaries at each dose. At the highest dose of all drugs, following focal plane recordings,

EDF recordings were made at, and around the window, as described above. To change the perfusion fluid, the stopcock was closed to the device to stop the flow and the reservoir was changed to the next dose, once the change was made the stopcock was returned to the flowing position. The first vasodilator, either ATP or ACh, was put through the device following baseline recordings starting at the lowest dose. The device was then immediately perfused with second vasodilator in the same fashion as the first vasodilator. Later experiments limited the dose response protocol to one vasodilator and extended Krebs solution washout to quantify the washout period. Pre-PE baseline recordings were completed following vasodilators using the previously mentioned buffered Krebs Solution. Increasing doses of PE, a vasoconstrictor, were administered to the muscle through the device following the Krebs solution.

In a subset of experiments, upon completion of the dose response protocol, the apparatus was perfused with Evan's blue dye (0.5 %) to verify the seal integrity between the muscle and the micro-outlet surface. Evan's blue is a biological dye that has a high affinity for albumin causing tissue coming in contact with the dye to be brightly stained, thus demarking the area of exposure to the fluid flowing through the channel. Further, any loss of integrity between the muscle and the device resulted in air being drawn into the device. While perfusing with the dye the interface between the tubing and supports at the inlet and outlet of the device was observed to ensure there were no leaks. Evan's blue was used to assess the contact interface between the exposed muscle surface and the fluid in the channel while also ensuring that there was adequate exchange throughout the entire length of the micro-outlet.

2.2.7. Offline Analysis

Analysis of individual capillaries was carried out using custom software written in MATLAB (Mathworks, Natick, Mass., USA). The captured TIFF images recorded during experiments were split into their respective wavelengths. The processing software also generated AVI videos and functional images including pseudo optical density, variance, and SAD images. A naming convention was used to ensure vessels were analyzed in all doses of the experiment. From these processed files, each experiment was loaded into a program used to generate STIs similar to that described previously (Ellis et al., 1992). In-focus capillaries with single file flow RBCs of focal plane recordings were selected, named and the walls of the capillaries were traced using a semi-automated algorithm (Fraser et al., 2012b). A third program was used for the final analysis of the generated STI to measure velocity and lineal density, and to calculate RBC supply rate in cells per second (Ellis et al., 1992).

Composite EDF maps were generated using a custom MATLAB program that has been described previously (Fraser et al., 2012b). In this program, individual functional images were loaded and registered to one another with common discernible features in overlapping images used as seed points for a two-dimensional fast Fourier transform based registration algorithm. This program was used to create a spatial map of all perfused vessels within the first 100 μm of the surface and their orientation with respect to the micro-outlet window for the highest dose of each of the drug interventions.

2.2.8. Hemodynamic Data

The resulting 60 second average of the hemodynamic data from the custom MATLAB program were organized by vasoactive drug, dose, and vessel identification number into Excel spreadsheets and copied into Prism (Graphpad, California, USA) for statistical analysis. Standard error of the mean was calculated in Prism based on the means of individual capillary data at each dose.

Analysis of Variance (ANOVA) and Kruskal-Wallis multiple comparisons tests were used on individual vessel hemodynamic data. There was a large variability in each animal at each dose because of this data from individual capillaries from various animals can be compared. Due to the heterogeneity in microvascular blood flow throughout each dose the data does not fit a normal distribution and was therefore considered non-parametric. ANOVA was used to analyze the mean values for each of the hemodynamic parameters. Following the significant result of one-way ANOVA tests, the Kruskal-Wallis multiple comparison test was used to compare each dose to the corresponding baseline and other respective doses. A p value of < 0.05 was considered significant.

2.2.9. Tissue Mass Transport Model

To aid with the interpretation of experimental results we applied a mathematical model that describes the expected tissue concentrations of each drug across the range of experimental conditions described above. Concentrations of vasoactive drugs were simulated in 3D over time. Concentration, C, was determined by numerically solving the following partial differential equation, for each drug:

$$\frac{\partial C}{\partial t} = D\nabla^2 C + q(C_b - C) - V_{max}\frac{C}{K_m + C}$$

where D is the diffusivity of the drug in tissue, ∇^2 is the Laplacian operator for the drug concentration, q is the rate of transport into/out of the blood, C_b is the concentration of the drug in the blood, V_{max} is the maximum rate of degradation of the drug in the tissue and K_m is the Michaelis constant representing the concentration at which the degradation rate is half of V_{max}. The parameters used in our model are summarized in Table 2.1.

Table 2.1 Parameters used in mathematical model.

	Parameter	Value	Source
Acetylcholine			
	D	4.00×10^{-6} cm^2 s^{-1}	(Land et al., 1984)
	q	1.037×10^{-1} s^{-1}	calculated†
	C_b	0	
	V_{max}	4.83×10^{-2} μM s^{-1}	(Miledi et al., 1984)
	K_m	6.2 mM	(Miledi et al., 1984)
ATP			
	D	5.035×10^{-6} cm^2 s^{-1}	(de Graaf et al., 2000)
	q	1.306×10^{-1} s^{-1}	calculated†
	C_b	1.06 μM	(Wood et al., 2009)
	V_{max}	1.00×10^{-2} μM s^{-1}	(Yegutkin, 1997) ‡
	K_m	143 μM	(Yegutkin, 1997)
Phenylephrine			
	D	9.00×10^{-6} cm^2 s^{-1}	(Bevan & Török, 1970)
	q	2.334×10^{-1} s^{-1}	calculated†
	C_b	0	
	V_{max}	0	
	†$q_x = \frac{D_x}{D_{O_2}} q_{O_2}$ with $D_{O_2} = 2.41 \times 10^{-5}\ cm^2 s^{-1}$ (Bentley et al., 1993) and $q_{O_2} = 0.625\ s^{-1}$ (Goldman, 2008) ‡ Calculated assuming a sarcoendoplasmic reticulum Ca^{2+}-ATPase density of 11.25 mg/mL.		

An implicit-explicit temporal discretization scheme was implemented as described previously (Ascher et al., 1995) where the linear source terms were evaluated at the current time step, and the other terms were evaluated at the previous time step. The spatial derivatives were discretized using a second order central difference scheme. The PDE was solved in parallel on a graphical processing unit (GPU) implemented in CUDA (J. Nickolls, 2008). The numerical grid was spatially decomposed onto a 1024-core GPU.

2.3. Results

2.3.1. Systemic Measurements

Animal weight, and systemic physiological animal monitoring data are shown in Table 2.2. Animal weights were measured immediately prior to experiment. Mean arterial, systolic, and diastolic blood pressures are the mean values recorded from the start of the capturing protocol and therefore include times immediately following administration of anaesthetic. Mechanical ventilation respiratory rate and fraction of inspired oxygen (FiO_2) are shown.

Arterial blood gas sample results are listed in Table 2.3. The temperature at the surface of the muscle, measured with a thermocouple positioned adjacent to the muscle belly ,was found to be 29 ℃ throughout the capture period. A minor variation in temperature was seen during the heat lamp cycling. Efforts were made to block the muscle from being directly exposed to the heat lamp by shielding the device and muscle as much as possible.

Table 2.2 Systemic physiological animal monitoring data of anaesthetized male Sprague-Dawley rats that completed the experimental protocol.

	Mean	Standard Deviation
Animal Weight (g)	174.1	14.2
Mean arterial pressure (mmHg)	88.6	6.4
Systolic blood pressure (mmHg)	94.0	7.0
Diastolic blood pressure (mmHg)	81.0	6.2
Heart rate (beats per minute)	412	25.4
Fluid infusion rate (ml/hour)	0.5	0
FiO_2 ($\%O_2$)	34.9	1.5
Respiratory rate (breaths/minute)	72	1.8

Note: FiO_2, fraction of inspired oxygen. N = 18 animals

Table 2.3 Arterial blood gas analyzer measurements of anaesthetized male Sprague-Dawley rats.

	Mean	Standard Deviation
pH	7.408	0.04
PCO_2 (mmHg)	46.9	5.00
PO_2 (mmHg)	136.0	20.84
BEecf (mmol/L)	4.83	2.87
HCO_3 (mmol/L)	29.5	2.45
TCO_2 (mmol/L)	30.8	2.66
sO_2 (%)	98.8	0.73
Lac (mmol/L)	1.28	0.51

Note: PCO_2, partial pressure of carbon dioxide; PO_2, partial pressure of oxygen; BEecf, base excess in the extracellular fluid compartment concentration; HCO_3, bicarbonate concentration; TCO_2, total carbon dioxide; sO_2, oxygen saturation; Lac, lactate concentration. N=18 animals

2.3.2. Hemodynamics Measurements

Hemodynamic measurements of analyzed capillaries in response to increasing doses of ATP are shown in Figure 2.6, Figure 2.7, and Figure 2.8. Individual analyzed capillaries from 9 anaesthetized Sprague-Dawley rats are shown in Table 2.4 for each sequential dose. The numbers of analyzed capillaries varied at each dose due to shifts in focal plane and ability to select vessel segments due to limitation of the analysis software relying on capillary hemodynamics (e.g. high hematocrit, high velocity). Capillaries from each animal were analyzed for each dose. Symbols correspond to the one minute mean of individual capillary measurements collected over 1800 frames (30 frames / s). The symbols represent individual capillary data from the 9 animals.

There was a significant increase in RBC velocity in capillaries between baseline and ATP 10^{-3} M ($p = 0.0064$). There was a significant increase in RBC supply rate from baseline to ATP 10^{-4} ($p = 0.0472$), and 10^{-3} M ($p = 0.0254$). There were no significant differences in capillary hematocrit values across all doses.

Table 2.4 Hemodynamic measurements in response to increasing doses of adenosine triphosphate.

	Baseline	**ATP 10^{-8} M**	**ATP 10^{-7} M**	**ATP 10^{-6} M**	**ATP 10^{-5} M**	**ATP 10^{-4} M**	**ATP 10^{-3} M**
n (Capillaries)	53	48	49	47	47	41	41
Hematocrit (%)	18.9 ± 2.3	12.8 ± 2.0	15.4 ± 2.1	14.5 ± 1.8	19.4 ± 2.1	22.4 ± 2.1	22.3 ± 2.2
Velocity (µm/s)	213.7 ± 23.5	210.0 ± 32.1	202.1 ± 26.0	183.9 ± 23.6	287.4 ± 33.9	393.2 ± 52.8	425.0* ± 49.1
Supply Rate (cells/s)	15.5 ± 3.2	10.6 ± 2.2	11.4 ± 2.3	11.0 ± 2.3	24.3 ± 4.4	34.4* ± 5.5	33.9* ± 6.4

Note: ATP, adenosine triphosphate. ± standard deviation; * $p < 0.0472$ compared to baseline; data from 9 animals.

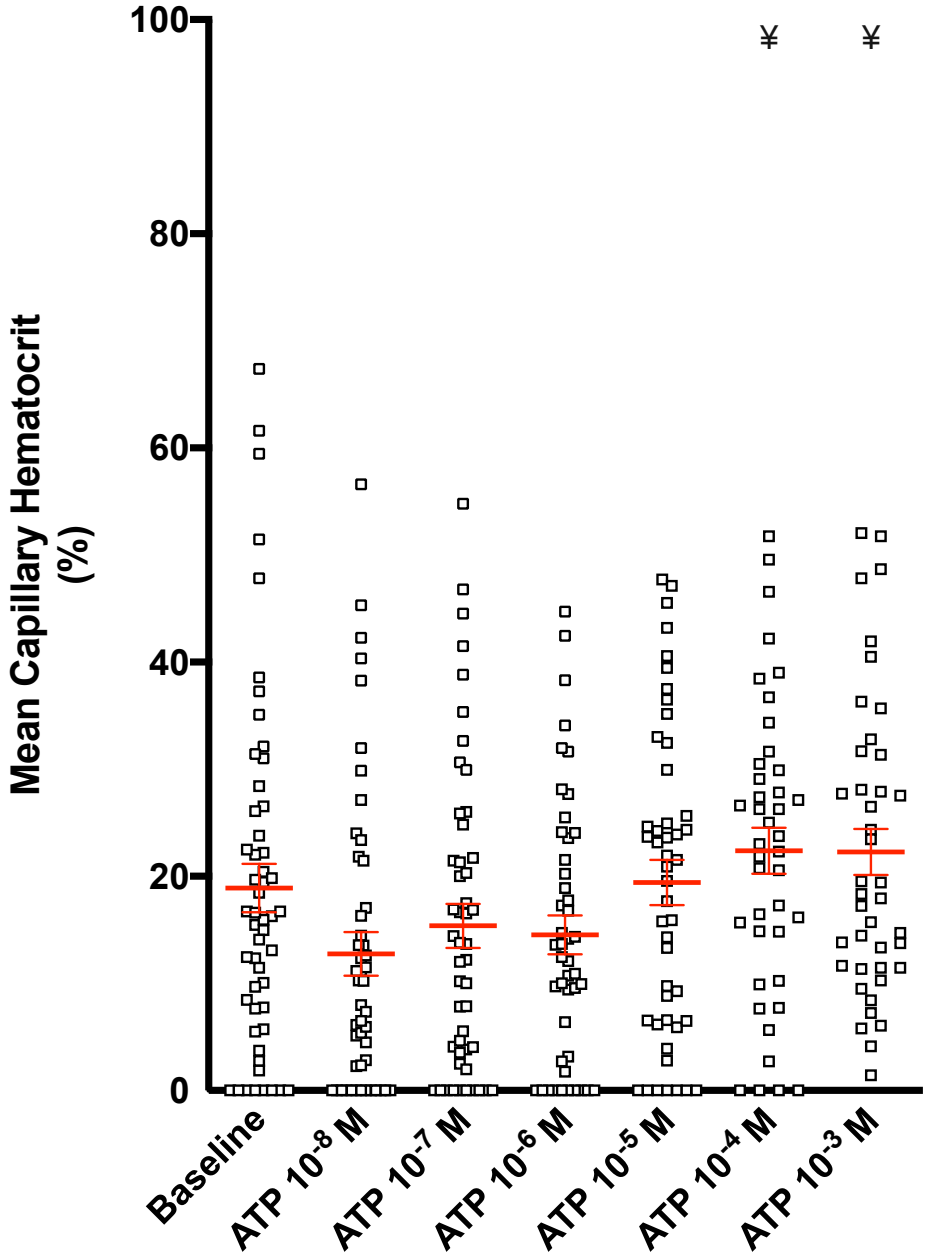

Figure 2.6 Capillary hematocrit in response to increasing doses of adenosine triphosphate. Doses of adenosine triphosphate (ATP) from 10^{-8} M to 10^{-3} M were delivered via the microfluidic device. The mean capillary hematocrit at each dose is indicated and error bars represent the standard error of the mean. ¥ $p < 0.0094$ compared to 10^{-8} M. n= 41-53 capillaries (in 9 animals)

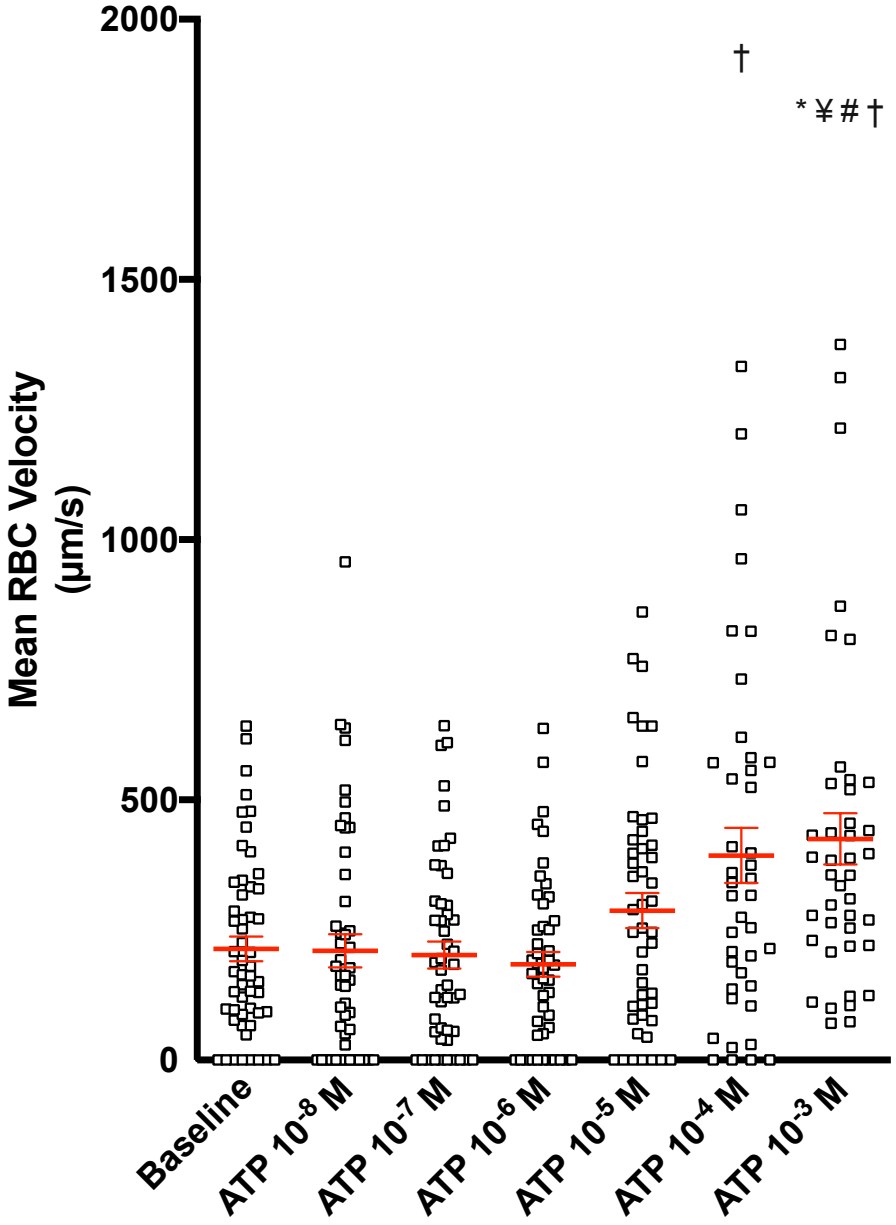

Figure 2.7 Capillary red blood cell velocity in response to increasing doses of adenosine triphosphate. Doses of adenosine triphosphate (ATP) from 10^{-8} M to 10^{-3} M were delivered via the microfluidic device. The mean red blood cell velocity at each dose is indicated and error bars represent the standard error of the mean. * $p = 0.0064$ compared to baseline, ¥ $p = 0.0009$ compared to 10^{-8} M, # $p = 0.0017$ compared to 10^{-7} M, † $p < 0.0269$ compared to 10^{-6} M. n= 41-53 capillaries (in 9 animals)

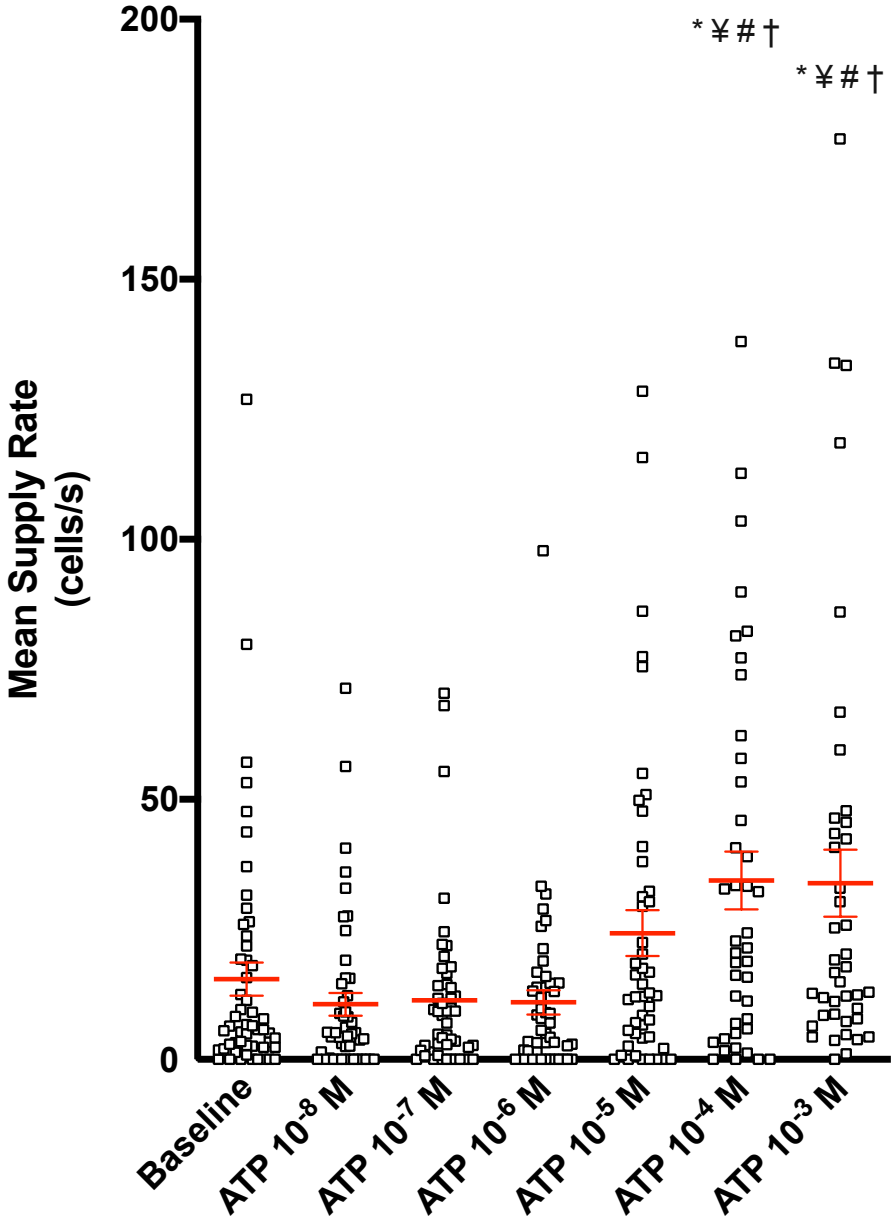

Figure 2.8 Capillary red blood cell supply rate in response to increasing doses of adenosine triphosphate. Doses of adenosine triphosphate (ATP) from 10^{-8} M to 10^{-3} M were delivered via the microfluidic device. The mean red blood cell supply rate at each dose is indicated and error bars represent the standard error of the mean. * $p < 0.0472$ compared to baseline, ¥ $p < 0.0012$ compared to 10^{-8} M, # $p = 0.0063$ compared to 10^{-7} M, † $p < 0.0071$ compared to 10^{-6} M . n= 41-53 capillaries (in 9 animals)

Hemodynamic measurements of analyzed capillaries in response to increasing doses of PE are shown in Figure 2.9, Figure 2.10, and Figure 2.11. Individual analyzed capillaries of 11 anaesthetized Sprague-Dawley rats are shown in Table 2.5 for each sequential dose. The numbers of analyzed capillaries varied at each dose due to shifts in focal plane and ability to select vessel segments due to limitation of the analysis software relying on capillary hemodynamics (e.g. high hematocrit, high velocity). Capillaries from each animal were analyzed for each dose. Symbols correspond to the one minute mean of individual capillary measurements collected over 1800 frames. The symbols represent individual capillary data from the 11 animals.

There was a significant decrease in RBC velocity, supply rate, and hematocrit between the pre-PE baseline and PE 10^{-4} ($p < 0.0001$) and PE 10^{-3} M ($p < 0.0001$) doses.

Table 2.5 Hemodynamic measurements in response to increasing doses of phenylephrine.

	Pre-PE Baseline	**PE 10^{-7} M**	**PE 10^{-6} M**	**PE 10^{-5} M**	**PE 10^{-4} M**	**PE 10^{-3} M**
n (Capillaries)	55	66	67	65	67	64
Hematocrit (%)	15.2 ± 2.3	15.5 ± 2.7	12.3 ± 1.6	8.6 ± 1.2	4.0* ± 0.9	4.2* ± 1.4
Velocity (µm/s)	280.9 ± 39.7	266.3 ± 34.6	272.3 ± 36.6	178.0 ± 27.3	82.0* ± 21.8	42.3* ± 12.5
Supply Rate (cells/s)	18.8 ± 3.8	15.13 ± 2.9	13.4 ± 2.7	7.8 ± 1.4	2.9* ± 1.1	2.4* ± 0.9

Note: PE, phenylephrine. ± standard deviation; * $p < 0.0001$ compared to pre-PE baseline; data from 11 animal.

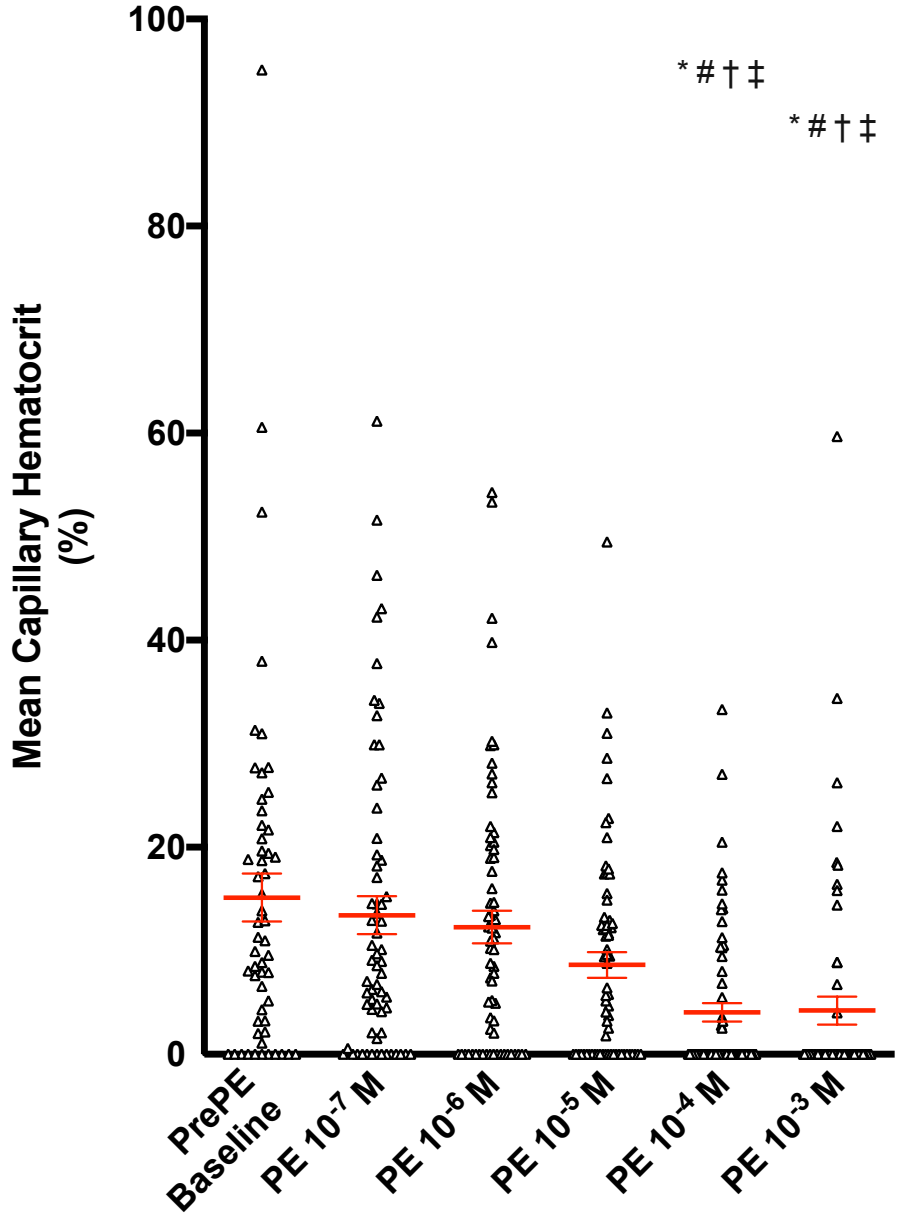

Figure 2.9 Capillary hematocrit in response to increasing doses of phenylephrine. Doses of phenylephrine (PE) from 10^{-7} M to 10^{-3} M were delivered via the microfluidic device. The mean capillary hematocrit at each dose is indicated and error bars represent the standard error of the mean. * p <0.0001 compared to pre-PE baseline, # $p < 0.0001$ compared to 10^{-7} M, † $p < 0.0001$ compared to 10^{-6} M, ‡ $p < 0.0429$ compared to 10^{-5} M. n= 55 to 70 capillaries (in 11 animals)

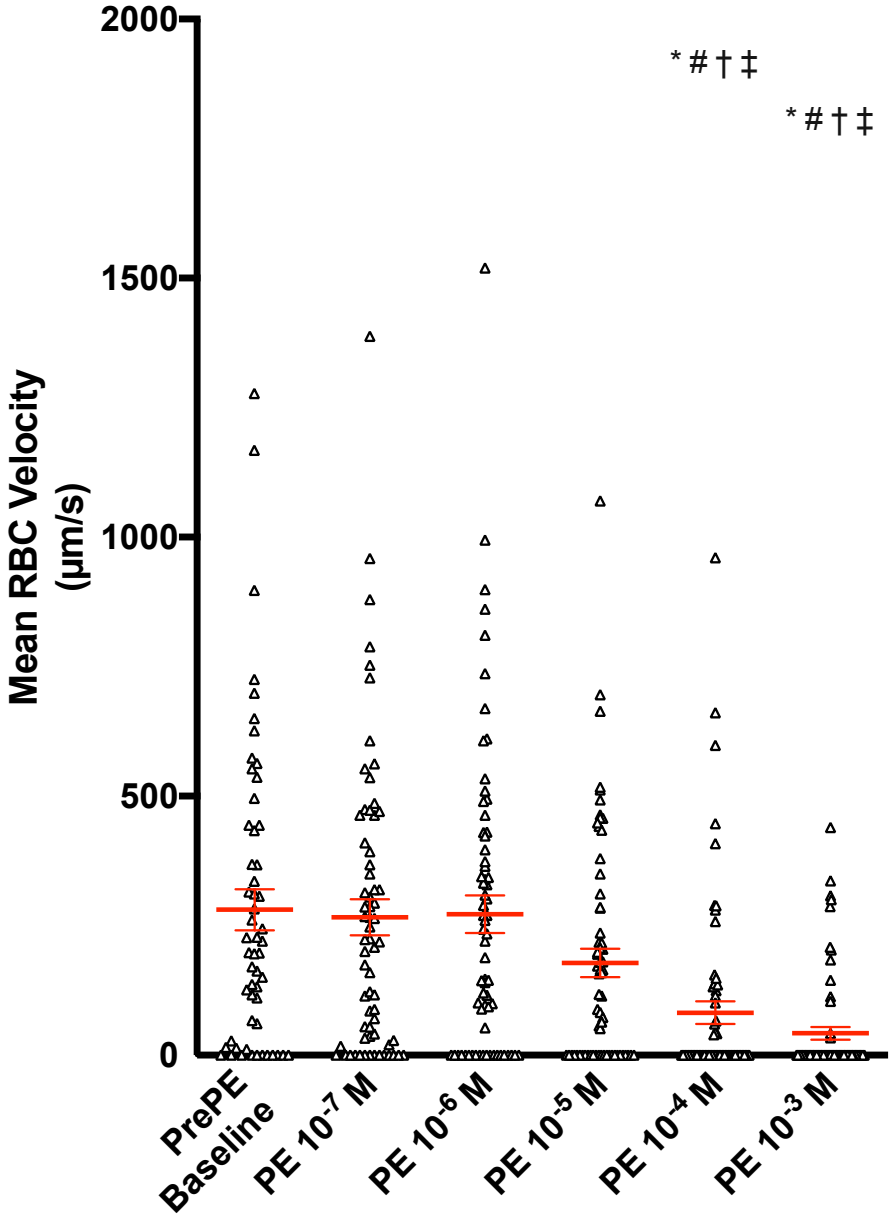

Figure 2.10 Capillary red blood cell velocity in response to increasing doses of phenylephrine. Doses of phenylephrine (PE) from 10^{-7} M to 10^{-3} M were delivered via the microfluidic device. The mean red blood cell (RBC) velocity at each dose is indicated and error bars represent the standard error of the mean. * p <0.0001 compared to pre-PE baseline, # $p < 0.0001$ compared to 10^{-7} M, † $p < 0.0001$ compared to 10^{-6} M, ‡ $p < 0.0268$ compared to 10^{-5} M. n= 55 to 70 capillaries (in 11 animals)

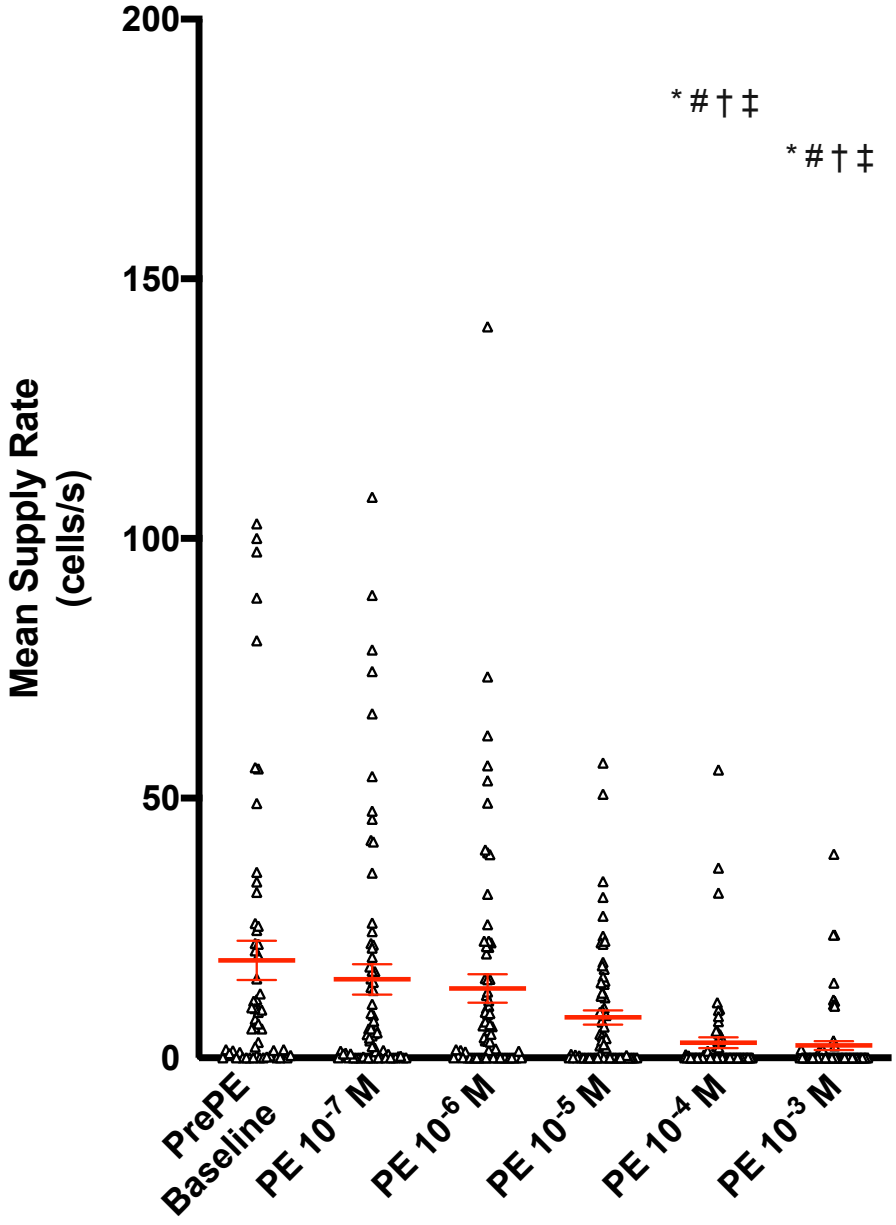

Figure 2.11 Capillary red blood cell supply rate in response to increasing doses of phenylephrine. Doses of phenylephrine (PE) from 10^{-7} M to 10^{-3} M were delivered via the microfluidic device. The mean red blood cell supply rate at each dose is indicated and error bars represent the standard error of the mean. * p <0.0001 compared to pre-PE baseline, # $p < 0.0001$ compared to 10^{-7} M, † $p < 0.0001$ compared to 10^{-6} M, ‡ $p <$ 0.0068 compared to 10^{-5} M. n= 55 to 70 capillaries (in 11 animals)

Hemodynamic measurements of analyzed capillaries in response to increasing doses of ACh are shown in Figure 2.12, Figure 2.13, and Figure 2.14. Individual analyzed capillaries from 5 anaesthetized Sprague-Dawley rats are shown in Table 2.6 for each sequential dose. The numbers of analyzed capillaries varied at each dose due to shifts in focal plane and ability to select vessel segments due to limitation of the analysis software relying on capillary hemodynamics (e.g. high hematocrit, high velocity). Capillaries from each animal were analyzed for each dose. Symbols correspond to the one minute mean of individual capillary measurements collected over 1800 frames. The symbols represent individual capillary data from the 5 animals.

There was a significant increase in RBC velocity between baseline and ACh 10^{-3} M ($p = 0.0014$). There was no significant difference in capillary hematocrit amongst all doses.

Table 2.6 Hemodynamic measurements in response to increasing doses of acetylcholine.

	Baseline	**ACh 10^{-7} M**	**ACh 10^{-6} M**	**ACh 10^{-5} M**	**ACh 10^{-4} M**	**ACh 10^{-3} M**
n (Capillaries)	57	56	57	64	66	67
Hematocrit (%)	18.1 ± 2.4	15.9 ± 2.2	15.0 ± 1.7	16.0 ± 1.9	18.8 ± 2.1	24.1 ± 2.3
Velocity (µm/s)	165.2 ± 20.4	155.4 ± 16.9	205.6 ± 40.4	209.3 ± 34.4	196.9 ± 20.6	270.3* ± 28.3
Supply Rate (cells/s)	9.9 ± 2.0	8.6 ± 1.8	11.4 ± 3.2	11.9 ± 2.7	13.0 ± 2.5	19.6 ± 2.6

Note: ACh, acetylcholine. ± standard deviation; * $p = 0.0014$ compared to baseline; data from 5 animals.

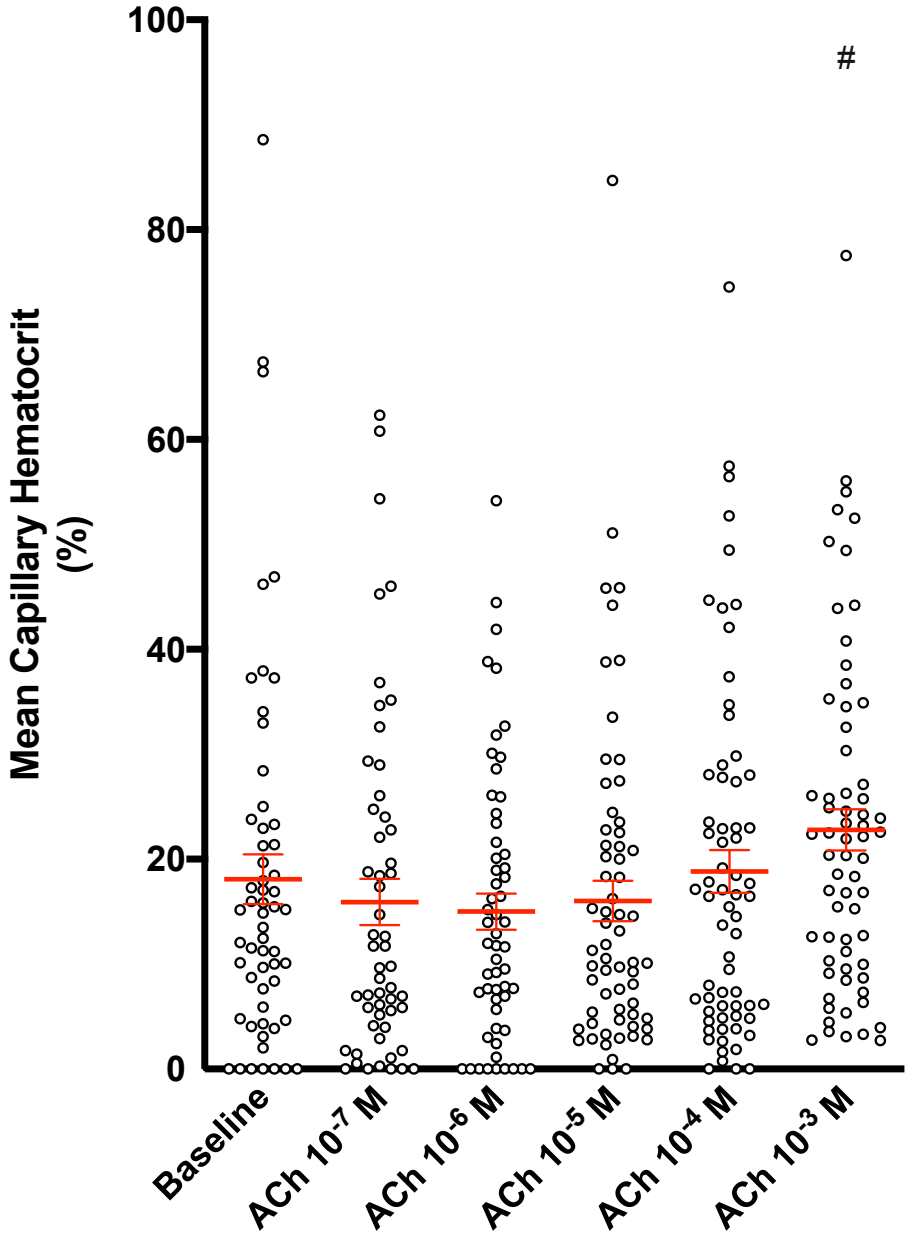

Figure 2.12 Capillary hematocrit in response to increasing doses of acetylcholine. Doses of acetylcholine (ACh) from 10^{-7} to 10^{-3} M were delivered via the microfluidic device. The mean capillary hematocrit at each dose is indicated and error bars represent the standard error of the mean. # $p = 0.0445$ compared to 10^{-7} M. n= 56 to 67 capillaries (in 5 animals)

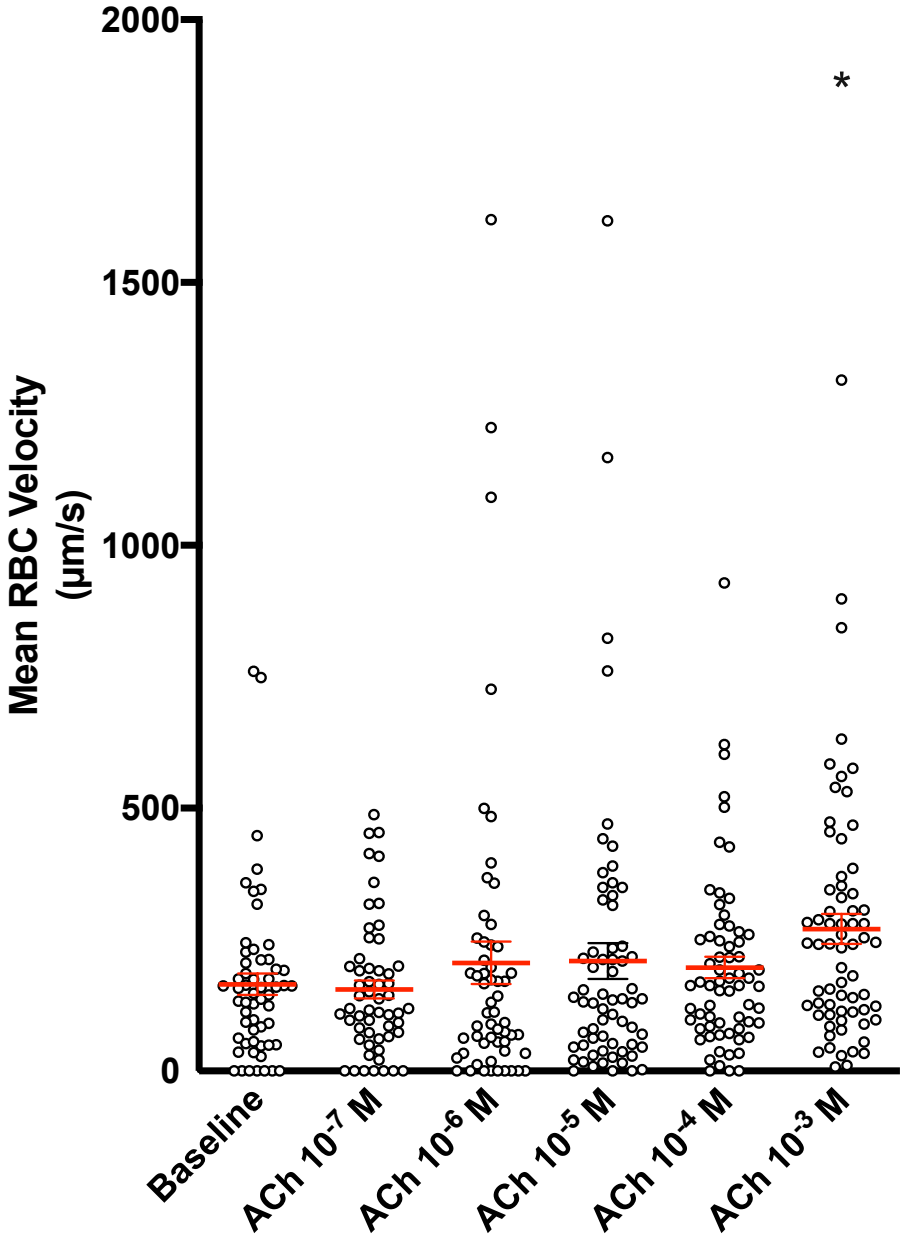

Figure 2.13 Capillary red blood cell velocity in response to increasing doses of acetylcholine. Doses of acetylcholine (ACh) from 10^{-7} to 10^{-3} M were delivered via the microfluidic device. The mean red blood cell (RBC) velocity at each dose is indicated and error bars represent the standard error of the mean. * $p = 0.0014$ compared to baseline. n= 56 to 67 capillaries (in 5 animals)

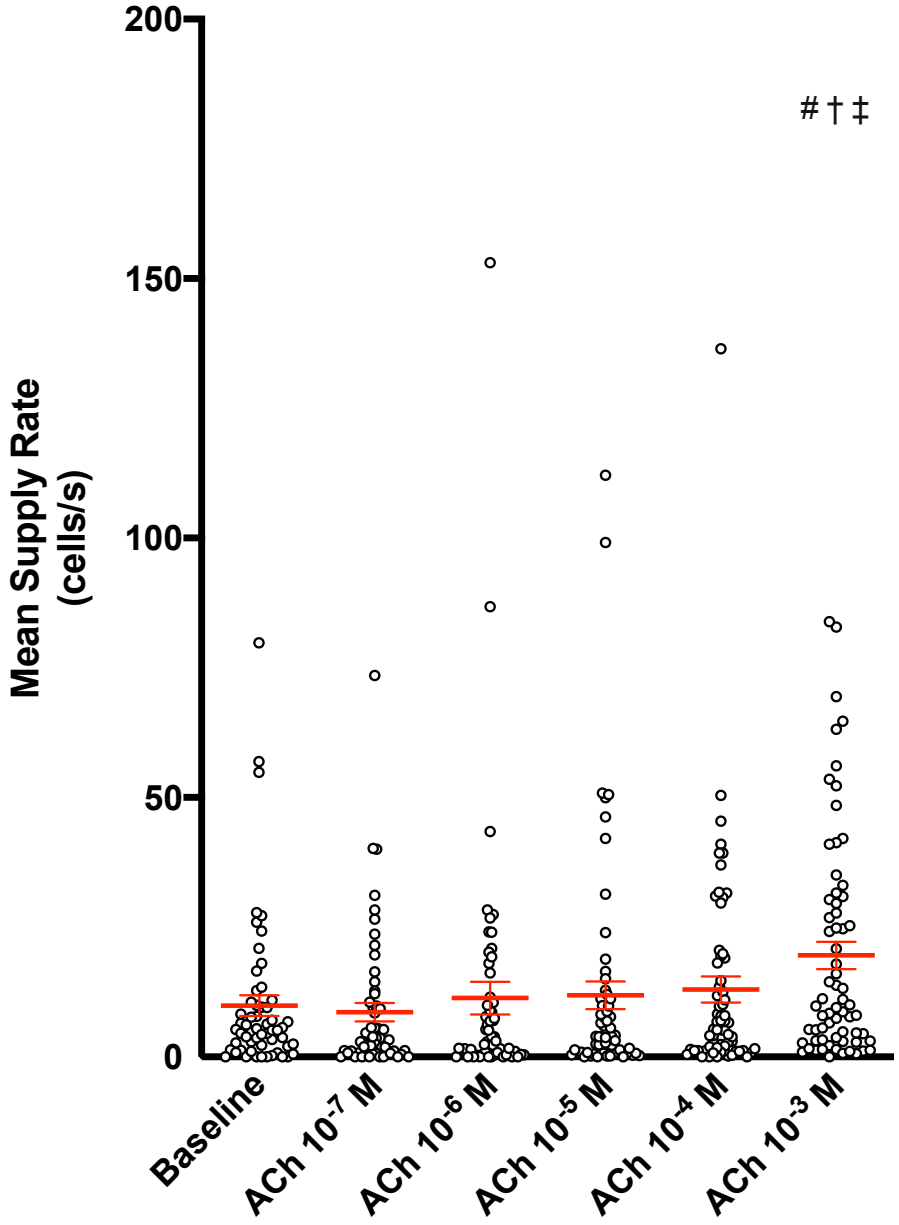

Figure 2.14 Capillary red blood cell supply rate in response to increasing doses of acetylcholine. Doses of acetylcholine (ACh) from 10^{-7} to 10^{-3} M were delivered via the microfluidic device. The mean red blood cell supply rate at each dose is indicated and error bars represent the standard error of the mean. # $p = 0.0013$ compared to 10^{-7} M, † $p = 0.0024$ compared to 10^{-6} M, ‡ $p = 0.0104$ compared to 10^{-5} M. n= 56 to 67 capillaries (in 5 animals)

2.3.3. Functional Perfusion Maps

Extended depth of field captures are used to record all RBC perfused vessels within the first 100 μm of the EDL muscle surface. These captures record vessels overlying and surrounding the micro-outlet while qualitatively showing the effect of the highest does of ATP, ACh, and PE. Figure 2.15 shows the highest dose of ATP (10^{-3} M) results in the area overlying the micro-outlet and the immediate surrounding areas have higher number of vessels perfused compared to the number of perfused vessels at baseline. The vasodilatory effect of 10^{-3} M ATP was limited to vessels within ~300 μm of the window and those which were connect to vessel segments passing directly over the micro-outlet. The vessels beyond this area, seen to the left and right sides of the micro-outlet, appear similar under baseline and ATP 10^{-3} M perfusion conditions. The extended depth of field map in Figure 2.16 shows the flowing vessels overlying the micro-outlet while PE 10^{-4} M was delivered to the muscle via the microfluidic device. The decrease in RBC supply, and visible vessels, overlying the window due to local vasoconstriction was limited to within 500 μm of the window compared to the vessels shown at baseline. The number of vessels beyond 500 μm from the micro-outlet in all directions appear similar in response to PE 10^{-4} M and baseline.

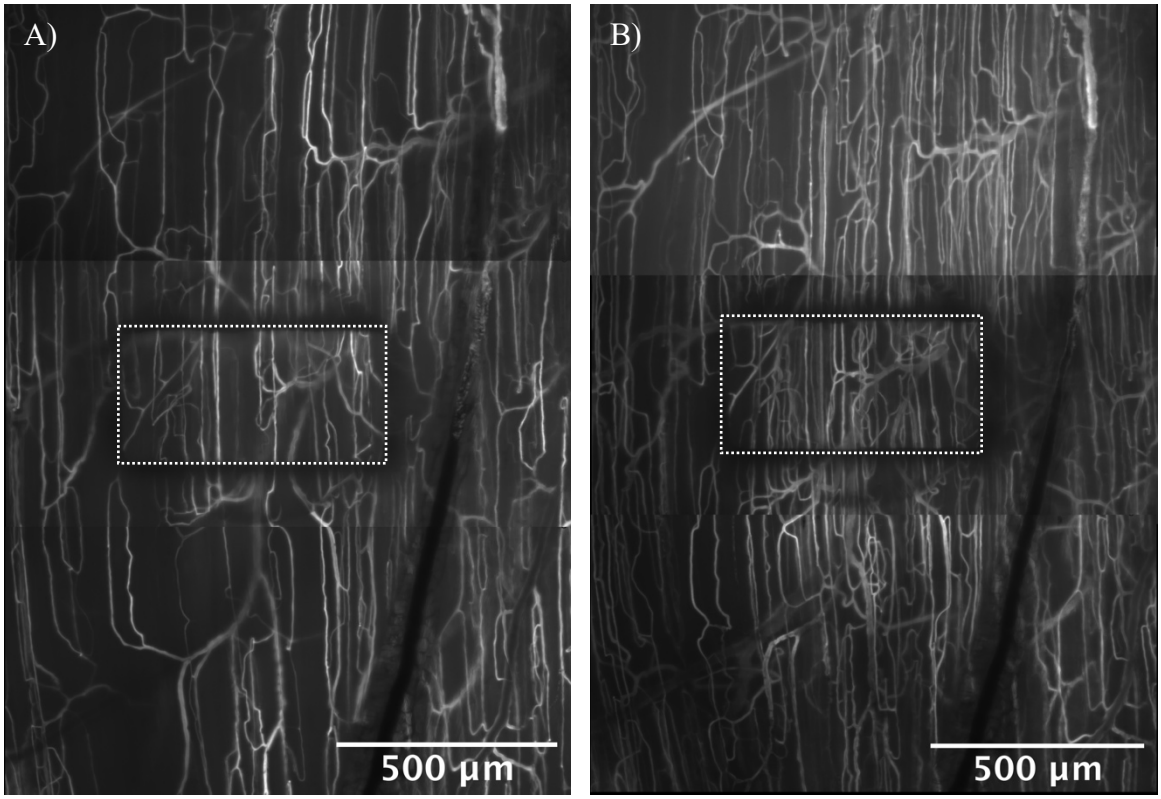

Figure 2.15 Sum of absolute difference functional image of microvascular flow at the highest dose of adenosine triphosphate. Images show perfused vessels within the first 100 µm of the surface of the extensor digitorum longus muscle of an anesthetized Sprague-Dawley rat positioned over a 300 x 600 µm micro-outlet indicated by the dotted rectangle and a liquid microfluidic device perfused with A) Krebs solution (baseline) and B) adenosine triphosphate 10^{-3} M concentration.

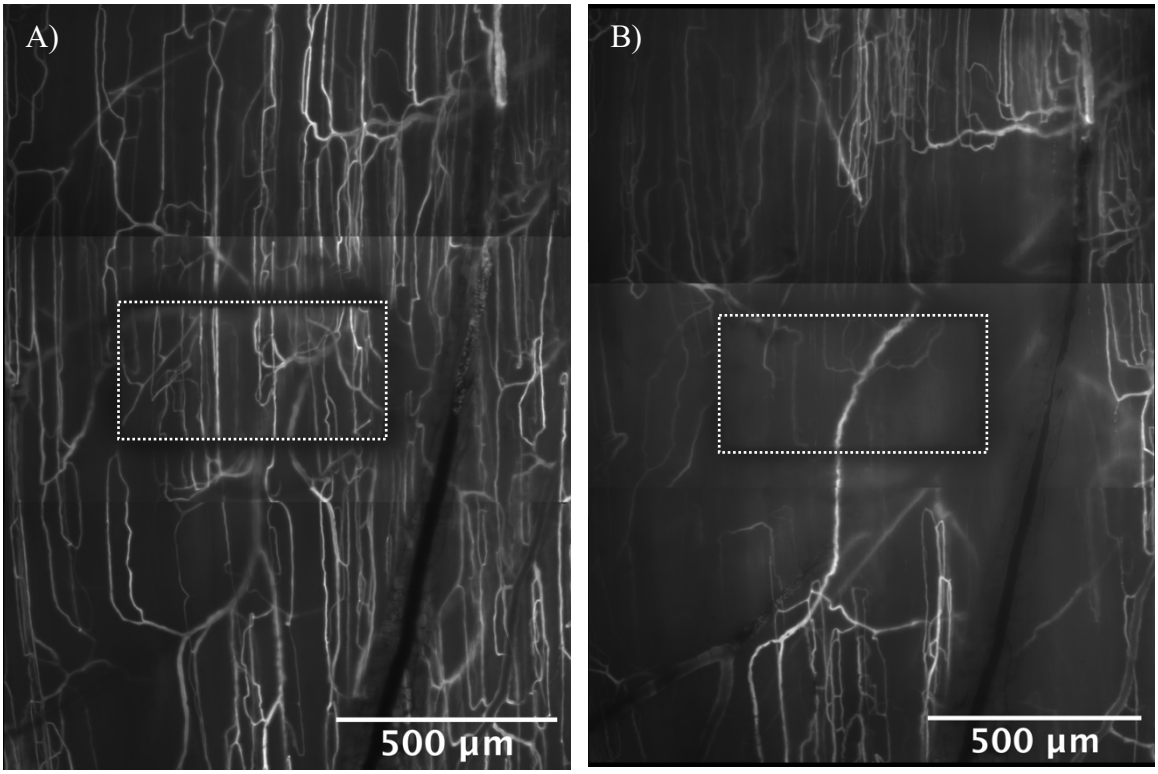

Figure 2.16 Sum of absolute difference functional image of microvascular flow at the highest dose of phenylephrine. Images show perfused vessels within the first 100 µm of the surface of the extensor digitorum longus muscle of an anesthetized Sprague-Dawley rat positioned over a 300 x 600 µm micro-outlet indicated by the dotted rectangle and a liquid microfluidic device perfused with A) Krebs solution (baseline) and B) phenylephrine 10^{-4} M concentration. Vessels receiving zero RBCs do not appear in the functional images.

2.3.4. Tissue Mass Transport Model Results

Simulations were completed to predict tissue concentrations for each dose of ACh, ATP, and PE. Drug levels in the modelled volume of tissue were largely dependent on the boundary condition set at the exchange window and rate of removal within the volume itself. Representative colour maps of the modelling results are shown for 10^{-4} M ATP in Figure 2.17. As expected, the highest concentration of ATP is found at the surface of the tissue in contact with the exchange window, with isolines illustrating the location of 10^{-5} and 10^{-6} M ATP. This result illustrates a steep decrease in concentration with increasing distance from the exchange window, falling by two orders of magnitude within 240 µm of the edge of the window in both the x and y directions, and by 300 µm in the z direction. The increase in the concentration of ATP within the simulated microfluidic channel raise the concentrations proportionally within the tissue. The tissue ATP concentration throughout the tissue volume was generally greater than 3.47×10^{-7} M primarily due to our initial assumption of ATP levels in the blood (C_b) (Wood et al., 2009). As such, concentrations below 10^{-7} M (data not shown) had little effect on increasing tissue ATP in our simulations.

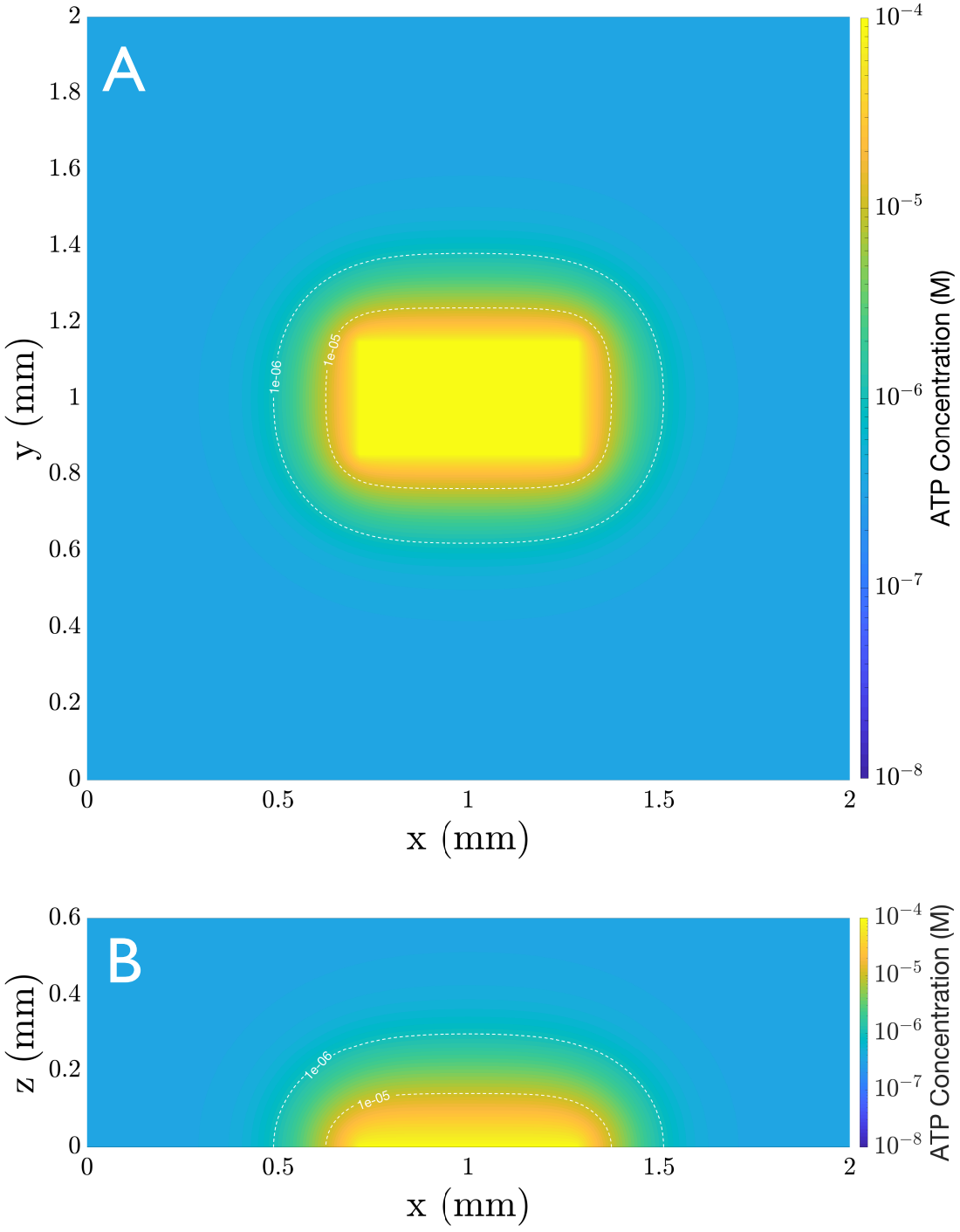
A
B
y (mm)
z (mm)
x (mm)
x (mm)
ATP Concentration (M)
ATP Concentration (M)
1e-06
1e-05
1e-06
1e-05

Figure 2.17 Mass transport model results for adenosine triphosphate 10^{-4} M. The log scale colour map shows the predicted tissue concentrations with 10^{-4} M adenosine triphosphate at the micro-outlet. Panel A shows the gradients at the surface of the tissue closest to the microfluidic device, in the same perspective as the micrographs shown in Figure 2.15. Panel B illustrates the tissue adenosine triphosphate concentrations perpendicular to the x-y plane centred at the middle of the micro-outlet. Contour lines indicate the position of 10^{-6} and 10^{-5} M adenosine triphosphate within the tissue volume in each panel. Concentrations throughout the volume were above 3.47×10^{-7} M due to the initial assumption of blood adenosine triphosphate as detailed in Table 2.1.

The modelling results for ACh and PE differ somewhat from ATP due to the assumed blood concentrations of zero for both drugs. In the model, gradients for both ACh and PE were extremely similar at equivalent concentrations due to low rates of degradation within the tissue volume (data not shown). Similarly, the simulation results largely scale with concentration at the micro-outlet. Predicted concentrations for PE at 10^{-4} M are shown in Figure 2.18 and provide a clear representation of the gradients within the tissue for both drugs. As with the simulations for ATP, there is a steep decrease in PE concentration with increasing distance as shown by the contour lines that indicate the spatial position of PE concentrations from 10^{-5} to 10^{-8} M at the tissue surface and in the tissue cross section. PE concentrations decrease by five orders of magnitude within 475 µm of the edge of the window in both the x and y directions, and by 550 µm in the z direction. PE concentrations decrease to below 2×10^{-13} M in the corners of the 2000 x 2000 µm tissue volume. The predicted time-dependent change in tissue concentration for the 10^{-4} M PE simulation in are shown in Figure 2.19. The curves illustrated are for points centred in the x-y plane of the micro-outlet at increasing distances from the window. These transients show a rapid time course to pseudo-steady state in regions that are within 200 µm of the micro-outlet. Time to pseudo-steady state for the entire volume was <6 minutes for each drug concentration simulated.

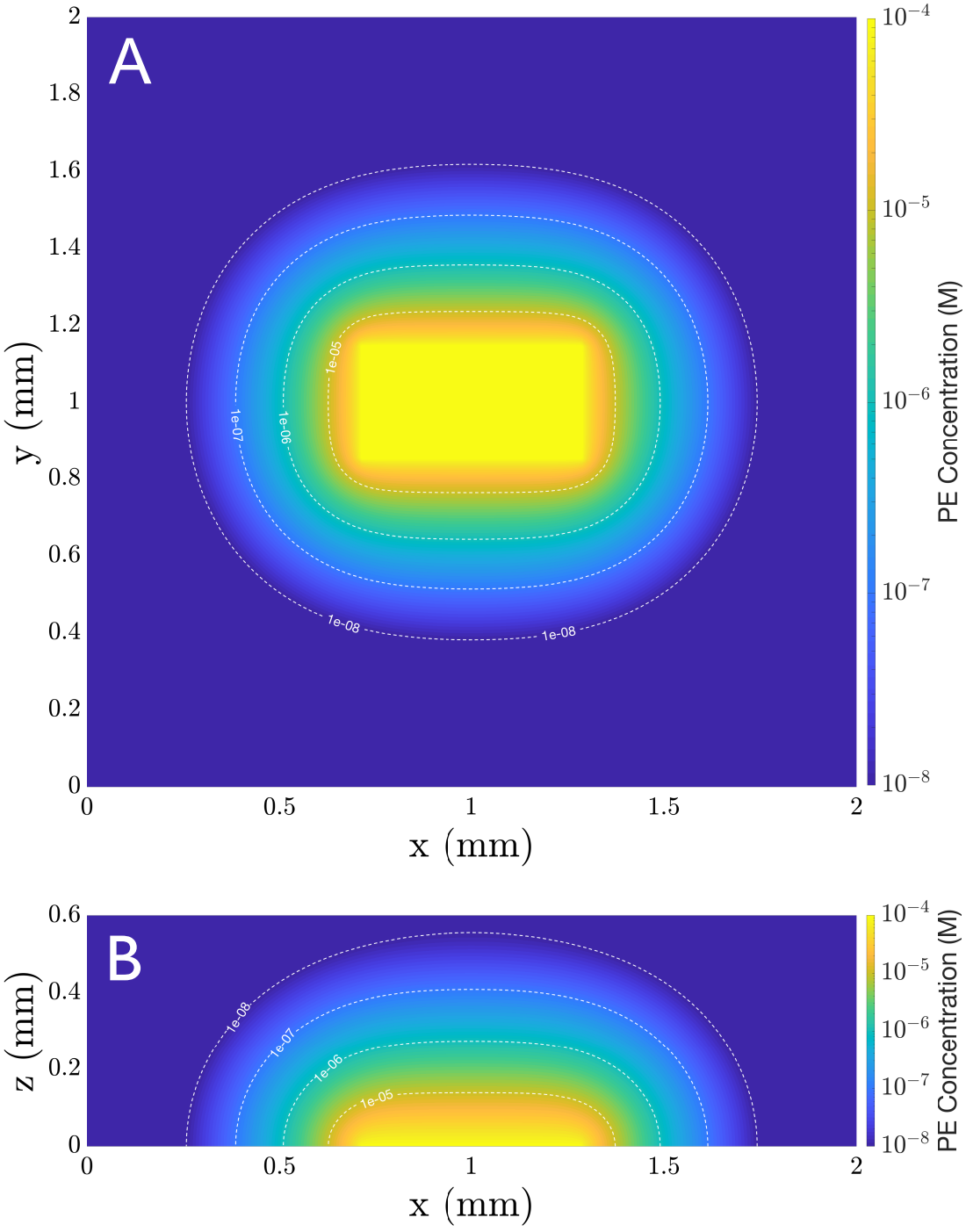
A
B
y (mm)
z (mm)
x (mm)
x (mm)
PE Concentration (M)
PE Concentration (M)
1e-05
1e-06
1e-07
1e-08
1e-08
1e-05
1e-06
1e-07
1e-08

Figure 2.18 Mass transport model results for 10^{-4} M phenylephrine. The log scale colour map shows the predicted tissue concentrations of phenylephrine with 10^{-4} M at the micro-outlet. Panel A shows the gradients at the surface of the tissue closest to the microfluidic device, in the same perspective as the micrographs shown in Figure 2.16. Panel B illustrates the tissue phenylephrine concentrations perpendicular to the x-y plane centred at the middle of the micro-outlet. Contour lines indicate the distribution PE concentrations ranging from 10^{-5} to 10^{-8} M phenylephrine within the tissue volume in each panel.

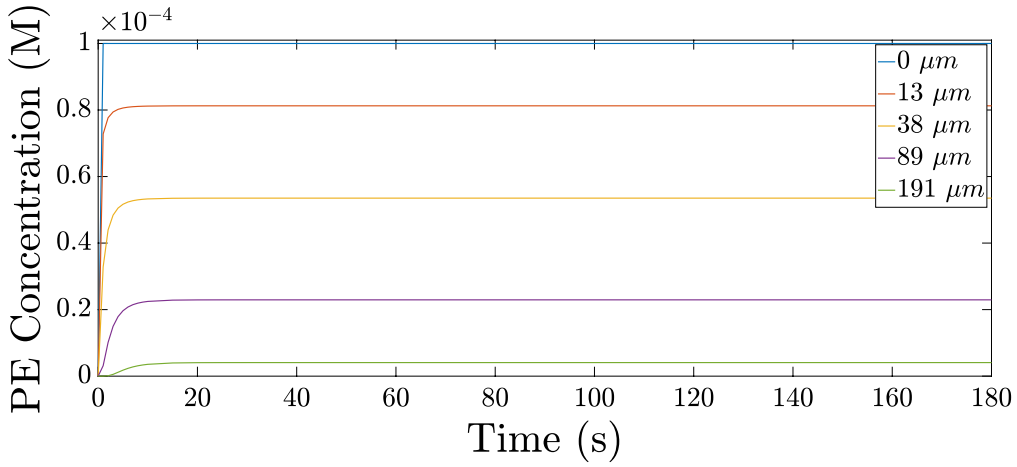

Figure 2.19 Time-dependant changes in tissue phenylephrine as predicted by the mass transport model for 10^{-4} M phenylephrine. The curves illustrate the concentration at different depths in the tissue centred at the middle of the micro-outlet when the device is perfused with 10^{-4} M phenylephrine. As expected, time to pseudo-steady state increases with distance from the micro-outlet surface. The time transients are consistent with experimentally observed changes in blood flow following introduction of high doses of phenylephrine.

2.4. Discussion

The goal of the current study was to develop a microfluidic apparatus capable of delivering vasoactive drugs to a microscale region of skeletal muscle while simultaneously visualizing and recording the capillary blood flow directly overlying the device and in surrounding areas for offline analysis. This was achieved by using soft lithographic techniques to mould a fluid channel into PDMS and bonding it to a glass slide. Precision laser cut micro-outlets were designed and manufactured using borosilicate glass coverslips. When mated to channel openings these 600 x 300 μm micro-outlets became the interface between the fluid in the channel and the EDL muscle itself. The apparatus was also composed of tubing inlet and outlet supports to allow fluid flow from a reservoir through the device and to the waste fluid collection point. The microfluidic apparatus was designed to establish a slight negative pressure at the window to both ensure a seal between the fluid channel and the muscle as well as facilitate flow of fluid through the device.

Administration of increasing doses of vasoactive drugs were used to validate that the device could deliver agents diffusively to the vasculature of skeletal muscle tissue. As expected, capillary RBC velocity and supply rate increased at the high doses of vasodilators, ATP and ACh. In contrast, the highest doses of PE resulted in a decrease in capillary velocity and supply rate. The capability to administer drugs to a microscale region of tissue continuously, while simultaneously visualizing microvascular blood flow in a specific region of tissue, is highly desirable when determining the interaction of multiple blood flow regulation mechanisms. The ability to position the micro-outlet to

interact with specific vascular structures also allows for targeted delivery to desired elements of the microcirculatory system including examining the effects caused by administering various substances to capillary networks, venules or arterioles. Thus, we have demonstrated that this novel technique allows for specific interactions with the microcirculation in a spatially confined micro scale region.

For the present study, we applied a range of ATP doses selected based on previous work in gluteus maximus superfusion preparations (Nyberg et al., 2013). Previous investigators showed significant vasodilation and increase in blood flow in second order arteriole (2A) and third order arteriole (3A) order arterioles in response to 5 x 10^{-6} M ATP administered via superfusion solution. Abluminal application of ATP has been documented to have a biphasic vasodilatory response in the cremaster muscle preparation (Dora, 2017). An increase in upstream vessel diameter leading to an increase in capillary RBC supply rate and velocity is expected from increasing doses of ATP. This is what was observed in the gluteus maximus muscle preparation as application of ATP causes vasodilation at 5 x 10^{-6} M (Lohman et al., 2012; Nyberg et al., 2013). In our preparation, the mean capillary supply rate and velocity response to ATP is similar to what was seen in other preparations, with the highest doses 10^{-4} and 10^{-3} M causing a significant increase in overall capillary supply rate, and a dose of 10^{-3} M resulting in a significant increase in velocity to the capillaries within the window. This increase may be partly due to ATP acting on $P2X_4$, $P2Y_1$, and $P2Y_2$ receptors of endothelial cells which leads to arteriolar vasodilation (Burnstock, 2006; Lohman et al., 2012). ATP is metabolised into adenosine diphosphate, adenosine monophosphate and adenosine, all of which have respective vasodilatory signalling mechanisms. Modelling results for ATP

indicate that vessels deeper than 100 μm in the tissue are expected to be exposed to concentrations an order of magnitude lower than the dose flowing through the microfluidic channel. Further, predicted concentrations of ATP within the majority of the tissue volume were ~3.47 x 10^{-7} M, which are comparable to reported interstitial concentrations of 1.6 x 10^{-7} M obtained via microdialysis (Li et al., 2005). If tissue ATP concentrations are indeed within this range, doses within two orders of magnitude of the mean tissue concentration will only affect microvessels close to the surface of the window, making targeting individual capillary beds and terminal arterioles near the surface highly viable.

The range of PE doses were also based on concentrations that cause significant vasoconstriction in superfusion preparations (Moore et al., 2010). Previous work has shown that a 10^{-7} M PE dose lead to a significant vasoconstriction at first order arterioles, as well as 2A, and 3A arterioles. We administered doses between 10^{-7} and 10^{-3} M through the microfluidic device which lead to the significant decrease in the red cell velocity, and supply rate from the 10^{-4} dose to 10^{-3} M. This suggests that these doses of PE lead to the constriction of arterioles leading to the capillary networks that we measured within the window, effectively shutting down RBC supply to this localized area. Predicted tissue gradients of PE based on the mass transport model (Figure 2.18) indicate a steep drop in tissue concentration with distance. The concentrations at a distance from the surface would be substantially lower than what would be expected if similar doses were applied in a superfusion solution. Indeed, PE concentration decreased to 10^{-8} M by 550 μm, and as the relative concentration scales with the delivered dose there is a strong potential to

target a given concentration to specific microvasculature based on distance from the window.

As detailed above, the vasodilator ACh was also applied with our device as it is a common positive control used in many preparations *in vivo* and *ex vivo* to test the vascular reactivity of the tissue (Furchgott & Zawadzki, 1980; Emerson & Segal, 2000; Welsh et al., 2018). The concentrations that were selected were based on those reported using superfusion solution using abluminal application of doses ranging from 10^{-9} to 10^{-4} M that resulted in vasodilation (Dua et al., 2009). We expected a strong vasodilatory response from ACh via action on endothelial muscarinic receptors, which stimulate the release of nitric oxide, and causes subsequent relaxation of smooth muscle cells. Surprisingly, the responses to the lower 4 doses of ACh were not significantly different from the baseline measurements. This is not what is seen in other preparations where the arteriolar diameter diameter response to ACh has an effect at doses as low as 10^{-8} M (Dua et al., 2009). The absence of a significant increase in RBC velocity and supply rate at lower doses is potentially due to the breakdown of ACh by acetylcholinesterase. However, at 10^{-3} M there was a significant increase in RBC velocity and supply rate. Although ACh effect the M3 receptors of endothelial cells results in vasodilation, a potential avenue for constriction may be the effect of ACh on the M3 and M2 receptors on the vascular smooth muscle cells at high doses, while nitric oxide release is impaired (Toda & Okamura, 2003; Amiya et al., 2014). This effect is unlikely in the current approach due to the limited area exposed to the high doses of ACh. A limitation of this approach is that prolonged exposure to high doses of ACh may cause confounding response to ACh over time. Similar gradients and scalability as described for PE was

observed in the simulations for ACh. We would expect lower tissue concentrations of ACh compared to PE due to the activity of acetylcholinesterase in skeletal muscle (Kiss et al., 2001). However, the modelling result derived from ACh degradation rates reported in the literature did not predict a notable impact in tissue ACh concentrations from enzymatic breakdown. Erythrocytes contain acetylcholinesterases and can contribute to the enzymatic breakdown of ACh at high and low flow states (Herz & Kaplan, 1973). It is possible that there is some heterogeneity of ACh breakdown across the tissue due to the variation in hematocrit between individual capillaries.

Extended depth of field maps provide qualitative information relating to the number of vessels flowing within the first 100 μm of the muscle. These maps include vessels close to the muscle surface both at and around the micro-outlet. Each EDF map taken at the highest doses of each vasoactive drug shows a spatially constrained region of effect of the vasoactive drugs. The vasoactive drugs are delivered through diffusive exchange from the channel and micro-outlets into the surface of the muscle. The relative tissue concentration of the drug from the micro-outlet decreases as it diffuses outwards from the window. This is similar to the previously described relative tissue O_2 concentrations using micro-outlets on a gas based microfluidic device (Ghonaim et al., 2011). The more distant from the micro-outlet, both into the tissue and surrounding area, the lower the drug concentration will be, therefore having less effect on the vasculature. Some convective exchange may be expected due to the drugs diffusing into the vasculature and being carried downstream to the venules which may have an effect on blood flow. However, the region of effect of the highest dose of vasoactive drugs, as shown by the EDF maps, is constrained to within 500 μm of the micro-outlet.

The protocol for changing between doses was to change the fluid and wait a minimum of 3 minutes to ensure equilibration within the tissue to the new dose flowing through the channel. Blood flow responses were observed in 30 to 45 seconds in pilot experiments and it was determined that a 3 minute wait time was sufficient to reach pseudo-steady state within the micro-outlet. Following sequential doses and administration of vasoactive drugs for extended periods of time surpassing one hour, the time to return to baseline was observed to extend to beyond one hour (data not shown). However, in a subset of experiments when vasoactive drugs were administered at highest doses for a shorter period of time, 10^{-3} M PE for 10 minutes, a 15 minute washout with Krebs solution led to a qualitative return to baseline flow (data not shown). The modelling results predict a much shorter time-dependant change in tissue concentration (Figure 2.19), which increases with distance from the micro-outlet. Indeed, based on the mathematical model we would expect the time to steady state of the capillaries observed *in vivo* to be well within the equilibration time at each experimental dose.

The positioning of the muscle over the micro-outlet is challenging. There is limited ability to reposition the muscle once the device and muscle are set up. Once assembled, the response to the doses administered by the device depends on the location of the micro-outlet and the vasculature around it. As each muscle has a different structure and orientation of the capillary networks it can be challenging to place the muscle in a location that allows for consistency in spatial orientation from the window to the terminal arterioles or collecting venules. Other preparations, such as superfusion with application via micropipette, allow for consistent selection of arterioles of the same level, 2A or 3A, amongst animals even in which there is individual variation in orientation and number of

vessels (Charter et al., 2018). However, applications via this method do not allow for continuous administration of substances to a spatially specific region of tissue. The underlying vasculature deeper in the muscle can also be affected by the drug concentrations as they diffuse into the muscle as previously described leading to a more widespread area of affect.

Due to the time to return to baseline, limiting drug administrations to one or two vasoactive substances in a single experiment would be beneficial for ensuring the muscle quickly returns to baseline function following high doses without extending the period of time during observation. Decreases in the time exposure of the drug would be another potential method to oppose this extended washout. However, due to the small number of capillaries overlying the micro-outlet, it is necessary to record multiple focal planes to maximize the data collected at each dose. Collection of additional focal plane recordings necessarily extends the duration of acquisition and hence exposure of the tissue to each drug dose. Future experiments could focus on administration of one vasoactive drug per experiment. Recording additional focal planes overlying the micro-outlet per dose, and recording microvascular blood flow at a distance adjacent to the window, would increase the number of capillaries sampled with the caveat of a longer overall recording time. Given technical limitations, the addition of recordings to each drug in one experiment is impractical as the additional time required causes concern of device failure, and data storage limits. Randomization and blinding during the experiment and analysis could also be incorporated in future experiments to avoid observer bias.

Additional experiments considering the area of effect using fluorescent dye would serve to quantify both the spatial gradients and total tissue volume affected with greater

accuracy. Direct empirical quantification of tissue concentrations using this approach could be used to further tune the predictions from the mass transport model. The use of substances that will act specifically on receptors of interest rather than molecules that have multiple conflicting responses would aid in determining the area of effect that we observed especially with ACh. The use of our microfluidic device and intravascular injection of various agents could be easily combined to investigate blood flow regulatory mechanisms at specific scales of vasculature. The microfluidic device could also be adapted for use in tissues other than skeletal muscle such as in the mesentery, other striated muscle, and the liver to deliver drugs of interest to microscale regions in a spatially confined area. Combining additional micro-outlets and channels to the devices would allow for simultaneous administration of various drug combinations to several networks for further studies into the area of effect. Further refinements of the current microfluidic device design could reduce the perfused fluid volumes facilitating studies utilizing reagents that are costly or otherwise difficult to procure.

This novel microfluidic device may allow researchers to study the signalling mechanisms of the microcirculation in animals in healthy and diseased states by manipulating the local microvasculature. This device is capable of maintaining continuous delivery of substance at known concentrations to a confined microscale region of tissue which cannot be accomplished with previous methods. Furthermore, blood flow regulatory mechanisms can be identified and interrogated, leading to development of potential pharmacological targets. This device can also be modified to target specific vasculature structures through the modification of the window size and orientation, along with selection of an appropriate dose of vasoactive drugs to limit the area of effect both

around the micro-outlet and into the tissue. Modifications to orientation of the channel within the device is possible to improve usage in other tissue and organ preparations for interrogation of local tissue environments.

References

Abgrall, P., & Gué, A.-M. (2007). Lab-on-chip technologies: making a microfluidic network and coupling it into a complete microsystem—a review. *Journal of Micromechanics and Microengineering, 17*(5), R15-R49. doi:10.1088/0960-1317/17/5/R01

Amiya, E., Watanabe, M., & Komuro, I. (2014). The Relationship between Vascular Function and the Autonomic Nervous System. *Annals of Vascular Diseases, 7*(2), 109-119. doi:10.3400/avd.ra.14-00048

Ascher, U. M., Ruuth, S. J., & Wetton, B. T. (1995). Implicit-explicit methods for time-dependent partial differential equations. *SIAM Journal on Numerical Analysis, 32*(3), 797-823.

Bagher, P., & Segal, S. S. (2011a). The Mouse Cremaster Muscle Preparation for Intravital Imaging of the Microcirculation. *Journal of Visualized Experiments*(52). doi:10.3791/2874

Bagher, P., & Segal, S. S. (2011b). Regulation of blood flow in the microcirculation: role of conducted vasodilation. *Acta Physiologica (Oxford, England), 202*(3), 271-284. doi:10.1111/j.1748-1716.2010.02244.x

Bentley, T. B., Meng, H., & Pittman, R. N. (1993). Temperature dependence of oxygen diffusion and consumption in mammalian striated muscle. *The American Journal of Physiology, 264*(6 Pt 2), H1825-1830. doi:10.1152/ajpheart.1993.264.6.H1825

Bevan, J. A., & Török, J. (1970). Movement of norepinephrine through the media of rabbit aorta. *Circulation Research, 27*(3), 325-331. doi:10.1161/01.res.27.3.325

Bosetti, F., Galis, Z. S., Bynoe, M. S., Charette, M., Cipolla, M. J., del Zoppo, G. J., . . . Zlokovic, B. V. (2016). "Small Blood Vessels: Big Health Problems?": Scientific Recommendations of the National Institutes of Health Workshop. *Journal of the American Heart Association, 5*(11), 657-612. doi:10.1161/JAHA.116.004389

Bridges, L. E., Williams, C. L., Pointer, M. A., & Awumey, E. M. (2011). Mesenteric artery contraction and relaxation studies using automated wire myography. *Journal of Visualized Experiments : JoVE*(55). doi:10.3791/3119

Brozovich, F. V., Nicholson, C. J., Degen, C. V., Gao, Y. Z., Aggarwal, M., & Morgan, K. G. (2016). Mechanisms of Vascular Smooth Muscle Contraction and the Basis for Pharmacologic Treatment of Smooth Muscle Disorders. *Pharmacological Reviews, 68*(2), 476-532. doi:10.1124/pr.115.010652

Burnstock, G. (2006). Vessel tone and remodeling. *Nature Medicine, 12*(1), 16-17. doi:10.1038/nm0106-16

Buus, N. H., VanBavel, E., & Mulvany, M. J. (1994). Differences in sensitivity of rat mesenteric small arteries to agonists when studied as ring preparations or as cannulated preparations. *British Journal of Pharmacology, 112*(2), 579-587. doi:10.1111/j.1476-5381.1994.tb13114.x

Charter, M. E., Lamb, I. R., & Murrant, C. L. (2018). Arteriolar and capillary responses to CO2 and H+ in hamster skeletal muscle microvasculature: Implications for active hyperemia. *Microcirculation (New York, N.Y. : 1994), 25*(7), e12494. doi:10.1111/micc.12494

de Graaf, R. A., van Kranenburg, A., & Nicolay, K. (2000). In vivo (31)P-NMR diffusion spectroscopy of ATP and phosphocreatine in rat skeletal muscle. *Biophysical Journal, 78*(4), 1657-1664. doi:10.1016/S0006-3495(00)76717-8

Dora, K. A. (2017). Conducted dilatation to ATP and K+ in rat skeletal muscle arterioles. *Acta Physiologica (Oxford, England), 219*(1), 202-218. doi:10.1111/apha.12656

Dua, A. K., Dua, N., & Murrant, C. L. (2009). Skeletal muscle contraction-induced vasodilator complement production is dependent on stimulus and contraction frequency. *American Journal of Physiology. Heart and Circulatory Physiology, 297*(1), H433-442. doi:10.1152/ajpheart.00216.2009

Duling, B. R., & Berne, R. M. (1970). Propagated vasodilation in the microcirculation of the hamster cheek pouch. *Circulation Research, 26*(2), 163-170. doi:10.1161/01.RES.26.2.163

Duza, T., & Sarelius, I. H. (2003). Conducted dilations initiated by purines in arterioles are endothelium dependent and require endothelial Ca2+. *American Journal of Physiology. Heart and Circulatory Physiology, 285*(1), H26-H37. doi:10.1152/ajpheart.00788.2002

Ellis, C. G., Ellsworth, M. L., Pittman, R. N., & Burgess, W. L. (1992). Application of image analysis for evaluation of red blood cell dynamics in capillaries. *Microvascular Research, 44*(2), 214-225. doi:10.1016/0026-2862(92)90081-Y

Emerson, G. G., & Segal, S. S. (2000). Endothelial cell pathway for conduction of hyperpolarization and vasodilation along hamster feed artery. *Circulation Research, 86*(1), 94-100.

Fraser, G. M., Milkovich, S., Goldman, D., & Ellis, C. G. (2012b). Mapping 3-D functional capillary geometry in rat skeletal muscle in vivo. *American Journal of Physiology. Heart and Circulatory Physiology, 302*(3), H654-664. doi:10.1152/ajpheart.01185.2010

Furchgott, R. F., & Zawadzki, J. V. (1980). The obligatory role of endothelial cells in the relaxation of arterial smooth muscle by acetylcholine. *Nature, 288*(5789), 373-376. doi:10.1038/288373a0

Ghannad-Rezaie, M., Wang, X., Mishra, B., Collins, C., & Chronis, N. (2012). Microfluidic chips for in vivo imaging of cellular responses to neural injury in Drosophila larvae. *PloS One, 7*(1), e29869. doi:10.1371/journal.pone.0029869

Ghonaim, N. W., Fraser, G. M., Ellis, C. G., Yang, J., & Goldman, D. (2013). Modeling steady state SO2-dependent changes in capillary ATP concentration using novel O2 micro-delivery methods. *Frontiers in Physiology, 4*, 260. doi:10.3389/fphys.2013.00260

Ghonaim, N. W., Lau, L. W. M., Goldman, D., Ellis, C. G., & Yang, J. (2011). A micro-delivery approach for studying microvascular responses to localized oxygen delivery. *Microcirculation (New York, N.Y. : 1994), 18*(8), 646-654. doi:10.1111/j.1549-8719.2011.00132.x

Goldman, D. (2008). A mathematical model of oxygen transport in intact muscle with imposed surface oscillations. *Mathematical Biosciences, 213*(1), 18-28. doi:10.1016/j.mbs.2008.01.010

Herz, F., & Kaplan, E. (1973). A review: human erythrocyte acetylcholinesterase. *Pediatric Research, 7*(4), 204-214. doi:10.1203/00006450-197304000-00024

J. Nickolls, I. B., and M. Garland. (2008). Scalable parallel programming,. *2008 IEEE Hot Chips 20 Symposium (HCS)*, 40-53.

Jackson, D. N., Moore, A. W., & Segal, S. S. (2010). Blunting of rapid onset vasodilatation and blood flow restriction in arterioles of exercising skeletal muscle with ageing in male mice. *The Journal of Physiology, 588*(Pt 12), 2269-2282. doi:10.1113/jphysiol.2010.189811

Kimura, H., Sakai, Y., & Fujii, T. (2018). Organ/body-on-a-chip based on microfluidic technology for drug discovery. *Drug Metabolism and Pharmacokinetics, 33*(1), 43-48. doi:10.1016/j.dmpk.2017.11.003

Kiss, G., Somogyi, J., Csermely, P., Szelényi, J., & Vér, A. (2001). Streptozotocin-induced diabetes alters the oligomerization pattern of acetylcholinesterase in rat skeletal muscle. *Diabetologia, 44*(2), 220-223. doi:10.1007/s001250051602

Krogh, A. (1919). The supply of oxygen to the tissues and the regulation of the capillary circulation. *The Journal of Physiology, 52*(6), 457-474. doi:10.1113/jphysiol.1919.sp001844

Land, B. R., Harris, W. V., Salpeter, E. E., & Salpeter, M. M. (1984). Diffusion and binding constants for acetylcholine derived from the falling phase of miniature endplate currents. *Proceedings of the National Academy of Sciences of the United States of America, 81*(5), 1594-1598. doi:10.1073/pnas.81.5.1594

Li, J., King, N. C., & Sinoway, L. I. (2005). Interstitial ATP and norepinephrine concentrations in active muscle. *Circulation, 111*(21), 2748-2751. doi:10.1161/CIRCULATIONAHA.104.510669

Lohman, A. W., Billaud, M., & Isakson, B. E. (2012). Mechanisms of ATP release and signalling in the blood vessel wall. *Cardiovascular Research, 95*(3), 269-280. doi:10.1093/cvr/cvs187

Ludmer, P. L., Selwyn, A. P., Shook, T. L., Wayne, R. R., Mudge, G. H., Alexander, R. W., & Ganz, P. (2009). Paradoxical Vasoconstriction Induced by Acetylcholine in Atherosclerotic Coronary Arteries. *The New England Journal of Medicine, 315*(17), 1046-1051. doi:10.1056/NEJM198610233151702

Marshall, J. M. (1982). The influence of the sympathetic nervous system on individual vessels of the microcirculation of skeletal muscle of the rat. *The Journal of Physiology, 332*(1), 169-186. doi:10.1113/jphysiol.1982.sp014408

Miledi, R., Molenaar, P. C., & Polak, R. L. (1984). Acetylcholinesterase activity in intact and homogenized skeletal muscle of the frog. *The Journal of Physiology, 349*(1), 663-686. doi:10.1113/jphysiol.1984.sp015180

Moore, A. W., Jackson, W. F., & Segal, S. S. (2010). Regional heterogeneity of α-adrenoreceptor subtypes in arteriolar networks of mouse skeletal muscle. *The Journal of Physiology, 588*(Pt 21), 4261-4274. doi:10.1113/jphysiol.2010.194993

Myneni, P., Terekhov, A., Wright, G., Hofmeister, W., & Janetopoulos, C. (2014). Intravital Microfluidic Windows for Delivery of Chemicals, Drugs and Probes. *Microscopy and Microanalysis, 20*(S3), 1352-1353. doi:10.1017/S1431927614008496

Nyberg, M., Al-Khazraji, B. K., Mortensen, S. P., Jackson, D. N., Ellis, C. G., & Hellsten, Y. (2013). Effect of extraluminal ATP application on vascular tone and blood flow in skeletal muscle: implications for exercise hyperemia. *American*

Journal of Physiology. Regulatory, Integrative and Comparative Physiology, 305(3), R281-290. doi:10.1152/ajpregu.00189.2013

Park, J. W., Kim, H. J., Kang, M. W., & Jeon, N. L. (2013). Advances in microfluidics-based experimental methods for neuroscience research. *Lab on a Chip, 13*(4), 509-521. doi:10.1039/c2lc41081h

Poole, D. C., Copp, S. W., Ferguson, S. K., & Musch, T. I. (2013). Skeletal muscle capillary function: contemporary observations and novel hypotheses. *Experimental Physiology, 98*(12), 1645-1658. doi:10.1113/expphysiol.2013.073874

Segal, S. S. (2005). Regulation of blood flow in the microcirculation. *Microcirculation (New York, N.Y. : 1994), 12*(1), 33-45. doi:10.1080/10739680590895028

Toda, N., & Okamura, T. (2003). The Pharmacology of Nitric Oxide in the Peripheral Nervous System of Blood Vessels. *Pharmacological Reviews, 55*(2), 271-324. doi:10.1124/pr.55.2.3

Tyml, K., & Budreau, C. H. (1991). A new preparation of rat extensor digitorum longus muscle for intravital investigation of the microcirculation. *International Journal of Microcirculation, Clinical and Experimental, 10*(4), 335-343.

van Duinen, V., Trietsch, S. J., Joore, J., Vulto, P., & Hankemeier, T. (2015). Microfluidic 3D cell culture: from tools to tissue models. *Current Opinion in Biotechnology, 35*, 118-126. doi:10.1016/j.copbio.2015.05.002

Welsh, D. G., Tran, C. H. T., Hald, B. O., & Sancho, M. (2018). The Conducted Vasomotor Response: Function, Biophysical Basis, and Pharmacological Control. *Annual Review of Pharmacology and Toxicology, 58*(1), 391-410. doi:10.1146/annurev-pharmtox-010617-052623

Winter, P., & Dora, K. A. (2007). Spreading dilatation to luminal perfusion of ATP and UTP in rat isolated small mesenteric arteries. *Journal of Physiology, 582*(1), 335-347. doi:10.1113/jphysiol.2007.135202

Wolfe, D. B., Qin, D., & Whitesides, G. M. (2010). Rapid Prototyping of Microstructures by Soft Lithography for Biotechnology. In *Microengineering in Biotechnology* (Vol. 583, pp. 81-107). Totowa, NJ: Humana Press, Totowa, NJ.

Wood, R. E., Wishart, C., Walker, P. J., Askew, C. D., & Stewart, I. B. (2009). Plasma ATP concentration and venous oxygen content in the forearm during dynamic handgrip exercise. *BMC Physiology, 9*(1), 24-29. doi:10.1186/1472-6793-9-24

Yan, Z., Huang, X., & Yang, C. (2017). Rapid prototyping of single-layer microfluidic PDMS devices with abrupt depth variations under non-clean-room conditions by using laser ablation and UV-curable polymer. *Microfluidics and Nanofluidics, 21*(6), 1-9. doi:10.1007/s10404-017-1943-2

Yegutkin, G. G. (1997). Kinetic analysis of enzymatic hydrolysis of ATP in human and rat blood serum. *Biochemistry. Biokhimiia, 62*(6), 619-622.

3. Summary

Manipulation of the microcirculation of tissues has been an area of interest for over 100 years. The delivery of O_2 and nutrients to tissues while removing waste products is accomplished through exchange across the microcirculation. The ability to observe and manipulate blood flow regulatory mechanisms has provided a great deal of insight into the dynamic processes that occur at steady state in tissues. Experimental manipulations of microvascular blood flow have included agent administration through superfusion solution, micropipetting, or through intravascular injection into upstream feed arteries of the area of interest. Currently, there is no effective way to restrict agonist or antagonist administration to a well-defined microscale region of tissue while simultaneously visualizing the change in blood flow in the microcirculation within the volume effected. The purposes of this thesis were to develop a novel microfluidic device combined with a perfusion system for *in vivo* use. Secondly, we aimed to validate that this novel approach was capable of continuous delivery of substances at fixed concentration to a targeted confined microscale region of skeletal muscle, *in vivo,* coupled with simultaneous visualization of intact capillaries and terminal arterioles.

3.1. Results Summary

We fabricated a novel microfluidic device capable of delivering a known concentration of vasoactive drugs to a microscale region of skeletal muscle. We demonstrated that our microfluidic device is capable of constant perfusion of a PSS to skeletal muscle in a controlled manner. Upon device completion, and once setup to the

remainder of the perfusion apparatus, continuous perfusion of the device from the reservoir fluid was successfully and reproducibly achieved. Administration of doses of well characterized vasoactive drugs were used to validate the novel perfusion device and system for *in vivo* use capable of maintaining continuous delivery of a solute at fixed concentration to a microscale region of skeletal muscle during intravital video imaging. Administration of the vasodilator ATP, from 10^{-8} to 10^{-3} M, through the microfluidic device resulted in an increase in RBC velocity (μm/s) in capillaries directly overlying the micro-outlet at ATP 10^{-3} M, and mean capillary RBC supply rate (cells/s) in the same vessels increased at 10^{-4}, 10^{-3} M doses. The effect of ATP on capillary blood flow is likely due to the effects of ATP on nearby terminal arterioles and higher order arterioles via conducted vasodilation through the binding of the $P2X_4$, $P2Y_1$, and $P2Y_2$ receptors previously discussed in Chapter 1 and Chapter 2.

Along with the dose response to ATP, the dose response to the vasoconstrictor PE was also successful. Increasing doses of PE showed a significant decrease in capillary hematocrit (%), RBC velocity (μm/s), and supply rate (cells/s) at 10^{-4} and 10^{-3} M doses. The response to PE administration to the skeletal muscle volume directly over the micro-outlet strongly indicates localized area of effect of PE at the level of terminal arterioles near the window. PE causes vasoconstriction due to the rise in intracellular Ca^{2+} through α_1-adrenergic receptors present along the vascular smooth muscle cells and activation of phospholipase C. Our response to PE indicates that the delivery of PE is effective for dynamic manipulations with both vasodilators and vasoconstrictors using our novel methodology.

Lastly, administration of ACh, a vasodilator, showed no significant increase in the mean capillary RBC supply rate (cells/s), velocity (μm/s), or hematocrit (%) throughout the 4 increasing doses from 10^{-7} to 10^{-4} M, and a significant increase in supply rate and velocity at 10^{-3} M. Although not expected this result is not inexplicable. The effect of ACh on muscarinic receptors, as previously described, leads to an increase in eNOS activity and NO production resulting in vasodilation. ACh can also lead to the hyperpolarization of endothelial cells resulting in the release of EDHFs that conducts upstream to stimulate vasodilation. The decrease in ACh concentration by cholinesterase found in the tissue is a potential cause for the lack of strong initial response to the increasing doses between 10^{-7} and 10^{-4} M. The observed result was in response to extended continuous exposure to high doses of ACh doses for over one hour upon completion of the entire ACh dose protocols. This prolonged exposure time potentially leads to counteracting stimuli responsible for maintaining vascular tone.

The effect of the highest dose of each drug demonstrated the area of effect was limited to areas directly adjacent to the micro-outlet. The extended depth of field recordings of all perfused vessels within the first 100 μm of the surface of the muscle show when exposed to the highest dose of vasoactive drugs. The area of effect is limited to within ~500 μm of the micro-outlet and is seen in vessels that traverse the area above the micro-outlet. Beyond this area of effect, capillary blood flow appears to be consistent across all three drugs compared to baseline as previously shown and described. This restriction to this area provides evidence that the designed device is capable of continuously delivering vasoactive drugs at fixed concentrations to a specific microscale region of tissue while allowing for simultaneous visualization of capillary blood flow.

3.2. Limitations

This method for investigation of microvascular blood flow using a novel microfluidic device has several limitations involving fabrication and technical limitations associated with the application of the device. The design of the device is specific to the tissue and vasculature of interest, requiring additional modification and testing to apply this approach to other tissues. In this project, channel and micro-outlet orientation were determined and fabricated to accommodate the optical limitations of the microscope, as well as to facilitate positioning the animal's hind limb. Due to this, the device design outlined in this thesis will require modifications based on the tissue preparation of choice and the working distance of the microscope objective. Another limitation is the ability to target a specific vascular structure, in this study a large area was exposed to the vasoactive drugs rather than confined to a single capillary network. This larger area of effect may have led to increased conducted signalling from arterioles which were much deeper in the tissue that we could not quantify. There is also limited ability to position the micro-outlet relative to a specific target vasculature as the desired structures must be at a distance from the edge of the muscle to maintain a seal with the micro-outlet, and they must be close enough to the surface to allow for diffusive exchange with the outlet. This inability to target certain areas of the tissue may result in the need for additional tissue preparations to administer solutes to a specific vascular structure.

In addition to these limitations, there are several technical challenges associated with the delivery of drugs using the perfusion system. Doses of potent vasoactive drugs were administered for extended periods to maximize the number of field recordings. As a

result, a prolonged period of perfusion with the Krebs buffered solution may be required to regain baseline blood flow. The prolonged delivery of fluid through the microfluidic device increases the risk of accumulating bubbles within the channel causing a reduced overall fluid flow rate that can impair flow to the micro-outlet. Accommodations are required to balance maximizing the number of field recordings and the prolonged period of exposure and washout time to limit the risk of bubble accumulation within the device. This method of investigation is challenging and has several limitations associated that should be considered when adapting this approach for use in other tissue preparations.

3.3. Future Directions

Future implications of this novel method for microvascular blood flow manipulation includes the use of microfluidics to deliver soluble agonists and antagonists to capillary networks in skeletal muscle. This technique will be used to determine potential mechanisms responsible for O_2 and CO_2 mediated blood flow regulation both in healthy and diseased states. The orientation of the device use can be modified to accommodate various other muscle preparations such as the cremaster, gluteus maximus, and spinotrapezius preparations that were previously described in Chapter 1. In superfusion preparations, manipulations can be achieved in several ways; when coupled with the microfluidic device, the continuous application of superfusion fluid can be maintained at physiological levels while the microfluidic device can simultaneously deliver substances of interest during visualization. This device could be the bridge between the superfusion preparation and isolation preparations due to the potential to modify existing methods to accommodate the microfluidic device and micro-outlet.

Potential uses beyond studying blood flow regulation in muscle include delivery of direct stimuli to cause immune cell influx into area of interest in a controlled manner. Use of the microfluidic device within other organ preparations could be beneficial to the study of cell migration as well as blood flow regulation in inflammatory conditions. This could be used to study cell signalling and migration across the vascular wall in response to a treatment at the window. The use of the microfluidics with the liver preparation in particular could be beneficial in understanding both blood flow and white cell migration within the tissue. The use of microfluidics in other organ preparations can provide valuable insight into the events that occur locally during various physiological events.

Future implementation of such a device with IVVM could provide insight in the study of blood flow regulation in healthy and diseased states including hypertension, and under other metabolic states of the tissue. The application of this and similar devices could be suited for examining how the local effects of substances that might cause adverse systemic reactions when administered via intravascular injection or through abluminal application. Microfluidic use *in vivo* could be manipulated to deliver substances of research interest for mechanistic studies but also in developing or identifying pharmacological targets.

3.4. Final Summary

In summary, this project provided a basis of future use of microfluidic devices for *in vivo* use with simultaneous IVVM imaging modalities. This device provides a novel method to interact with the microcirculation of skeletal muscle to study blood flow regulation *in vivo*. The successful delivery and dose response of vasoactive agents

provides promising results that local dynamic tissue manipulation of capillary networks can lead to a blood flow response to a spatially confined region. This can have future implications in the study of mechanisms related to O_2 and ATP mediated blood flow within tissues and subsequent pharmacological targets in healthy and diseased states.